

Ph. D Dissertation

**Design and Functions of Imine-Linked Covalent  
Organic Frameworks**

イミン連結した共有結合性有機構造の設計と機能

**2015. 1**

**Hong XU**

**The Graduate University for Advanced Studies**

# Contents

<b>Chapter 1. General Introduction</b> .....	<b>1</b>
1.1 Covalent Organic Frameworks .....	2
1.2 Design and Synthesis .....	3
1.2.1 Dynamic Covalent Chemistry.....	3
1.2.2 Design Principles .....	4
1.2.3 Synthetic Methods .....	10
1.2.4 Linkage of COFs.....	17
1.3 Functions and Properties.....	25
1.3.1 Gas Adsorption and Storage.....	26
1.3.2 Photoelectric Applications .....	29
1.3.3 Heterogeneous Catalysis.....	33
1.4 Scope of This Thesis .....	34
1.5 References.....	37
<b>Chapter 2. Catalytic Covalent Organic Frameworks <i>via</i> Pore Surface</b>	
<b>Engineering</b> .....	<b>42</b>
2.1 Introduction.....	44
2.2 Results and Discussions .....	46
2.2.1 Synthesis and Structural Characterization .....	46
2.2.2 Preparation of the COF-Catalysts .....	52
2.2.3 PXRD Pattern and Theoretical Calculation .....	54
2.2.4 Gas Sorption Property.....	57
2.2.5 Heterogeneous Organocatalysis.....	59
2.3 Conclusion .....	66
2.4 Experimental Section .....	67
2.4.1 Methods.....	67
2.4.2 Coordinates and Atomic Net Charges.....	68
2.4.3 Materials and Synthetic Procedures.....	76
2.4.4 Characterization of Products.....	83

2.5 References.....	86
<b>Chapter 3. Construction of High Crystalline Meso-Porous Imine-based Covalent Organic Frameworks.....</b>	<b>89</b>
3.1 Introduction.....	91
3.2 Results and Discussions.....	93
3.2.1 Synthesis and Structural Characterization .....	93
3.2.2 PXRD Pattern and Theoretical Calculation .....	95
3.2.3 Gas Sorption Property.....	98
3.2.4 Chemical Stability.....	99
3.3 Conclusion .....	102
3.4 Experimental Sections .....	103
3.4.1 Materials and Methods.....	103
3.4.2 Crystallographic Information of Modeled COFs.....	104
3.4.3 Stability in Different COF Systems .....	109
3.5 References.....	114
<b>Chapter 4. Chiral Covalent Organic Frameworks for High-Performance Heterogeneous Asymmetric Catalysis .....</b>	<b>118</b>
4.1 Introduction.....	120
4.2 Results and Discussions.....	122
4.2.1 Synthesis and Structural Characterization .....	122
4.2.2 Preparation of the COF Catalysts .....	123
4.2.3 Gas Sorption Property.....	126
4.2.4 Heterogeneous Organocatalysis.....	128
4.2.5 Kinetic Study .....	133
4.2.6 Cycle Performance.....	134
4.3 Conclusion .....	137
4.4 Experimental Sections .....	138
4.4.1 Materials and Methods.....	138
4.4.2 Characterization of Products.....	141

4.4.3 Comparison of Different Heterogeneous Organocatalysts .....	145
4.5 References.....	150
<b>Chapter 5. Summary and Perspectives .....</b>	<b>152</b>
<b>List of Publications .....</b>	<b>155</b>
<b>Acknowledgements .....</b>	<b>157</b>

# **Chapter 1.**

## **General Introduction**

## 1.1 Covalent Organic Frameworks

Over the past two decades, interests in the field of crystalline porous materials has grown tremendously because of their unique crystalline structure, high surface area and broad applications, such as gas storage, gas separation, energy conversion, energy storage, optoelectronics and heterogeneous catalysis. Chemists have developed various strategies to prepare porous materials; however, it had proven difficult to synthesize porous organic polymer networks with highly order structure until the concept of reticular chemistry, which uses topologically designed building blocks, was proposed to construct these crystalline porous materials. The first family of crystalline porous materials to be synthesized under the principle of Reticular Chemistry was Metal Organic Frameworks (MOFs)<sup>[1-2]</sup>, which consisting of metal ions or clusters coordinated to rigid organic molecules to form ordered one-, two, or three- dimensional structures. The coordination versatility of the constituent metal ions combines with the functional diversity of the organic linker molecules to create enormous possibilities.

In 2005, Yaghi and co-workers demonstrated the utility of the topological design principle in their synthesis of porous organic frameworks connected via covalent bonds, which produced the first successful examples of Covalent Organic Frameworks (COFs)<sup>[3]</sup>. COFs are a class of crystalline porous polymers that enable the atomically precise integration of building blocks into periodicities. Since then, the COF materials have attracted tremendous interest since its unique structure feature and possess great potential for functional exploration.

COFs are composed of lightweight elements (usually C, H, O, N and B) and linked by strong covalent bonds, therefore they own low densities, possess high thermal stabilities, and provide permanent porosity. According to the geometry of the crystalline structures, COFs can be categorized into two- (2D) or three-dimensional (3D) COFs. 2D-COFs consist of 2D sheets, which stack further to constitute layered structures, lead to the periodically aligned columnar  $\pi$  arrays and ordered one-dimensional channel arrays. The periodic columnar structure provides a powerful platform to construct ordered  $\pi$  systems that are difficult to create via conventional

covalent linked polymers. The ordered columns in 2D COFs could facilitate charge carrier transport through the pre-organized and build-in pathways, which possess great potential for developing new type light-emitting, semiconducting, photoconductive, and charge-separating materials.<sup>[4-14]</sup> Meanwhile highly ordered skeletal alignment, high surface area together with open-channel structure of the 2D COFs provides a high potential to develop high-performance heterogeneous catalysts.<sup>[15]</sup> On the other hand, 3D COFs consisting of three-dimensional network structure have a higher potential to achieve high surface areas, which makes them ideal candidates for gas adsorption and storage.<sup>[16-48]</sup>

## 1.2 Design and Synthesis

### 1.2.1 Dynamic Covalent Chemistry

Dynamic covalent chemistry (DCC) relates to chemical reactions carried out reversibly under the conditions of thermodynamic control. The reversible nature of the reactions could introduce the mechanisms of "error checking" and "proof-reading" during synthetic process. Synthesis of covalent linked polymers has generally been dominated by kinetically controlled reactions, which irreversibly form covalent bonds. In contrast, dynamic covalent chemistry leads to the reversible formation of covalent bonds, which can be formed, broken, and reformed.<sup>[49-50]</sup> Therefore, unlike conventional covalent bond formation, DCC is thermodynamically controlled and offers reversible reaction systems with "error checking" and "proof-reading" characteristics, leading to the formation of the most thermodynamically stable structures (**Figure 1**). By utilizing DCC concept for the construction of COF materials, the polymer skeleton formation occurs alongside the crystallization process, while the self-healing feedback reduces the incidence of structural defects and assists in the formation of ordered structure. As a result, the final COF product possesses the ordered crystalline structure with the highest thermodynamic stability.

The design and synthesis of COFs have two key issues that should be satisfied to achieve thermodynamic control: the first is the topological structure of the building blocks and the second is the synthetic method.

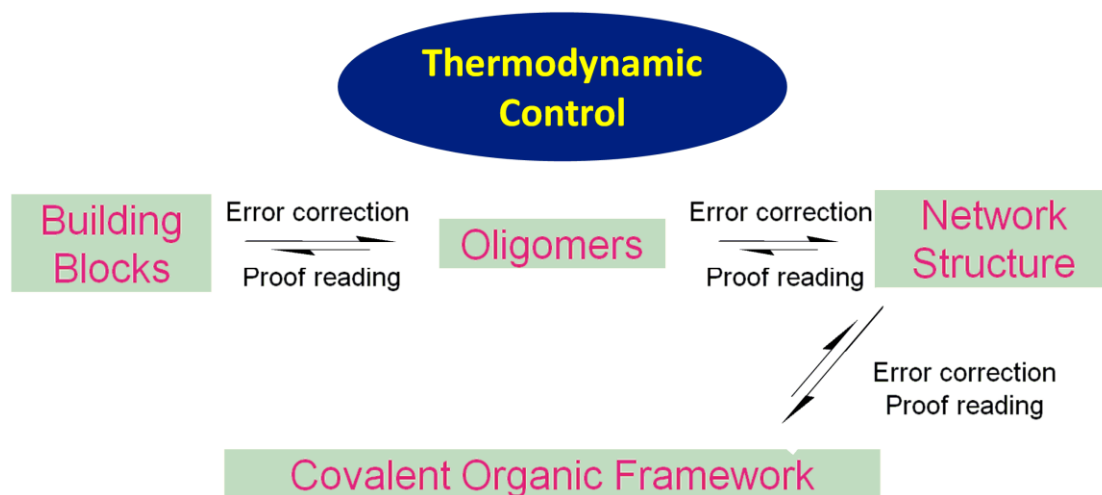


**Figure 1.** Synthesis of covalent organic frameworks under the principle of dynamic covalent chemistry, in which crystalline polymers were formed under the thermodynamic control mechanism.

### 1.2.2 Design Principles

Similar to the case of MOFs, the COF materials could be designed through the principles of Reticular Chemistry. The basic concerns for design and synthesis of such porous crystalline materials mainly focus on the porosity and the structural regularity. Under this notion, experiences and techniques have been obtained from the MOF systems<sup>[1-2]</sup>, which should be applicable to the COF synthesis as well. However, self-assembly of the building blocks (metal and organic linkers) to construct crystalline MOFs *via* coordination chemistry is much easier than that to construct crystalline COFs *via* the less reversible covalent bonds. Further, additional concerns for constructing functional COFs for certain applications should also be invoked.

#### 1.2.2.1 Structural Regularity

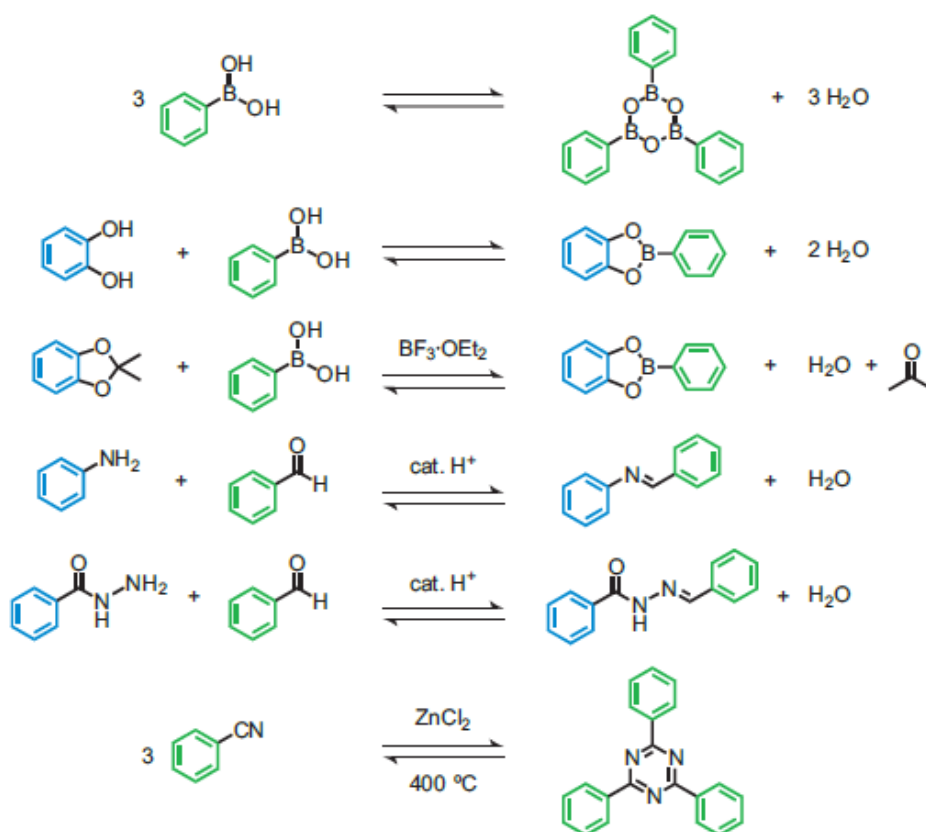


**Figure 2.** Reversible reactions used for the construction of COFs.

COFs are synthesized under the principle of Dynamic Covalent Chemistry, reversibility of the formation reaction is crucial important for getting a crystalline framework. (Figure 2) A majority of the known COFs rely on the boron chemistry because of the high reversibility of these condensation reactions, in which the boronic acids can be self-condensed or co-condensed with catechol to obtain six-membered boroxine or the five membered boronate-ester linkages. (Figure 3) The boron-based COFs own higher crystallinity in the COF family because of its high reversibility, however, this feature makes this class of COF own a poor chemical stability which are susceptible to attack of the nucleophilic reagent and are even hydrolysed by water vapours in the air.<sup>[51]</sup>

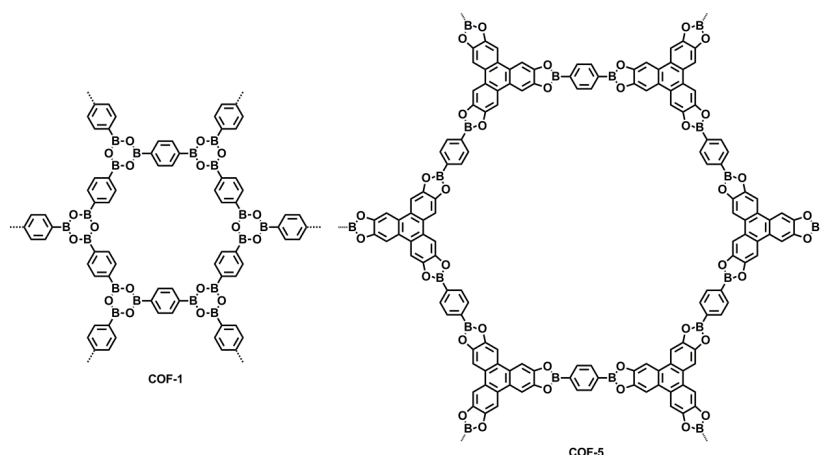


**Figure 3.** Schematic representation of COFs with boroxine and boronate-ester linkages.

Yaghi's group has pioneered in new connection chemistry for COFs, developed dynamic pH-dependent, reversible condensation reactions that form both imine<sup>[52-53]</sup> and hydrazone<sup>[54]</sup> linkages. Another class of COFs which called Covalent Triazine-based Frameworks (CTFs), has been developed *via* the cyclical trimerization of cyano-groups under ionothermal conditions in high temperatures (>400 °C).<sup>[55-57]</sup> Such CTFs demonstrate high thermal, chemical and mechanical stabilities along with a high degree of conjugation; however, they typically possess low crystallinity since the poor reversibility of the trimerization reaction.

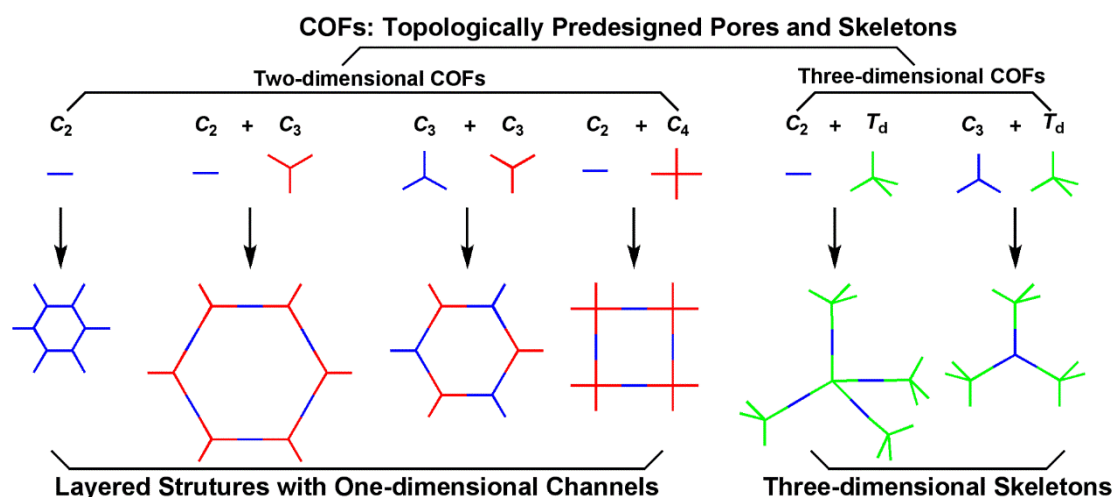


**Figure 4.** The combination of building blocks with different geometries to design 2D and 3D COFs.

The rigid conformation of the building blocks enables the topological design of the COFs. As shown in **Figure 4**, the geometry of the building blocks determines the crystalline structure of COF. As a result, the combinations such as 3D- $T_d$  + 3D- $T_d$ , 3D- $T_d$  + 2D- $C_2$ , or 3D- $T_d$  + 2D- $C_3$  can generate 3D COFs with different crystalline space groups. In contrast, the combinations of the 2D building blocks (*e.g.*, 2D- $C_2$  + 2D- $C_3$ , 2D- $C_3$  + 2D- $C_3$  or 2D- $C_2$  + 2D- $C_4$ ) will endow 2D COFs with designed topology and pore structures (**Figure 4**). The rigid nature and discrete bonding direction of arenes makes aromatic  $\pi$  conjugated systems suitable building blocks for COFs. Meanwhile, the diversity of aromatic systems allows numerous building blocks combinations, which endows COF with high flexibility in their structure design.

### 1.2.2.2 Porosity

The second concern for the construction of COF materials, as for other porous organic polymers, is the issue of porosity. Under this notion, the design strategy applied to other covalent linked porous solids could be adapted to the COF synthesis. For example, the templating strategy for the preparation of microporous zeolites or mesoporous silicas which employs the structural-directing agents to assemble the building blocks,<sup>[58-60]</sup> removing the template from the as-synthesized materials could provide the porous materials. Another strategy is to utilize the rigid building blocks to construct the porous structures. For example, the synthesis method for conjugated porous polymers *via* coupling reactions.<sup>[61-64]</sup>

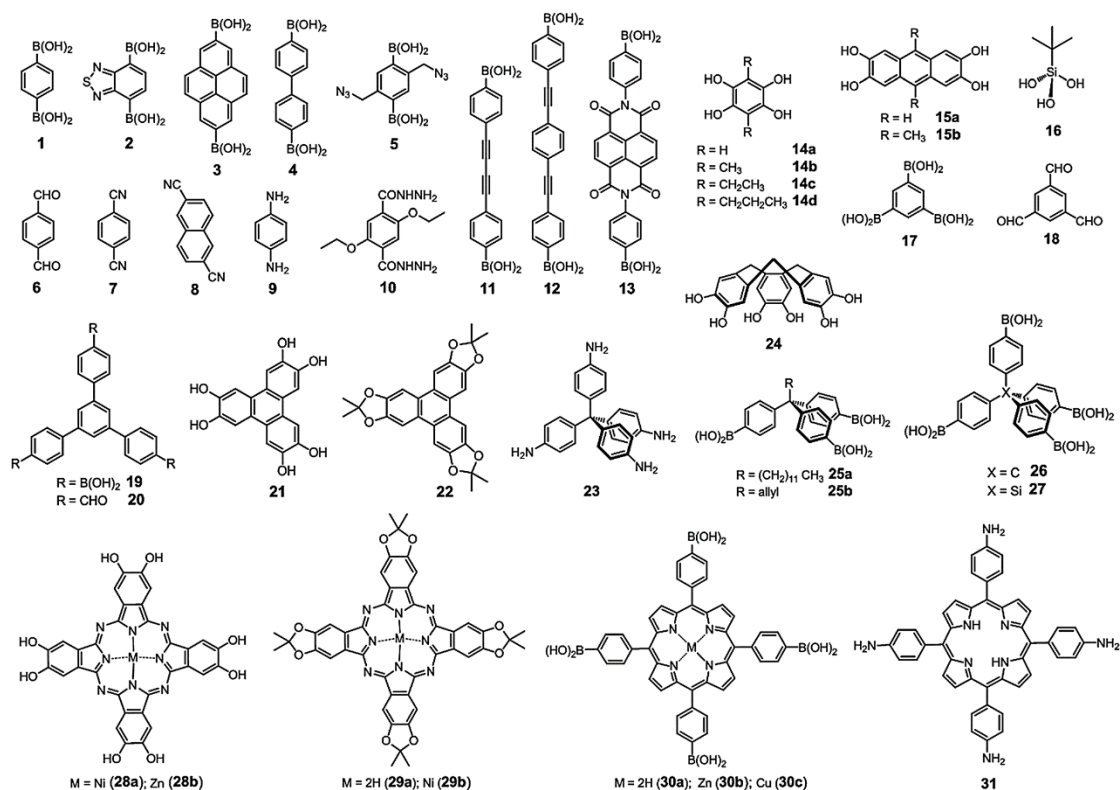


**Figure 5.** Building blocks utilized for the synthesis of COFs.

Up to now, most COF materials are utilized the latter strategy by designing the rigid building blocks to create the extended porous structures. The size of the building blocks will, accordingly, govern the pore size of the framework; while the shape of the building blocks will determine the topology of the crystalline structure (as discussed in Section 1.2.2.1). To date, the linking groups formed are boroxines,<sup>[3, 5, 65]</sup> boronate esters,<sup>[3-4, 6-7, 53, 65-75]</sup> imines,<sup>[5, 52]</sup> hydrazones,<sup>[43, 54, 76]</sup> triazines,<sup>[55-57]</sup> phenazines<sup>[77]</sup> and azines,<sup>[78]</sup> which are all rigid with a planar geometry. For the efficient construction of crystalline porous structure, building blocks (as shown in **Figure 5**) with rigid aromatic moieties are preferable, as found in most of the MOF materials and also the amorphous porous organic materials.

### 1.2.2.3 Functionality

The principles discussed above (Section 1.2.2.1 and 1.2.2.2) mainly focus on the periodicity and porosity towards design and synthesis of the crystalline porous COF materials. However, in order to construct the functionalized COF for a certain applications, further concerns on how to introduce the functional groups into the COF

channel walls should be invoked. The two general strategies were shown in **Figure 6**, which is similar to those applied for constructing functional materials.

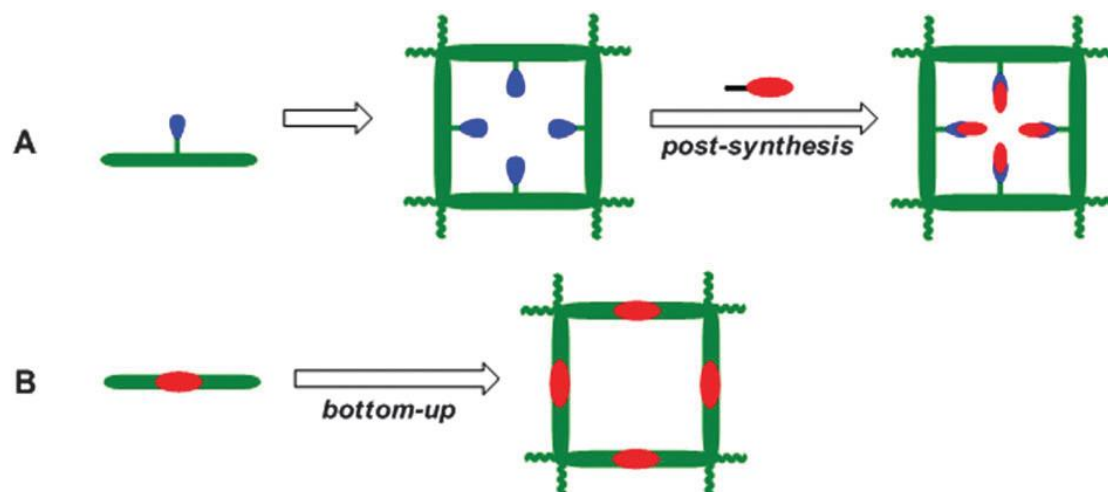


**Figure 6.** General strategy for synthesis of functional COF materials. The red oval represents the functional moieties.

The strategy B involves introducing reactive groups into functional monomers and polymerization of these monomers from each other, which is a facile and common method in traditional linear polymers and porous organic polymers. However, when the functional molecular is partially bigger, asymmetric or flexible, constructing crystalline frameworks require a tedious solvothermal synthesis if not impossible. On the other hand, the post-synthesis strategy (route A, **Figure 6**), which introduces the functional moieties into the given crystalline structure *via* the subsequent modification, such as coordination or chemical transformation become to be better option. Under this notion, our lab has established a facile but effective method for engineering the surface of 2D COF pores to allow the incorporation of organic functional moieties into the channels.<sup>[73]</sup> This method utilized the azido-contained building blocks for the synthesis of boronate-ester-based COFs with a designable content of azide units. These azide units undergo a quantitative click reaction with ethynyl-contained molecular to produce pore surfaces with desired groups. The pore size can be finely tuned by introduce different alkynes, from 1.2 nm to 3.0 nm for the hexagonal COF-5 family.

### 1.2.3 Synthetic Methods

Optimizing thermodynamic equilibrium during covalent bond formation is the key to form highly ordered crystalline frameworks. Therefore, the reaction conditions such as: temperature, pressure, catalyst and template should be taken into account for the formation of thermodynamically stable crystalline structures. Regarding the reaction media, mix-solvents system and molten salts have been developed to provide solvothermal and ionothermal conditions, respectively, for the synthesis of COFs. Microwave and sonochemical reactions under solvothermal conditions have been explored for quickly preparation of large-scale COF materials. Very recently, a novel mechanochemical synthesis method has been demonstrated to synthesize COF under solvent-free conditions. In contrast to these bulky synthesis methods, COF monolayers or films have been explored *via* reactions on substrates, such as metal surfaces and graphene surfaces.

#### 1.2.3.1 Solvothermal Synthesis

Most COF materials are obtained *via* the solvothermal synthesis method, which is similar to those for synthesizing metal organic frameworks in autoclaves, the solvothermal condition often takes 2 to 15 days and require heating (80-120 °C) within a sealed vessel. Pressure inside the sealed vessel is of importance, which may affect the reaction yields and crystallinity. Yaghi and co-workers found that 150 mTorr is the optimal pressure before the vessel is sealed within a given volume (ca. 10 cm<sup>3</sup>).<sup>[3]</sup> Meanwhile, Lavigne and co-workers developed a reflux procedure under ambient pressure to synthesize COFs.<sup>[66]</sup> Utilize this method, COF-18Å could be obtained under ambient pressure without the use of sealed vessels in 3 days, it is easy for operation and suitable for large-scale preparation.

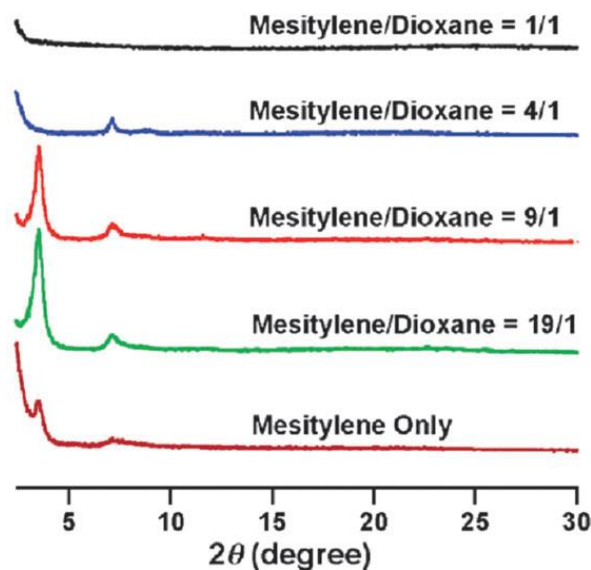


**Figure 7.** PXRD pattern of ZnP-COF prepared in different solvent combinations after 6 days.

Notably, the solvent chosen for the solvothermal synthesis is crucial important, since it governs the solubility of the monomers and self-assemble behavior. Our lab have carefully investigated the influence of solvents on the crystallinity of boronate-ester-based COFs.<sup>[71]</sup> Co-condensation of zinc(II) 5,10,15,20-tetrakis(4-(dihydroxyboryl)phenyl) porphyrin (monomer **30b**, **Figure 5**) and 1,2,4,5-tetrahydroxybenzene (monomer **14a**, **Figure 5**) in a co-solvents of mesitylene and dioxane with  $v/v = 1/1$  resulted in amorphous solids (as indicated by the PXRD spectra, **Figure 7**, black line). In contrast, when the volume ratio of mesitylene and dioxane was changed to  $v/v = 19/1$  or  $9/1$ , COF materials with high crystallinity could be obtained (**Figure 7**, red line and green line).

Dichtel and co-workers synthesized the boronate-ester based COF *via* the solvothermal procedure assisted with a Lewis acid.<sup>[70]</sup> This approach employs acetamide-protected catechol as monomers which could be deprotected in the presence of the Lewis acid catalyst ( $\text{BF}_3 \cdot \text{OEt}_2$ ) during the solvothermal procedure. This strategy avoids the use of unstable (sensitive to oxygen) and insoluble catechol monomers, and thus, broadens the scope of the building blocks for the COFs. Further mechanistic study revealed that the self-condensation of boronic acids (form six-membered boroxines)

and the formation of boronic acid–BF<sub>3</sub> complex contributed to the reversibility of the reaction and influence the formation rate of boronate esters in the reaction system.<sup>[79]</sup>

### 1.2.3.2 Ionothermal Synthesis

Thomas and co-workers developed an ionothermal synthesis approach to produce covalent triazine-based frameworks (CTFs) (**Figure 8**).<sup>[55-57]</sup> The cyclotrimerization of aromatic nitrile building blocks (*e.g.*, 1,4-dicyanobenzene, as presented in **Figure 8**) in molten ZnCl<sub>2</sub> at 400 °C affords crystalline conjugated CTFs with robust chemical and thermal stabilities. Such molten ZnCl<sub>2</sub> saults act as both the solvent and also the catalyst for the trimerization reaction. However, such harsh ionothermal conditions largely limited the scope of the building blocks. On the other hand, due to the poor reversibility of the trimerization reaction, most synthesized CTFs displayed low crystallinity characterization that lacks long-range order structure.

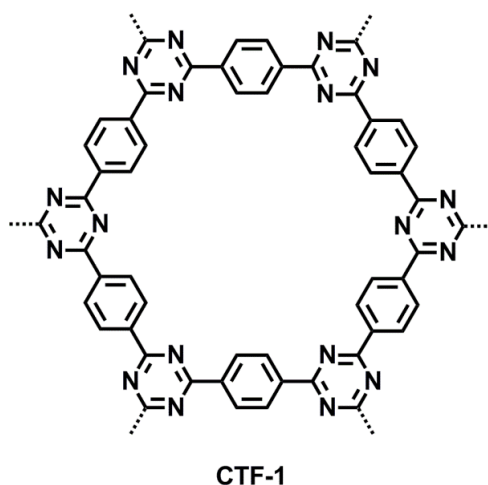


**Figure 8.** Schematic representation of COFs with triazine linkages (Covalent Triazine-based Frameworks).

### 1.2.3.3 Microwave Synthesis

Microwave synthesis has been widely used as a protocol for accelerating chemical reactions.<sup>[80]</sup> It has been found that crystalline metal organic frameworks materials could be synthesized using microwaves.<sup>[81-82]</sup> Accordingly, Cooper and co-workers demonstrated a rapid microwave-assisted method to rapidly synthesize boronate-ester linked COFs (**Figure 9**).<sup>[83]</sup> Such microwave synthesis possess several advantages over

the classical solvothermal methods. (1) Microwave synthesis produces COFs rapidly (COF-5 and COF-102 could be obtained *via* microwave conditions in 20 minutes, which is more than 200 times faster than the reaction time of 72 h required in the solvothermal conditions) (2) A sealed vessel is not required for microwave synthesis, simplified the operation procedures. Combine with the first advantage, it makes large-scale synthesis possible. (3) The solvent extraction under the microwave conditions could easily remove residues and impurities trapped in the pores, which promotes better porosity (the BET surface area of COF-5 (2019 m<sup>2</sup>/g) obtained *via* microwave synthesis is higher than that solvothermally synthesized in a sealed vessel (1590 m<sup>2</sup>/g). Therefore, such microwave-assisted protocol provides a potential replacement for the solvothermal method.

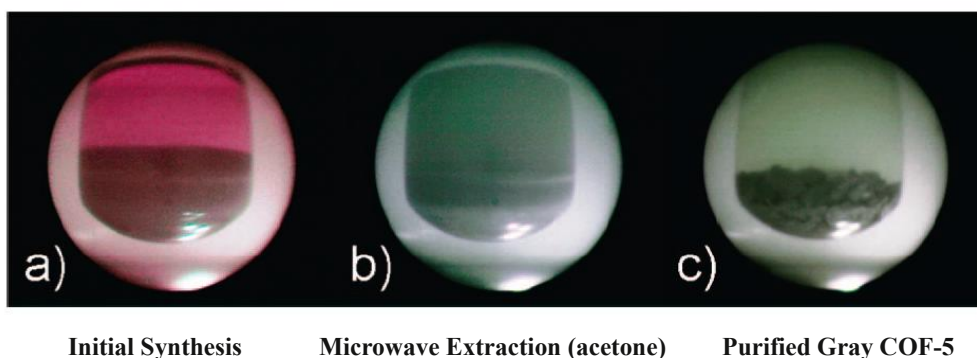


**Figure 9.** Digital camera images of the microwave-assisted synthesis of COF-5 and purification procedure.

#### 1.2.3.4 Mechanochemical Synthesis

Very recently, Banerjee and co-workers explored a mechanochemical method for COF synthesis (**Figure 10**).<sup>[20, 84]</sup> Utilizing this novel method, three chemically stable COFs [TpPa-1 (MC), TpPa-2 (MC), and TpBD (MC)] are obtained at room temperature under solvent-free conditions. These COFs possess moderate crystallinity compared with solvothermal synthesis since the poor reversibility of the COF formation reaction under this unique condition. However, the materials obtained from this strategy could demonstrate a graphene-like thin-layered morphology (exfoliated layers), quite

different from the analogues synthesized under solvothermal conditions because the exfoliate mechanism induced by grinding procedure.<sup>[20]</sup>



**Figure 10.** Schematic representation of the mechanochemical (MC) synthesis of TpPa-1 (MC), TpPa-2 (MC), and TpBD (MC).

### 1.2.3.5 Covalent Organic Frameworks on Surface

Solvothermal synthesis strategy produces the COF materials as unprocessable powders, which limited their applications, such as, interface incorporated devices, thin films or monolayer devices. To overcome this challenge and take advantage of COF's highly ordered yet covalent linked structure feature, several methods have been developed: Abel and co-workers demonstrated the Surface Covalent Organic Frameworks (SCOFs), which introduce the COF monolayers on the metal surface. Wan and co-workers utilized the highly ordered pyrolytic graphite surface instead of metal surface to prepare monolayer COFs. Dichtel and co-workers developed a solvothermal method for producing 2D COF materials as thin films on single-layer graphene.

#### 1.2.3.5.1 Synthesis of Monolayers on Metal Surface

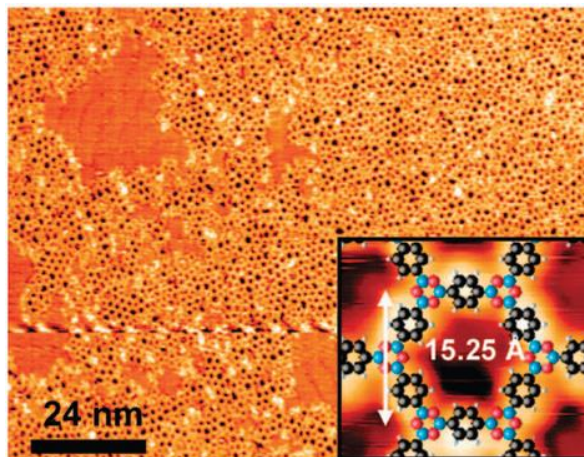


**Figure 11.** STM image (120 nm  $\times$  90 nm) of near-complete monolayer SCOOF-1 films synthesized from the deposition of 1,4-benzenediboronic acid on Ag (111) surface. The inset shows the overlaid chemical structure obtained by DFT calculation.

In contrast to the bulky synthesized COFs discussed in Section 1.2.3.1-1.2.3.4, condensation of the building blocks on the metal surface to form monolayers of COF-1 and COF-5 have been demonstrated by Abel and co-workers (**Figure 11**).<sup>[85]</sup> The covalently linked SCOOF-1 and SCOOF-2 nano-architectures can be prepared by sublimating corresponding building blocks onto the Ag(111) surface under ultrahigh vacuum. Such SCOOFs could be directly observed *via* scanning tunneling microscopy (STM), which reveals the presence of hexagonal pore structure along with small numbers of irregular pores (as shown in **Figure 11**). This is the first example of manufacturing covalent organic frameworks on the substrate surface, however, preparation of high quality or defect-free monolayers on the metal surface may require optimization reaction conditions, improving the purity of the building blocks, and using suitable metal substrate to direct the building block alignment.

#### 1.2.3.5.2 Synthesis of Monolayers on a HOPG Surface

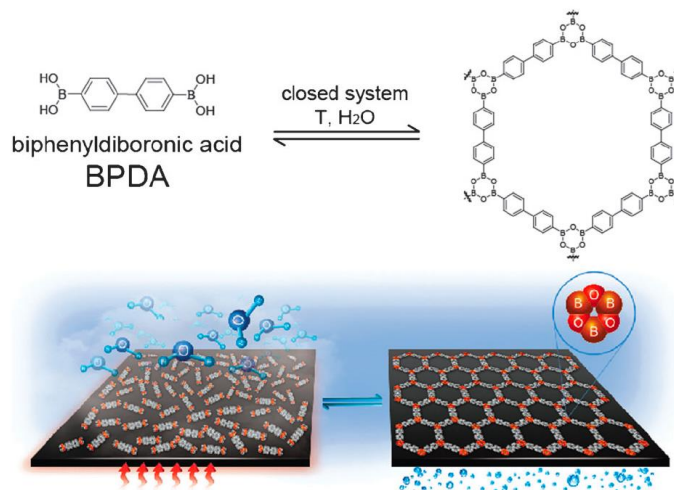


**Figure 12.** Schematic representation of synthesis of SCO on HOPG surface.

Wan and co-workers utilized the highly ordered pyrolytic graphite (HOPG) surface instead of metal substrate to prepare monolayer COFs (**Figure 12**).<sup>[86]</sup> Biphenyldiboronic acid (BPDA), 1,4-benzene diboronic acid (BDDBA), and 9,9-dihexylfluorene-2,7-diboronic acid were deposited onto the HOPG surface from their THF solutions, and the resulting HOPG substrates were heated in sealed autoclave at 150 °C for 1 h to form COF monolayers. To gain a high quality SCOFs, this paper introduced  $\text{CuSO}_4 \cdot 5\text{H}_2\text{O}$  serves as a water “reservoir” to regulate the chemical equilibrium. In the absence of  $\text{CuSO}_4 \cdot 5\text{H}_2\text{O}$ , the coverage of the HOPG surface by the monolayer was only approximately 7%, which increased dramatically to 98% in the presence of  $\text{CuSO}_4 \cdot 5\text{H}_2\text{O}$ . The water molecules released from  $\text{CuSO}_4 \cdot 5\text{H}_2\text{O}$  during the reaction process can act as an “equilibrium-manipulating agent” that increase the reversibility of the formation reaction and thus promotes the defect remedy process, which endows the synthesized SCOFs with highly order structure (**Figure 12**). Meanwhile, these water molecules can be reabsorbed by the  $\text{CuSO}_4$  during the cooling process, which prevents the decomposition of the boroxine-based COFs.

### 1.2.3.5.3 Synthesis of Oriented Thin Films on Graphene Surface

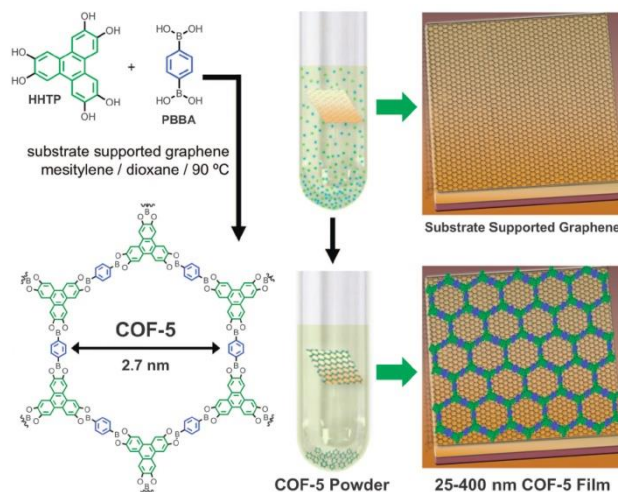


**Figure 13.** Solvothermal condensation of HHTP and PBBA on SLG surface provides COF-5 as both a film on the graphene surface, as well as a powder precipitated in the bottom of the reaction vessel.

COFs prepared using these methods discussed above are either unprocessable powders or monolayers, which cannot be reliably interfaced with electrodes or incorporated into real devices. Therefore, preparation of COF thin films on substrates is of broad scientific interest and significant technological importance. Dichtel and co-workers have reported the preparation of highly oriented 2D COF films onto single-layer graphene (SLG on SiO<sub>2</sub>) surfaces.<sup>[74, 87-88]</sup> By placing SLG/SiO<sub>2</sub> substrate in the solvothermal reaction systems, oriented COF thin films formed on the SLG surface *via*  $\pi$ - $\pi$  interaction (**Figure 13**). Various COF films, such as COF-5, TP-COF, and HHTP-DPB-COF could be successfully prepared *via* this method, and their thicknesses can be well controlled by tuning the reaction time. As demonstrated by synchrotron X-ray diffraction analysis, the obtained COF materials exhibit improved crystallinity in comparison with the powder samples, meanwhile the layers in the thin films are vertically aligned.

#### 1.2.4 Linkage of COFs

COFs are designed and synthesized under the principle of dynamic covalent chemistry (DCC), utilizing the reversible formation of covalent bonds, which can be formed, broken, and reformed. Reactions involved in COF formation is reversible,

according to the reversibility of the formation reactions, I divide the COF materials into two classes. The first class of COFs are boroxine<sup>[3, 5, 65]</sup> or boronate-ester<sup>[3-4, 6-7, 53, 65-75]</sup> based COF, which shows high crystallinity and porosity because of the high reversibility of the boroxine or boronate-ester formation reactions. However, all of them are not stable in the presence of water or other protonic solvents. Utilizing less reversible formation reactions, the second class COF, including imine-,<sup>[5, 52]</sup> hydrazone-,<sup>[43, 54, 76]</sup> phenazine-,<sup>[77]</sup> azine-<sup>[78]</sup> and triazine-<sup>[55-57]</sup> linked COF have been developed which showed improved stability compared with the first class COF. However, almost all of them suffer from low crystallinity and poor surface area.

#### 1.2.4.1 First Class COFs

Since the ingenious construction of the first COF materials (COF-1 and COF-5) demonstrated by Yaghi and co-workers,<sup>[3]</sup> various examples of boron-containing COFs through the formation of boroxine and boronate ester has been attracted intensive research interest, because of its high reversibility which endows these COFs with highly order crystalline structure and also high porosity. According to the synthetic strategies, these boron-containing materials could be further sorted into two categories.

##### 1.2.4.1.1 Boroxine-based COFs

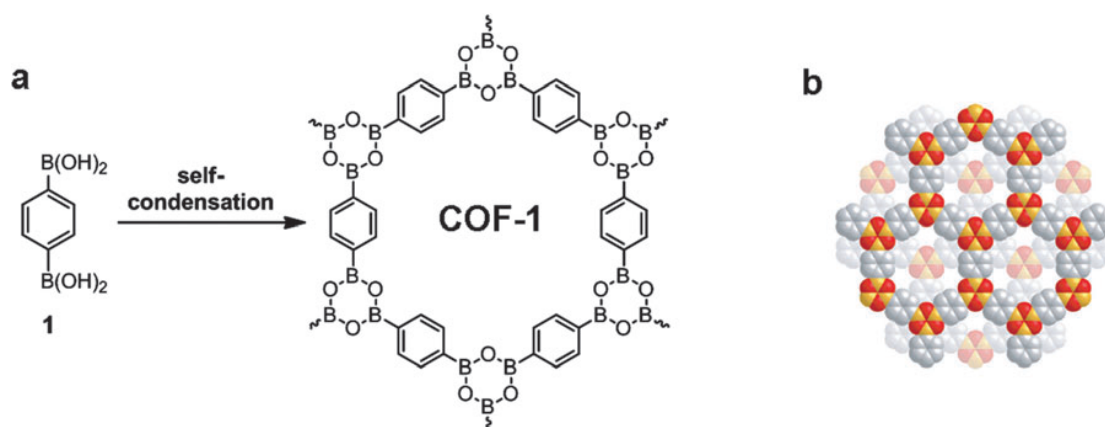


**Figure 14.** a. Self-condensation of 1,4-benzenediboronic acid to form 2D COF-1; b. proposed crystalline structure for COF-1.

One category of boron-containing COFs is boroxine-based COFs which constructed *via* the self-condensation of dibenzenediboronic acid monomer to form the six-membered boroxine ring. For example, COF-1 which was synthesized through the self-condensation reaction of 1,4-benzenediboronic acid (BDBA).<sup>[3]</sup> As shown in the **Figure 14**, self-condensation of benzenboronic acid groups forms boronate anhydrides with planar six-membered B<sub>3</sub>O<sub>3</sub> rings. As a result, the synthesized COF-1 exhibits a layered staggered structure (**Figure 14, b**) with a BET surface area of 711 m<sup>2</sup>/g and a pore size of 0.7 nm. Under this notion, 3D boron-containing COFs have also been successfully synthesized *via* the self-condensation of tetrahedrally-structured building blocks, which exhibit extremely high surface areas. For example, COF-103 synthesized from the tetrahedrally boronic acid monomer (monomer **27**, **Figure 5**) own a BET surface area of 4210 m<sup>2</sup>/g,<sup>[65]</sup> which possess the champion data in the COF family. So far, monomers **1**,<sup>[3]</sup> **3**,<sup>[5]</sup> **26**,<sup>[65]</sup> and **27**<sup>[65]</sup> (**Figure 5**) have been successfully applied to synthesize the boroxine-based COFs *via* the self-condensation strategy.

#### 1.2.4.1.2 Boronate-ester based COFs

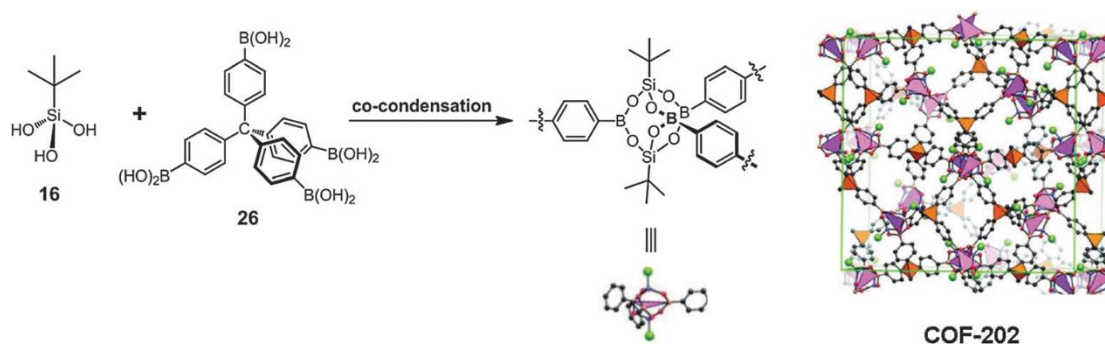


**Figure 15.** Co-condensation of monomers **16** and **26** to synthesize 3D COF-202 and the proposed crystalline structure.

Another large category of boron-containing COFs is boronate-ester based COFs which constructed *via* the co-condensation of two or more building blocks.<sup>[3-4, 6-7, 53, 65-75]</sup> The dehydration reaction of benzenboronic acid and catechol lead to the formation of five-membered rings (boronate ester, **Figure 2**). Under this strategy, the layered

eclipsed stacking structures are generated, in the cases of 2D COFs. If tetrahedrally-structured building blocks are used, 3D COFs with more complicated structures could be obtained. One significant advantage of this co-condensation strategy is the diverse combination of benzenboronic acid and catechol building blocks, by which serious of COFs with different properties and functionalities could be easily designed and synthesized. For instance, *via* the co-condensation of *tert*-butylsilane triol [*t*-BuSi(OH)<sub>3</sub>] and tetra(4-dihydroxyborylphenyl) methane (**Figure 15**), 3D COF-202 with butyl functional groups was synthesized due to the borosilicate formation reaction.<sup>[68]</sup> Different from the dehydration reaction of boronic acids with catechol, in this case, the two hydroxyl groups of one -B(OH)<sub>2</sub> react individually with different triols.

In general, the boron-containing COFs possess high crystallinity because of the high reversibility of the boron-chemistry, thus the first class COFs displayed low densities and high BET surface areas. Specifically, the 3D boron-containing COFs demonstrated the highest surface area in the COF family and the lowest densities among the porous materials reported. Meanwhile, such boron-containing COFs possess excellent thermal stabilities (up to 450–600 °C), as revealed by the thermogravimetric analysis. Based on these attractive features and diverse combination of various functional building blocks, further practical applications of functional COF materials are highly expected. However, it should be noted that most of the synthesized boron-based COF materials are unstable in moist air<sup>[89]</sup> or in water,<sup>[51]</sup> since its high reversible nature. The hydrolysis experiments on COF-5, COF-18Å, and COF-14Å indicate that significant loss of structural regularity in the presence of water (**Figure 16**).<sup>[51]</sup> Such inevitable disadvantages might, to some extent, limit the practical applications of first COFs materials.

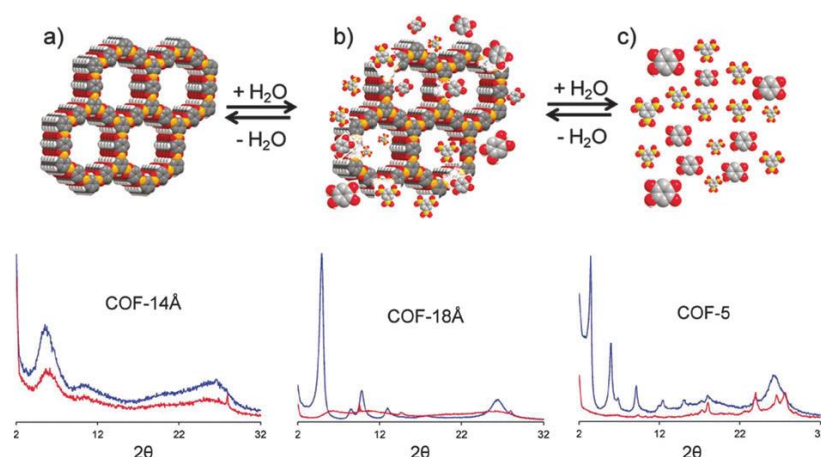


**Figure 16.** Top: The proposed mechanism for hydrolyzation of boron-containing COFs. **a.** the initial crystalline structure of COF; **b.** partial hydrolysis; **c.** complete hydrolysis. Bottom: hydrolysis experiments of COFs, PXRD patterns of COF-14Å, COF-18Å, and COF-5 before (blue) and after (red) hydrolysis in water.

### 1.2.4.2 Second Class COFs

Utilizing less reversible formation reactions, the second class COF, including imine-,<sup>[5, 52]</sup> hydrazone-,<sup>[43, 54, 76]</sup> phenazine-,<sup>[77]</sup> azine-<sup>[78]</sup> and triazine-<sup>[55-57]</sup> linked COF have been developed which are stable in most organic solvents and insensitive to water; however, they generally showed poor crystallinity compare to the first class COFs because of the reversible issue.

#### 1.2.4.2.1 Imine-based COFs

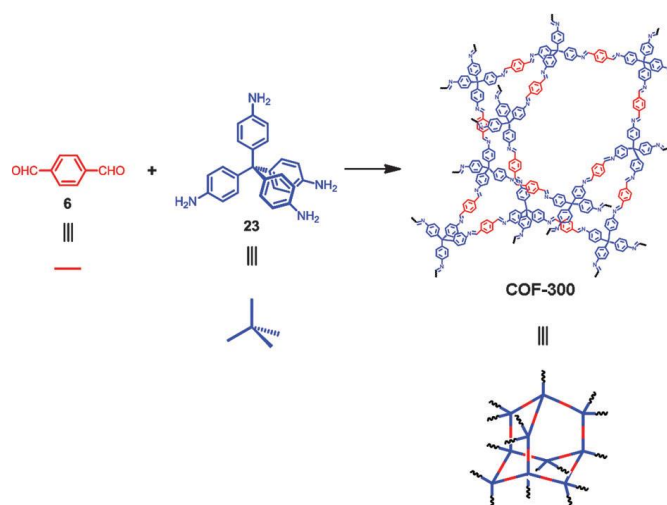


**Figure 17.** Synthesis of the imine-based three dimensional covalent organic framework, COF-300.

Current developed imine-based COFs could be divided into the "Schiff base" type and its derivatives include hydrazone-type, phenazine-type, and azine-type. In this section, the primary type, Schiff base linked COF will be introduced and the other three imine derivatives will be discussed in subsequent sections. In 2009, Yaghi and co-workers developed the first imine-based COF, COF-300, *via* the dehydration reaction of dialdehyde monomer (monomer **6**, **Figure 5**) and tetrahedrally amine monomer (monomer **23**, **Figure 5**).<sup>[52]</sup> COF-300 possesses a three-dimensional diamond-like structure with a BET surface area of 1360 m<sup>2</sup>/g and an average pore size of 7.8 Å because of its interpenetrated crystalline structure (**Figure 17**). Stimulated by this result, our lab has developed various imine-based COFs. For example, CuP-TFPhx COF synthesized *via* co-condensation of copper 5,10,15,20-tetrakis(4-phenylamino)porphyrin (CuP) with co-aldehyde monomer (2,3,5,6-tetrafluoroterephthalaldehyde and terephthalaldehyde), aims at synthetic control of the crystallinity and porosity of imine-COF by managing interlayer interactions based on self-complementary  $\pi$ -electronic forces.<sup>[90]</sup> The Py-DHPH COF, Py-2,3-DHPH COF, Py-2,2'-BPyPh COF and Py-3,3'-BPyPh series COFs with open docking sites.<sup>[91]</sup> These COFs feature ordered alignment of binding sites and pre-designable skeletons. Metallation converts the open frameworks into supramolecular COFs with dense and aligned catalytic V=O sites confined within the nanochannels.

#### 1.2.4.2.2 Hydrazone-based COFs

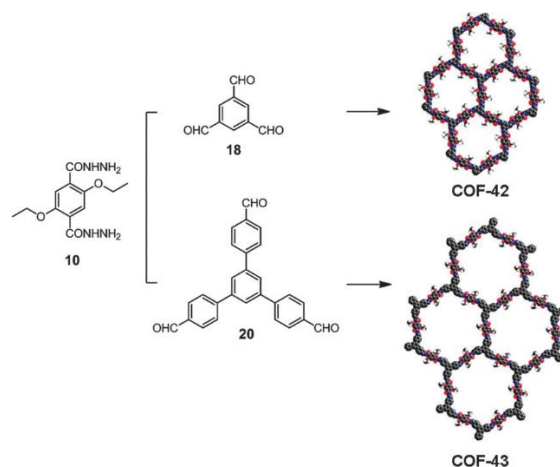


**Figure 18.** Synthesis and crystalline structure of the hydrazone-based covalent organic frameworks, COF-42 and COF-43.

Hydrazone-linked COF is a derivative of the imine-based COFs, the synthesis of which was pioneered by Yaghi and co-workers *via* the co-condensation reaction of aldehydes monomers and hydrazides monomers. By employing hydrazide (monomer **10**, **Figure 5**) and aldehydes (monomer **18** or **20**, **Figure 5**) as the building blocks, COF-42 and COF-43 were successfully synthesized *via* the solvothermal method (**Figure 18**).<sup>[54]</sup> These two COFs possess hexagonal pore structure with the pore size of 2.8 nm and 3.5 nm and own the BET surface areas of 710 and 620 m<sup>2</sup>/g, respectively. The intramolecular hydrogen bonds locked the conformation of the hydrazine monomers benefit the formation of the ordered crystalline structures. Since the hydrogen bonding is highly important for the formation of COFs, the nonsubstituted terephthalohydrazides or slight change in the solvothermal conditions will lead to amorphous solids.

#### 1.2.4.2.3 Phenazine-based COFs

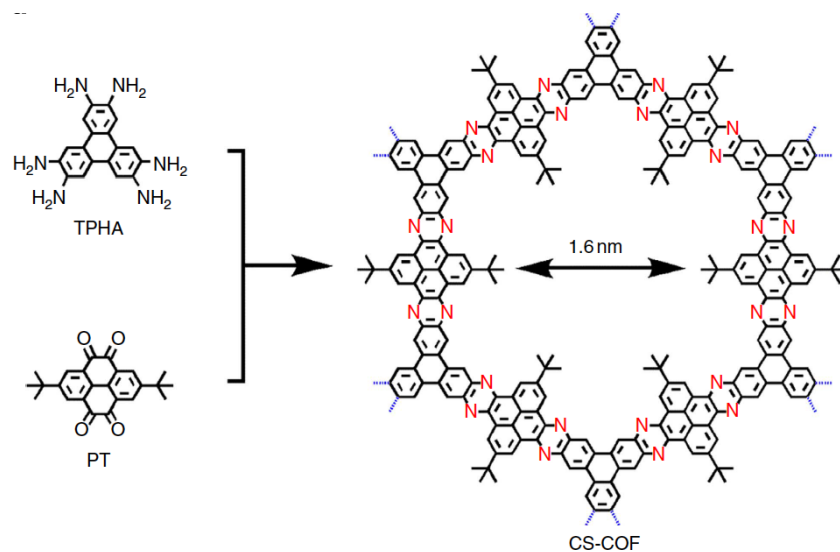


**Figure 18.** Synthesis of phenazine-based covalent organic frameworks, CS-COF.

Recently, our lab developed the first example of phenazine-linked COF, another derivative of the imine-based COF. The crystalline phenazine-linked CS-COF was synthesized by co-condensation of C3-symmetric building block triphenylene hexamine (TPHA) and C2-symmetric building block *tert*-butylpyrene tetraone (PT) *via*

solvothermal method (**Figure 18**).<sup>[77]</sup> The *tert*-butyl side groups in PT were employed for enhancing the solubility of monomer. However, the poor reversibility of the formation reaction (phenazine-ring) and the highly conjugated architectures lead to the CS-COF with a moderate crystallinity. This COF material has a pore size of 1.6 nm and a BET surface area of 776 m<sup>2</sup>/g. The unique crystalline structure permits inborn periodic ordering of conjugated chains in all three dimensions and exhibits a number of striking features: chemical stability, extended  $\pi$ -delocalization, ability to host guest molecules and hole mobility.

#### 1.2.4.2.4 Azine-based COFs

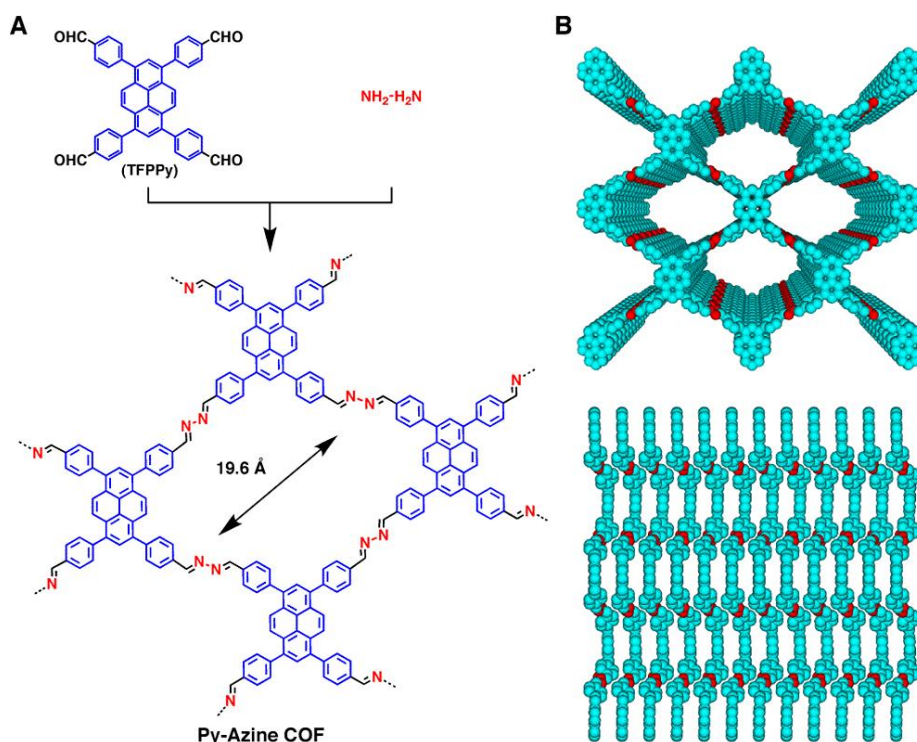


**Figure 19.** Synthesis and crystalline structure of the azine-linker COF, Py-Azine COF.

The third derivative of the imine-based covalent organic frameworks, azine-linked COF was firstly demonstrated by our lab. The Py-Azine COF was synthesized by co-condensation of hydrazine with 1,3,6,8-tetrakis(4-formylphenyl)pyrene (TFPPy) under solvothermal conditions (**Figure 19**).<sup>[78]</sup> Py-Azine COF demonstrated rhombic-shaped polygon sheets, which further stack in an AA-stacking mode to constitute periodically

ordered pyrene columns and one-dimensional microporous channels. The pore size of this azine COF is 1.9 nm with a BET surface area of 1210 m<sup>2</sup>/g. By virtue of the highly ordered pyrene column, such azine-linked frameworks are highly luminescent, meanwhile the azine units could serve as open docking sites for hydrogen-bonding interactions. These feature endows this COF material with high sensitivity and selectivity in chemosensing, for example, the selective detection of 2,4,6-trinitrophenol explosive.

#### 1.2.4.2.5 Triazine-based COFs

Other than the imine-derivate COFs, Thomas and co-workers exploited the ionothermal synthesis method to produce covalent triazine-based frameworks (CTFs) with crystallinity together with excellent chemical and thermal stabilities.<sup>[55-57]</sup> The cyclotrimerization of aromatic nitrile building blocks (e.g., 1,4-dicyanobenzene, as presented in **Figure 8**) in molten ZnCl<sub>2</sub> at 400 °C affords CTF materials. The molten ZnCl<sub>2</sub> salt plays important roles in the CTF synthesis, not only as the solvent but also as the catalyst for the reversible, CTFs demonstrated poor crystallinity since the reversible issue of the cyclotrimerization reactions. Further, the requirement of high reaction temperature narrows the scope of building blocks and limited their further applications.

### 1.3 Functions and Properties

Covalent organic frameworks have attracted intensive research interest, because of their high surface area, highly order crystalline structure together with tunable chemical and physical properties. As predesignable porous materials, COFs have been emerged as new candidates for gas adsorption and storage.<sup>[16-48]</sup> Meanwhile, because of their unique topology and stacking layer structures, 2D COFs possess highly ordered columnar arrays throughout their building blocks, which are difficult to achieve in traditional linear polymers, supramoleculars or porous materials. Under this notion, our lab has developed various  $\pi$ -electronic two-dimensional frameworks, which exhibited unique semiconducting, photo-conducting, and charge transfer properties.<sup>[4-14]</sup> On the

other hand, highly ordered skeletal alignment, high surface area together with open-channel structure of the 2D COFs provides an intriguing motif for exploring well-defined nanoreactors, thus, exhibit a high potential to develop high-performance heterogeneous catalysts.<sup>[15]</sup>

### 1.3.1 Gas Adsorption and Storage

COFs are composed of light elements linked by strong covalent bonds to form highly order porous structures, which regarded as ideal materials for gas storage. Utilize COF materials, adsorption and storage capabilities of gases, such as hydrogen,<sup>[16-47]</sup> methane,<sup>[21, 24, 46]</sup> carbon dioxide<sup>[21]</sup> and ammonia<sup>[48]</sup> have been investigated. Generally, the gas adsorption capacity of the COF material depends on the porosity, components and topologies of its frameworks. Benefit from the larger surface area and pore volume, 3D COFs exhibited significantly higher uptake capacities than 2D COFs.

#### 1.3.1.1 Hydrogen

Hydrogen storage has attracted tremendous public interest, because it represents as a future clean energy resource based on its high chemical abundance, high energy density, environmentally friendly characteristics and the ability to direct convert chemical energy into electric energy *via* the fuel cell technology. The DOE (Department of Energy, USA) target for hydrogen storage is set to 9 wt% and 81 kg H<sub>2</sub> m<sup>-3</sup> at 253-323 K with a pressure of 100 atm by the year 2015 (**Figure 20**). Only porous materials with very high specific-surface areas (> 3000 m<sup>2</sup> g<sup>-1</sup>) and optimized pore sizes in the range of 0.7 to 1.2 nm have the potential to meet the DOE 2015 target.

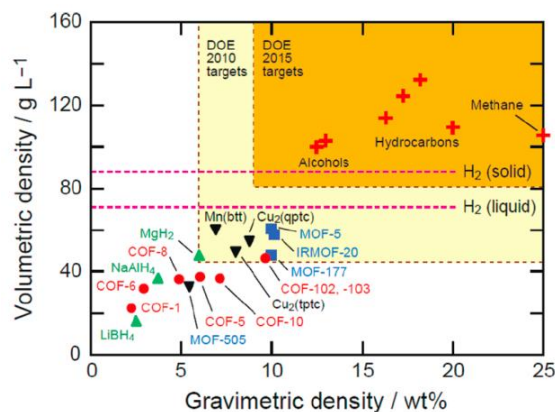


**Figure 20.** Hydrogen storage capacity of COFs and MOFs and DOE 2010/2015 target at 77 K.

Among COF materials, the highest hydrogen storage capacity is achieved by three dimensional boroxine-based COF, COF-102 (**Figure 21**,  $S_{\text{BET}}$ : 3620 m<sup>2</sup>/g, pore size: 1.2 nm),<sup>[21]</sup> which showed H<sub>2</sub> uptake of 72 mg/g under 1 bar and 77 K. This capacity is comparable to well-developed MOF systems: MOF-177 (75 mg/g,  $S_{\text{BET}}$ : 4500 m<sup>2</sup>/g), MOF-5 (76 mg/g,  $S_{\text{BET}}$ : 3800 m<sup>2</sup>/g), and the porous organic polymers PAF-1 (75 mg/g,  $S_{\text{BET}}$ : 5600 m<sup>2</sup>/g). Besides boroxine-based COFs, El-Kaderi and co-workers developed imine-based COF (IL COF-1) for high-pressure gas uptake application.<sup>[92]</sup> IL COF-1 possess a high argon capacity ( $S_{\text{BET}} = 2723$  m<sup>2</sup>/g) and a moderate hydrogen uptake, about 1.3 wt.% under 1bar and 77 K. This value was further enhanced to 4.7 wt.% at high pressure (40 bar, 77 K), which is higher than most of the porous materials with similar surface area. These capacities suggest high potential of COFs as hydrogen storage materials.

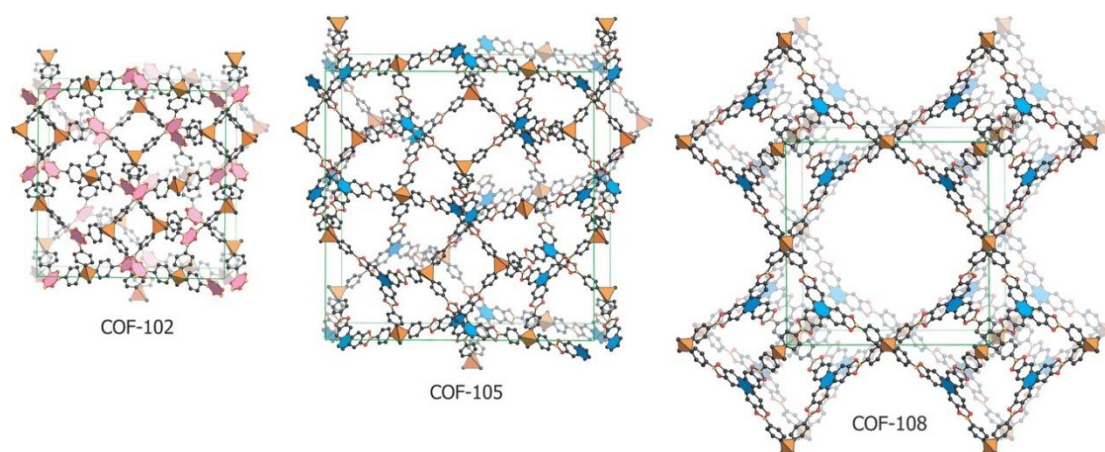


**Figure 21.** Schematic representation of three-dimensional covalent organic frameworks, COF-102, COF-105 and COF-108.

### 1.3.1.2 Methane

As the major component of natural gas, methane is abundant and inexpensive, compare with conventional fossil fuels. The target value for methane storage set by DOE is 180 cm<sup>3</sup> (STP) at 35 bar. In order to utilize methane on vehicles in a practical manner, effective and safe storage systems need to be developed.<sup>[93]</sup> Similar to the cases of hydrogen storage, the capacities of methane storage in 3D COFs are higher than

those of 2D COFs. The highest COF storage capacity was achieved by 3D COF-102 (**Figure 21**), which had a value of 187 mg/g. COF-103 also demonstrated a high capacity, about 175 mg/g. These results are comparable to the highest observed values in MOF systems (220 mg/g, MOF-210).<sup>[94]</sup> Besides boroxine-based COFs, El-Kaderi and co-workers developed imine-based COF (IL COF-1), which showed moderate methane uptake, about 0.9 wt.% under 1 bar and 273 K; meanwhile, under high pressure conditions, the absolute absorbed amount was estimated to be 129 L/L (92 g/L) at 35 bar and 298 K, which was comparable to COF-102 (136 L/L), but still lower than DOE 2015 target (180 L/L).<sup>[92]</sup>

### 1.3.1.3 Carbon Dioxide

Nowadays, carbon dioxide emitting from the combustion of fossil fuels has been thought to be a major contribution to the global warming. Therefore, how to efficiently capture and store carbon dioxide is an urgent issue and attracted broad interest. Among current techniques for CO<sub>2</sub> capture, porous materials approach is considered to be an energetically efficient and technically feasible way. Yaghi and co-workers have investigated series of COFs and reported that the CO<sub>2</sub> uptake of 3D COF-102 (**Figure 21**) reaches 27 mmol/g at 298 K and 35 bar,<sup>[21]</sup> which is higher than the uptake of MOF materials (MOF-5, 22 mmol/g)<sup>[95]</sup> and also zeolites (5-8 mmol/g).<sup>[96]</sup> El-Kaderi and co-workers reported the volumetric CO<sub>2</sub> adsorption capacity under 35 bar and 298 K for ILCOF-1 is about 587 g/L (299 L/L). Meanwhile, under 40 bar and 298K, the value was estimated to 29.3 mmol/g, which exceeds the capacity of COF-102.<sup>[92]</sup>

### 1.3.1.4 Ammonia

COFs have demonstrated high capacities for the adsorption of H<sub>2</sub>, CH<sub>4</sub>, and CO<sub>2</sub>, although these gas molecules just have weak physisorption interaction with the COF pore walls. Recently, Yaghi and co-workers demonstrated that boronate-ester based COF materials are useful for adsorbing ammonia<sup>[48]</sup> because the boron sites are Lewis acids and could coordinate with Lewis base guest molecular (**Figure 22**), such as ammonia<sup>[48]</sup> or pyridine.<sup>[97]</sup> Among the series of boronate-ester linked COFs, COF-10 emerged as one of the best materials for ammonia adsorption. It possesses an extremely

high ammonia uptake up to 15 mol/kg under 298 K and 1 bar condition. Although the chemisorption was utilized in this system and the boronate-ester based COFs are chemically unstable, such COF material can be cycled several times without significant deterioration in performance. This research represents a nice example of applying COF materials in functional applications and suggests that the molecularly designed COFs containing functional groups on their walls can be a practical means to develop new materials for the storage of specific gas.

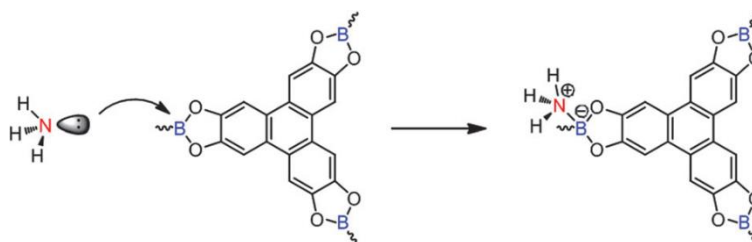


**Figure 22.** The proposed Lewis acid-Lewis base interaction upon the adsorption of ammonia on COF-10.

### 1.3.2 Photoelectric Applications

In 2D COFs, the building blocks for the vertices and edges are covalently linked to form extended 2D polygon sheets that stack to constitute layered frameworks, the out-of-plane  $\pi$  interactions are the primary driving force in the formation crystalline structure. Such unique crystalline structure induces a large electronic coupling between the  $\pi$ -orbitals of the stacking layers, which could facilitates the transport of charge carriers and excitons through pre-organized and built-in pathways (**Figure 23**). Notably, this stacking structure is inherent to 2D COFs, and the building blocks periodically align within the crystalline frameworks, which are difficult to achieve by traditional linear polymers, supramoleculars or porous materials. Under this notion, our lab has developed various  $\pi$ -electronic two-dimensional frameworks, which exhibit unique semiconducting, photo-conducting, and charge transfer properties.<sup>[4-14]</sup>

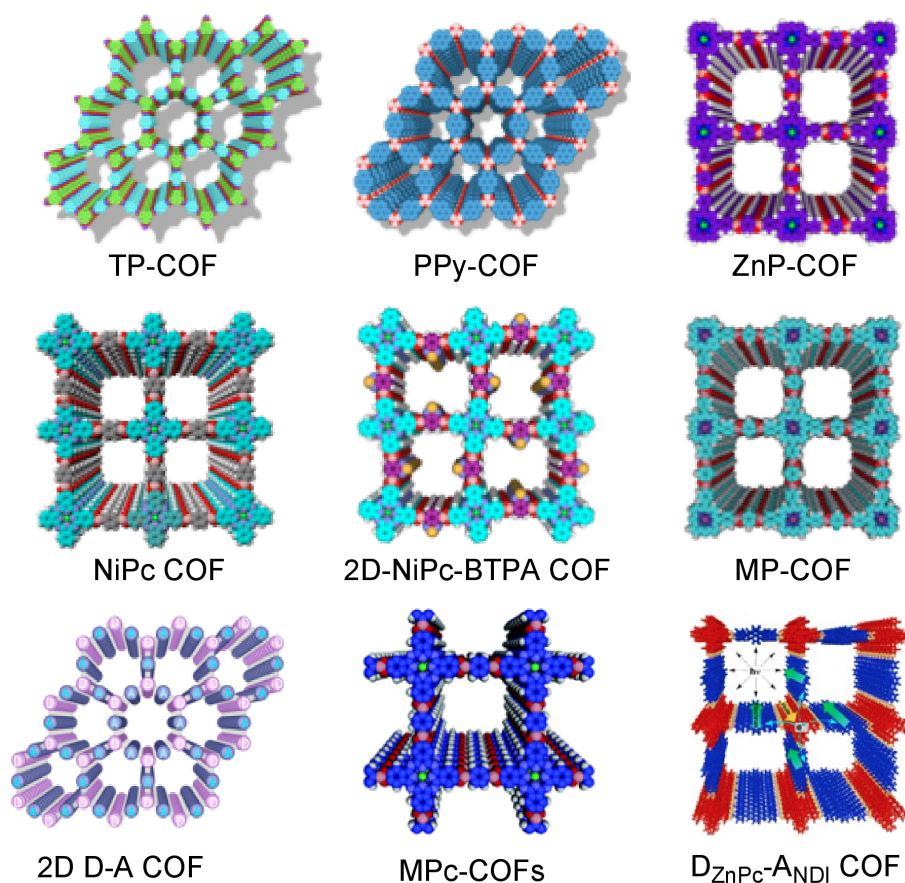


**Figure 23.** Schematic representation of the stacked crystalline structure of 2D COFs with pre-organized and built-in  $\pi$  columns.

### 1.3.2.1 Semiconduction

Our lab demonstrated the first semi-conductive covalent organic framework, TP-COF,<sup>[4]</sup> which is consisting of 2,3,6,7,10,11-hexahydroxytriphenylene (HHTTP) molecules at the vertices and pyrene-2,7-diboronic acid (PDBA) groups at the edges (**Figure 23**). Upon excitation of the pyrene building blocks, TP-COF emitted a strong blue luminescence. Interestingly, the excitation of triphenylene moieties also leads to a blue emission from only the pyrene units. This result indicates that the excitation energy of triphenylene was not localized but could transfer to the pyrene units through large electronic coupling between the  $\pi$ -orbitals. As a result, TP-COF demonstrates a wide range of photons from the ultraviolet to visible regions, and convert them into a brilliant blue luminescence.

Based on this pioneering work, several metallophthalocyanine based  $\pi$ -electronic COFs for semi-conductive application have been successfully developed by our lab<sup>[6, 8, 71]</sup> and Dichtel et al.<sup>[70, 88]</sup> Because of abundant  $\pi$ -electronic, photochemical, and redox properties of phthalocyanine building blockings, the 2D NiPc-COF<sup>[6]</sup> (**Figure 23**) displays hole mobility up to  $1.3 \text{ cm}^2/\text{V s}$ , whereas the 2D-NiPc-BTDA COF<sup>[71]</sup> (**Figure 23**) demonstrates *n*-type semi-conductive with the electron mobility as high as  $0.6 \text{ cm}^2/\text{V s}$ . Further, the effect of metal ions (such as Cu, Zn, and Co) in the phthalocyanine building blocks on the performance of carrier mobility was systematic studied, which suggests that central metal species have significant affect to carrier transport.<sup>[8]</sup>

### 1.3.2.2 Photoconduction

The exploration of photo-functional materials has attracted tremendous interests since its importance for the developing of artificial photo-synthesis, light-energy conversion, and optoelectronics. The molecular ordering of the  $\pi$ -electronic components plays a vital role in determining the performance of these devices. The highly ordered stacking structure and periodic alignment of the  $\pi$  columns endow COFs with a high potential in photoconductivity.<sup>[4-6, 8-9, 71]</sup>

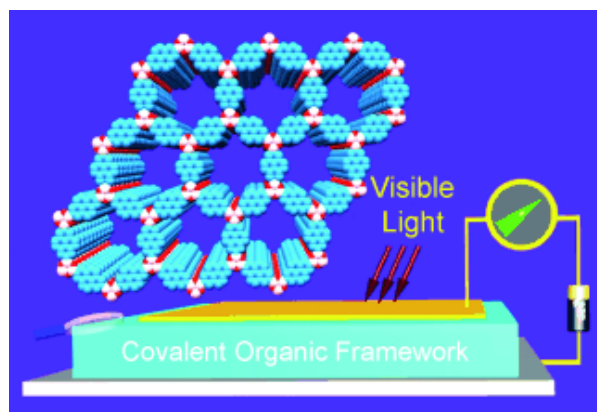


**Figure 24.** Schematic representation of photoconductive COFs covalent organic framework, PPy-COF.

Our lab demonstrated the first example of a photoconductive covalent organic framework, PPy-COF which is prepared *via* the self-condensation of pyrene-2,7-diboronic acid (PDBA) to form the boroxine-based COF (**Figure 23**).<sup>[5]</sup> The micro-

crystal of PPy-COF exhibited highly blue luminescent because of the formation of excimer in the stacked pyrenes. Photoconductivity observed in devices consisting of the COF powder sandwiched between Au and Al electrodes (**Figure 24**) suggested long-range exciton delocalization through the stacked pyrene moieties.<sup>[4]</sup> Unlike previously introduced semi-conductive TP-COF, which contains two components (HTTP and PDBA) with different energy gaps; excitons in the single-component PPy-COF can flow not only over the sheet but also across the stacking layers. Thus, PPy-COF could generate a prominent photocurrent with a quick response to light irradiation.

Based on this work, our lab developed a series of porphyrin and phthalocyanine based photoconductive COFs, which exhibits broad absorbance from the ultraviolet to near infrared region. On irradiation with a xenon light source (>400 nm), NiPc COF (**Figure 23**) displayed significant increased current from 20 nA (dark current) to 3  $\mu$ A (photocurrent) with an on-off ratio of 100 Hz.<sup>[6]</sup> Benefit from the broad absorbance of the phthalocyanine building block, NiPc-COF is panchromatic and responds to photos with various wavelengths. Metalloporphyrin COFs are panchromatically photoconductive, however, their photoconductivity is highly rely on the metal ions in the porphyrin species. ZnP-COF shows an on-off ratio of  $5 \times 10^4$  Hz, which is 150 and 10000 fold higher than H<sub>2</sub>P-COF and CuP-COF. These results gave insights into the conducting nature and its remarkable effect on photoconductivity, which could provide guidance for the photoconductive application of the 2D COFs.<sup>[9]</sup>

### 1.3.2.3 Charge Separation

Charge separation in COFs has been studied for COFs in which the donor and acceptor are both incorporated into the framework (D<sub>ZnPc</sub>-A<sub>NDI</sub>-COF)<sup>[11]</sup>, and also for non-covalent post-synthetic functionalization using a soluble fullerene derivative acceptor (TT-COF:PCBM).<sup>[98]</sup> In these works, ultra-fast charge transfer on the timescale of picoseconds occurred from the electron donors to acceptors. Charge-separated states with long-lived lifetimes of 1.5  $\mu$ s at 280 K and 1500  $\mu$ s at 80 K, respectively, were observed in the D<sub>ZnPc</sub>-A<sub>NDI</sub>-COF system.<sup>[11]</sup> By loading PCBM into

the pores of TT-COF, the first COF-based photovoltaic device was obtained, with an photoconversion efficiency of 0.053%.<sup>[98]</sup>

These studies suggest that the highly ordered structural features of 2D COFs are beneficial the transport of charge carriers and excitons. Such unique feature endows the 2D COF with a strong potential in developing high performance semiconducting, photoconducting, and charge transfer materials.

### 1.3.3 Heterogeneous Catalysis

Utilization of porous materials with large surface areas for heterogeneous catalysis has been acknowledged for several decades. For example, porous zeolites have been widely studied and used as heterogeneous catalysts in refining and petrochemical industries.<sup>[58]</sup> Porous organic polymers (POPs) have also considered to be new candidates for efficient heterogeneous catalysts.<sup>[99-101]</sup> Recently, the porous crystalline analogue, MOFs has been employed for heterogeneous catalysis and showed exciting performance.<sup>[102-104]</sup> Under this notion, COF materials especially the 2D COFs possess highly ordered skeletal alignment, high surface area together with open-channel structure which could serve as efficient mass transport pathways, provides an intriguing motif for exploring well-defined nano-reactors, thus, exhibit a high potential to develop high-performance heterogeneous catalysts. On the other hand, to meet the requirements of heterogeneous catalysts, the COF materials should incorporate robust catalytic sites and possess high stability to thermal treatments, water, and most of the organic solvents. Furthermore, to guarantee high catalytic performance, the accessibility to the catalytic sites and efficient mass transport inside COF catalyst should also be satisfied.

Wang and co-workers demonstrated the first example of COF-based heterogeneous catalyst; the imine-based COF-LZU1<sup>[15]</sup> can load Pd ions into its pores *via* the coordination reaction between nitrogen atoms in the COFs (**Figure 25**). Interestingly, the Pd loaded COF materials are catalytically active and accessible to both the substrates and the reactants, forming a heterogeneous catalytic system. The synthesized COF catalyst, Pd/COF-LZU1 could catalyze the Suzuki-Miyaura coupling

reaction and exhibits good activity. Such COF catalyst is effective for different reactants, produced excellent yields, and could be reused for many cycles.

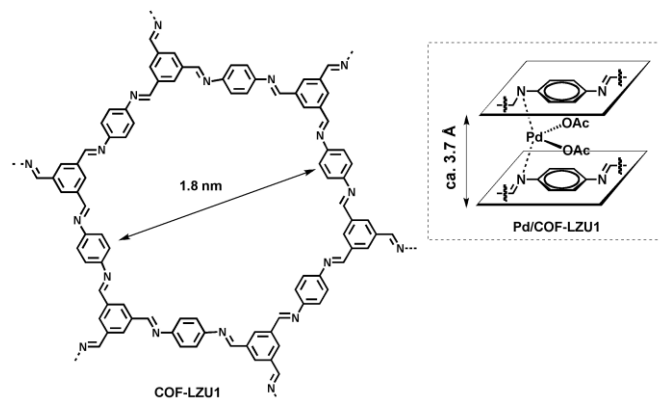


**Figure 25.** Chemical structure of COF-LZU1 and the COF-based catalyst, Pd/COF-LZU1.

To date, this is the only example of utilizing the COF materials for heterogeneous catalyst, although COFs have attracted tremendous interests and possess high potential in this field. Because currently, there is no effective method to introduce the catalytic active sites into the crystalline frameworks and the stability issue of the COF materials thus far developed hard to meet the requirement of catalyst carriers. These two challenges largely limited its applications and thus, precluded any practical implementations.

## 1.4 Scope of This Thesis

In 2D COFs, the building blocks for the vertices and edges are covalently linked to form extended 2D polygon sheets that stack to constitute layered frameworks. This covalently linked and topologically crystallized 2D architecture merges two structural characters, i.e., periodic  $\pi$  arrays and ordered one-dimensional channels. The 2D COFs offer a unique platform for constructing periodic columnar  $\pi$  arrays of arenes, porphyrins, phthalocyanines, and thiophenes, which exhibit remarkable light-emitting, semiconducting, photoconductive, charge-transferring, and charge-separating

properties. In addition, 2D COFs provide ordered one-dimensional (1D) channels whose size and shape can be tailored for gas adsorption and guest encapsulations.

If catalytic active sites can be successfully integrated into the frameworks, the highly ordered skeletal alignment and open-channel structure of 2D COFs provide an intriguing motif for exploring well-defined nanoreactors. Two strategies can be used for constructing catalytic COFs. Incorporating building blocks that possess catalytic sites constitute the direct method. However, this technique requires a tedious solvothermal synthesis. Particularly, if the catalytic site is bulky, forming a crystalline porous COF structure becomes difficult. Another methodology for constructing catalytic COFs involves the post-synthetic integration of catalytic sites into a crystalline COF skeleton. This approach can reduce the influence of the bulky catalytic sites on the COF scaffold crystallinity and the undesired effect of harsh solvothermal conditions on the catalytic sites. The construction of a covalently linked, yet highly active catalyst remains a synthetic challenge in the field.

Homogenous organocatalysts remain problematic with respect to their practical application because of the difficulty of separating expensive catalysts for repeated use. The development of immobilized, easily recoverable, and reusable catalysts appears to be one of the most promising strategies for overcoming these problems. Most heterogeneous organocatalysts are based on linear polymer supporters; however, such polymers exhibit low activity as a result of inefficient access to catalytic sites. To overcome this issue, metal-organic framework (MOF)-based organocatalysts have been developed. However, the MOF-based organocatalysts are problematic in terms of pore size, enantioselectivity, and the stability issue of the coordination bonds. High performance, including recyclability, is crucial for the practical application of catalysts; however, satisfactory results have thus far rarely been reported for open framework catalysts, even among reported COFs and MOFs; the combination of stability, crystallinity, and porosity of open frameworks remains a major issue to be solved before practical functional explorations can be undertaken.

This thesis consists of the design and synthesis of chiral covalent organic frameworks and demonstrated their functions as unique platform for designing high-performance heterogeneous asymmetric organocatalysts. In Chapter 2, I developed a pore surface engineering strategy for the controlled functionalization of imine-linked COFs using a three-component condensation system in conjunction with click chemistry. Engineering pyrrolidine units onto the pore walls creates COF based heterogeneous organocatalysts, which showed significantly improved activity because of the ordered nano-channel structure and the high surface area. In Chapter 3, I will introduce a novel mesoporous imine COF which combines high crystallinity, porosity and excellent stabilities. This discovery makes a breakthrough in the field of crystalline frameworks, providing an efficient solution to the contradiction of high performance with high stability. In Chapter 4, I combined the pore surface engineering strategy with the highly crystallized mesoporous imine COF to create a high-performance heterogeneous asymmetric organocatalyst. The mesoporous nature together with highly ordered 1D nano-channels and extremely high surface area endow this crystalline catalyst a number of striking features, including enhanced activity, high enantioselectivity, excellent stability and cycle performance and environmental benignity; these advantages offer a plausible solution to long-standing challenges for real application of organocatalysts.

In this thesis, structural calculations that were carried out by co-workers have been listed: Prof. Stephan Irle, Dr Matt Addicoat of Nagoya University carried out structural optimization using DFTB methods; Mr. Jia Gao in our group contributed to PXRD pattern simulation.

## 1.5 References

- [1] Eddaoudi, M.; Moler, D. B.; Li, H.; Chen, B.; Reineke, T. M.; O'Keeffe, M.; Yaghi, O. M., *Acc. Chem. Res.* **2001**, *34*, 319-330.
- [2] Yaghi, O. M.; Li, H.; Eddaoudi, M.; O'Keeffe, M., *Nature* **1999**, *402*, 276-279.
- [3] Cote, A. P.; Benin, A. I.; Ockwig, N. W.; O'Keeffe, M.; Matzger, A. J.; Yaghi, O. M., *Science* **2005**, *310*, 1166-1170.
- [4] Wan, S.; Guo, J.; Kim, J.; Ihee, H.; Jiang, D., *Angew. Chem. Int. Ed.* **2008**, *47*, 8826-8830.
- [5] Wan, S.; Guo, J.; Kim, J.; Ihee, H.; Jiang, D., *Angew. Chem. Int. Ed.* **2009**, *48*, 5439-5442.
- [6] Ding, X.; Guo, J.; Feng, X.; Honsho, Y.; Guo, J.; Seki, S.; Maitarad, P.; Saeki, A.; Nagase, S.; Jiang, D., *Angew. Chem. Int. Ed.* **2011**, *50*, 1289-1293.
- [7] Feng, X.; Chen, L.; Dong, Y.; Jiang, D., *Chem. Commun.* **2011**, *47*, 1979-1981.
- [8] Ding, X.; Feng, X.; Saeki, A.; Seki, S.; Nagai, A.; Jiang, D., *Chem. Commun.* **2012**, *48*, 8952-8954.
- [9] Feng, X.; Liu, L.; Honsho, Y.; Saeki, A.; Seki, S.; Irle, S.; Dong, Y.; Nagai, A.; Jiang, D., *Angew. Chem. Int. Ed.* **2012**, *51*, 2618-2622.
- [10] Feng, X.; Dong, Y.; Jiang, D., *CrystEngComm* **2013**, *15*, 1508.
- [11] Jin, S.; Ding, X.; Feng, X.; Supur, M.; Furukawa, K.; Takahashi, S.; Addicoat, M.; El-Khouly, M. E.; Nakamura, T.; Irle, S.; Fukuzumi, S.; Nagai, A.; Jiang, D., *Angew. Chem. Int. Ed.* **2013**, *52*, 2017-2021.
- [12] Jin, S.; Furukawa, K.; Addicoat, M.; Chen, L.; Takahashi, S.; Irle, S.; Nakamura, T.; Jiang, D., *Chem. Sci.* **2013**, *4*, 4505.
- [13] Chen, L.; Furukawa, K.; Gao, J.; Nagai, A.; Nakamura, T.; Dong, Y.; Jiang, D., *J. Am. Chem. Soc.* **2014**, *136*, 9806-9809.
- [14] Jin, S.; Sakurai, T.; Kowalczyk, T.; Dalapati, S.; Xu, F.; Wei, H.; Chen, X.; Gao, J.; Seki, S.; Irle, S.; Jiang, D., *Chem. Eur. J.* **2014**, *20*, 14608-14613.
- [15] Ding, S. Y.; Gao, J.; Wang, Q.; Zhang, Y.; Song, W. G.; Su, C. Y.; Wang, W., *J. Am. Chem. Soc.* **2011**, *133*, 19816-19822.
- [16] Assfour, B.; Seifert, G., *Microporous Mesoporous Mater.* **2010**, *133*, 59-65.
- [17] Assfour, B.; Seifert, G., *Chem. Phys. Lett.* **2010**, *489*, 86-91.
- [18] Cao, D.; Lan, J.; Wang, W.; Smit, B., *Angew. Chem. Int. Ed.* **2009**, *48*, 4730-4733.
- [19] Choi, Y. J.; Lee, J. W.; Choi, J. H.; Kang, J. K., *Appl. Phys. Lett.* **2008**, *92*, 173102.
- [20] Das, G.; Balaji Shinde, D.; Kandambeth, S.; Biswal, B. P.; Banerjee, R., *Chem. Commun.* **2014**, *50*, 12615-12618.

- [21] Furukawa, H.; Yaghi, O. M., *J. Am. Chem. Soc.* **2009**, 131, 8875-8883.
- [22] Ganz, E.; Dornfeld, M., *J. Phys. Chem. C* **2012**, 116, 3661-3666.
- [23] Gao, T.-F.; Zhang, H., *Struct. Chem.* **2013**, 25, 503-513.
- [24] Garberoglio, G.; Vallauri, R., *Microporous Mesoporous Mater.* **2008**, 116, 540-547.
- [25] Guo, J. H.; Zhang, H.; Miyamoto, Y., *Phys. Chem. Chem. Phys.* **2013**, 15, 8199-8207.
- [26] Guo, J. H.; Zhang, H.; Tang, Y.; Cheng, X., *Phys. Chem. Chem. Phys.* **2013**, 15, 2873-2881.
- [27] Guo, J.-H.; Zhang, H.; Gong, M.; Cheng, X.-L., *Struct. Chem.* **2012**, 24, 691-703.
- [28] Guo, J.-H.; Zhang, H.; Liu, Z.-P.; Cheng, X.-L., *J. Phys. Chem. C* **2012**, 116, 15908-15917.
- [29] Han, S. S.; Furukawa, H.; Yaghi, O. M.; Goddard, W. A., 3rd, *J. Am. Chem. Soc.* **2008**, 130, 11580-11581.
- [30] Han, S. S.; Mendoza-Cortes, J. L.; Goddard, W. A., 3rd, *Chem. Soc. Rev.* **2009**, 38, 1460-1476.
- [31] Kalidindi, S. B.; Fischer, R. A., *Phys. Status Solidi* **2013**, 250, 1119-1127.
- [32] Kalidindi, S. B.; Oh, H.; Hirscher, M.; Esken, D.; Wiktor, C.; Turner, S.; Van Tendeloo, G.; Fischer, R. A., *Chem. Eur. J.* **2012**, 18, 10848-10856.
- [33] Kandambeth, S.; Shinde, D. B.; Panda, M. K.; Lukose, B.; Heine, T.; Banerjee, R., *Angew. Chem. Int. Ed.* **2013**, 52, 13052-13056.
- [34] Kim, D.; Jung, D. H.; Kim, K.-H.; Guk, H.; Han, S. S.; Choi, K.; Choi, S.-H., *J. Phys. Chem. C* **2012**, 116, 1479-1484.
- [35] Klontzas, E.; Tylianakis, E.; Froudakis, G. E., *J. Phys. Chem. C* **2008**, 112, 9095-9098.
- [36] Koenig, A. R. V.; Desgranges, C.; Delhommelle, J., *Mol. Simul.* **2013**, 40, 71-79.
- [37] Li, F.; Zhao, J.; Johansson, B.; Sun, L., *Int. J. Hydrogen Energy* **2010**, 35, 266-271.
- [38] Li, L.-L.; Gao, T.-F.; Zhang, R.-Y.; Zhang, H., *Chin. Phys. Lett.* **2014**, 31, 097101.
- [39] Li, X.-D.; Guo, J.-H.; Zhang, H.; Cheng, X.-L.; Liu, X.-Y., *R. Soc. Chem. Adv.* **2014**, 4, 24526.
- [40] Li, X.-D.; Zang, H.-P.; Wang, J.-T.; Wang, J.-F.; Zhang, H., *J. Mater. Chem. A* **2014**, 2, 18554-18561.
- [41] Makhseed, S.; Samuel, J., *Chem. Commun.* **2008**, 4342-4344.
- [42] Oh, H.; Kalidindi, S. B.; Um, Y.; Bureekaew, S.; Schmid, R.; Fischer, R. A.; Hirscher, M., *Angew. Chem. Int. Ed.* **2013**, 52, 13219-13222.

- [43] Stegbauer, L.; Schwinghammer, K.; Lotsch, B. V., *Chem. Sci.* **2014**, *5*, 2789.
- [44] Thote, J.; Aiyappa, H. B.; Deshpande, A.; Diaz Diaz, D.; Kurungot, S.; Banerjee, R., *Chem. Eur. J.* **2014**, *20*, 15961-15965.
- [45] Tylianakis, E.; Klontzas, E.; Froudakis, G. E., *Nanoscale* **2011**, *3*, 856-869.
- [46] Yang, Z.; Cao, D., *J. Phys. Chem. C* **2012**, *116*, 12591-12598.
- [47] Zou, X.; Zhou, G.; Duan, W.; Choi, K.; Ihm, J., *J. Phys. Chem. C* **2010**, *114*, 13402-13407.
- [48] Doonan, C. J.; Tranchemontagne, D. J.; Glover, T. G.; Hunt, J. R.; Yaghi, O. M., *Nature Chem.* **2010**, *2*, 235-238.
- [49] Rowan, S. J.; Cantrill, S. J.; Cousins, G. R.; Sanders, J. K.; Stoddart, J. F., *Angew. Chem. Int. Ed.* **2002**, *41*, 898-952.
- [50] Belowich, M. E.; Stoddart, J. F., *Chem. Soc. Rev.* **2012**, *41*, 2003-2024.
- [51] Lanni, L. M.; Tilford, R. W.; Bharathy, M.; Lavigne, J. J., *J. Am. Chem. Soc.* **2011**, *133*, 13975-13983.
- [52] Uribe-Romo, F. J.; Hunt, J. R.; Furukawa, H.; Klock, C.; O'Keeffe, M.; Yaghi, O. M., *J. Am. Chem. Soc.* **2009**, *131*, 4570-4571.
- [53] Wan, S.; Gándara, F.; Asano, A.; Furukawa, H.; Saeki, A.; Dey, S. K.; Liao, L.; Ambrogio, M. W.; Botros, Y. Y.; Duan, X.; Seki, S.; Stoddart, J. F.; Yaghi, O. M., *Chem. Mater.* **2011**, *23*, 4094-4097.
- [54] Uribe-Romo, F. J.; Doonan, C. J.; Furukawa, H.; Oisaki, K.; Yaghi, O. M., *J. Am. Chem. Soc.* **2011**, *133*, 11478-11481.
- [55] Kuhn, P.; Antonietti, M.; Thomas, A., *Angew. Chem. Int. Ed.* **2008**, *47*, 3450-3453.
- [56] Bojdys, M. J.; Jeromenok, J.; Thomas, A.; Antonietti, M., *Adv. Mater.* **2010**, *22*, 2202-2205.
- [57] Zhang, W.; Liang, F.; Li, C.; Qiu, L. G.; Yuan, Y. P.; Peng, F. M.; Jiang, X.; Xie, A. J.; Shen, Y. H.; Zhu, J. F., *J. Hazard. Mater.* **2011**, *186*, 984-990.
- [58] Corma, A., *Chem. Rev.* **1997**, *97*, 2373-2420.
- [59] Davis, M. E., *Nature* **2002**, *417*, 813-821.
- [60] Hoffmann, F.; Cornelius, M.; Morell, J.; Froba, M., *Angew. Chem. Int. Ed.* **2006**, *45*, 3216-3251.
- [61] McKeown, N. B.; Budd, P. M., *Chem. Soc. Rev.* **2006**, *35*, 675-683.
- [62] Jiang, J. X.; Su, F.; Trewin, A.; Wood, C. D.; Campbell, N. L.; Niu, H.; Dickinson, C.; Ganin, A. Y.; Rosseinsky, M. J.; Khimiyak, Y. Z.; Cooper, A. I., *Angew. Chem. Int. Ed.* **2007**, *46*, 8574-8578.
- [63] Ben, T.; Ren, H.; Ma, S.; Cao, D.; Lan, J.; Jing, X.; Wang, W.; Xu, J.; Deng, F.; Simmons, J. M.; Qiu, S.; Zhu, G., *Angew. Chem. Int. Ed.* **2009**, *48*, 9457-9460.
- [64] Cooper, A. I., *Adv. Mater.* **2009**, *21*, 1291-1295.

- [65] El-Kaderi, H. M.; Hunt, J. R.; Mendoza-Cortes, J. L.; Cote, A. P.; Taylor, R. E.; O'Keeffe, M.; Yaghi, O. M., *Science* **2007**, 316, 268-272.
- [66] Tilford, R. W.; Gemmill, W. R.; zur Loye, H. C.; Lavigne, J. J., *Chem. Mater.* **2006**, 18, 5296-5301.
- [67] Cote, A. P.; El-Kaderi, H. M.; Furukawa, H.; Hunt, J. R.; Yaghi, O. M., *J. Am. Chem. Soc.* **2007**, 129, 12914-12915.
- [68] Hunt, J. R.; Doonan, C. J.; LeVangie, J. D.; Cote, A. P.; Yaghi, O. M., *J. Am. Chem. Soc.* **2008**, 130, 11872-11873.
- [69] Tilford, R. W.; Mugavero, S. J., 3rd; Pellechia, P. J.; Lavigne, J. J., *Adv. Mater.* **2008**, 20, 2741-2746.
- [70] Spitler, E. L.; Dichtel, W. R., *Nature Chem.* **2010**, 2, 672-677.
- [71] Ding, X.; Chen, L.; Honsho, Y.; Feng, X.; Saengsawang, O.; Guo, J.; Saeki, A.; Seki, S.; Irle, S.; Nagase, S.; Parasuk, V.; Jiang, D., *J. Am. Chem. Soc.* **2011**, 133, 14510-14513.
- [72] Dogru, M.; Sonnauer, A.; Gavryushin, A.; Knochel, P.; Bein, T., *Chem. Commun.* **2011**, 47, 1707-1709.
- [73] Nagai, A.; Guo, Z.; Feng, X.; Jin, S.; Chen, X.; Ding, X.; Jiang, D., *Nature Commun.* **2011**, 2, 536.
- [74] Spitler, E. L.; Koo, B. T.; Novotney, J. L.; Colson, J. W.; Uribe-Romo, F. J.; Gutierrez, G. D.; Clancy, P.; Dichtel, W. R., *J. Am. Chem. Soc.* **2011**, 133, 19416-19421.
- [75] Bunck, D. N.; Dichtel, W. R., *Angew. Chem. Int. Ed.* **2012**, 51, 1885-1889.
- [76] Bunck, D. N.; Dichtel, W. R., *J. Am. Chem. Soc.* **2013**, 135, 14952-14955.
- [77] Guo, J.; Xu, Y.; Jin, S.; Chen, L.; Kaji, T.; Honsho, Y.; Addicoat, M. A.; Kim, J.; Saeki, A.; Ihee, H.; Seki, S.; Irle, S.; Hiramoto, M.; Gao, J.; Jiang, D., *Nature Commun.* **2013**, 4, 2736.
- [78] Dalapati, S.; Jin, S.; Gao, J.; Xu, Y.; Nagai, A.; Jiang, D., *J. Am. Chem. Soc.* **2013**, 135, 17310-17313.
- [79] Spitler, E. L.; Giovino, M. R.; White, S. L.; Dichtel, W. R., *Chem. Sci.* **2011**, 2, 1588.
- [80] Kappe, C. O., *Angew. Chem. Int. Ed.* **2004**, 43, 6250-6284.
- [81] Ni, Z.; Masel, R. I., *J. Am. Chem. Soc.* **2006**, 128, 12394-12395.
- [82] Jhung, S. H.; Lee, J. H.; Yoon, J. W.; Serre, C.; Ferey, G.; Chang, J. S., *Adv. Mater.* **2007**, 19, 121-+.
- [83] Campbell, N. L.; Clowes, R.; Ritchie, L. K.; Cooper, A. I., *Chem. Mater.* **2009**, 21, 204-206.
- [84] Biswal, B. P.; Chandra, S.; Kandambeth, S.; Lukose, B.; Heine, T.; Banerjee, R., *J. Am. Chem. Soc.* **2013**, 135, 5328-5331.

- [85] Zwaneveld, N. A.; Pawlak, R.; Abel, M.; Catalin, D.; Gimes, D.; Bertin, D.; Porte, L., *J. Am. Chem. Soc.* **2008**, 130, 6678-6679.
- [86] Guan, C. Z.; Wang, D.; Wan, L. J., *Chem. Commun.* **2012**, 48, 2943-2945.
- [87] Colson, J. W.; Woll, A. R.; Mukherjee, A.; Levendorf, M. P.; Spitler, E. L.; Shields, V. B.; Spencer, M. G.; Park, J.; Dichtel, W. R., *Science* **2011**, 332, 228-231.
- [88] Spitler, E. L.; Colson, J. W.; Uribe-Romo, F. J.; Woll, A. R.; Giovino, M. R.; Saldivar, A.; Dichtel, W. R., *Angew. Chem. Int. Ed.* **2012**, 51, 2623-2627.
- [89] Li, Y. W.; Yang, R. T., *AIChE J.* **2008**, 54, 269-279.
- [90] Chen, X.; Addicoat, M.; Irle, S.; Nagai, A.; Jiang, D., *J. Am. Chem. Soc.* **2013**, 135, 546-549.
- [91] Chen, X.; Huang, N.; Gao, J.; Xu, H.; Xu, F.; Jiang, D., *Chem. Commun.* **2014**, 50, 6161-6163.
- [92] Rabbani, M. G.; Sekizkardes, A. K.; Kahveci, Z.; Reich, T. E.; Ding, R.; El-Kaderi, H. M., *Chem. Eur. J.* **2013**, 19, 3324-3328.
- [93] Wu, H.; Gong, Q.; Olson, D. H.; Li, J., *Chem. Rev.* **2012**, 112, 836-868.
- [94] Furukawa, H.; Ko, N.; Go, Y. B.; Aratani, N.; Choi, S. B.; Choi, E.; Yazaydin, A. O.; Snurr, R. Q.; O'Keeffe, M.; Kim, J.; Yaghi, O. M., *Science* **2010**, 329, 424-428.
- [95] Millward, A. R.; Yaghi, O. M., *J. Am. Chem. Soc.* **2005**, 127, 17998-17999.
- [96] Cavenati, S.; Grande, C. A.; Rodrigues, A. E., *J. Chem. Eng. Data* **2004**, 49, 1095-1101.
- [97] Du, Y.; Mao, K.; Kamakoti, P.; Ravikovitch, P.; Paur, C.; Cundy, S.; Li, Q.; Calabro, D., *Chem. Commun.* **2012**, 48, 4606-4608.
- [98] Dogru, M.; Handloser, M.; Auras, F.; Kunz, T.; Medina, D.; Hartschuh, A.; Knochel, P.; Bein, T., *Angew. Chem. Int. Ed.* **2013**, 52, 2920-2924.
- [99] Kaur, P.; Hupp, J. T.; Nguyen, S. T., *Acs Catalysis* **2011**, 1, 819-835.
- [100] Zhang, Y.; Riduan, S. N., *Chem. Soc. Rev.* **2012**, 41, 2083-2094.
- [101] Chen, L.; Yang, Y.; Jiang, D., *J. Am. Chem. Soc.* **2010**, 132, 9138-9143.
- [102] Banerjee, M.; Das, S.; Yoon, M.; Choi, H. J.; Hyun, M. H.; Park, S. M.; Seo, G.; Kim, K., *J. Am. Chem. Soc.* **2009**, 131, 7524-7525.
- [103] Dang, D.; Wu, P.; He, C.; Xie, Z.; Duan, C., *J. Am. Chem. Soc.* **2010**, 132, 14321-14323.
- [104] Lun, D. J.; Waterhouse, G. I.; Telfer, S. G., *J. Am. Chem. Soc.* **2011**, 133, 5806-5809.

**Chapter 2.**  
**Catalytic Covalent Organic Frameworks**  
***via* Pore Surface Engineering**

*Chem. Commun.*, 2014, **50**, 1292-1294

Hong Xu, Xiong Chen, Jia Gao, Jianbin Lin, Matthew Addicoat,  
Stephan Irleb and Donglin Jiang

## **Abstract**

A synthetic strategy for the pore surface engineering of imine-linked covalent organic frameworks to predesign pore functions by using click chemistry was demonstrated. This method enables the precise tune of pore wall surfaces with desired functional groups and controlled densities. The integration of organocatalytic sites onto the pore walls creates robust organocatalytic frameworks with significantly enhanced activity and retained stereoselectivity in aqueous solution. The COF catalyst combines a number of striking features, including broad applicability, good recyclability, and high capability to perform quantitative transformation under continuous columnar flow.

## 2.1 Introduction

Covalent organic frameworks (COFs) are a class of crystalline porous polymers that enable the atomically precise integration of building blocks into two- or three-dimensional (2D or 3D, respectively) periodicities.<sup>[1]</sup> In 2D COFs, the building blocks for the vertices and edges are covalently linked to form extended 2D polygon sheets that stack to constitute layered frameworks. This covalently linked and topologically crystallized 2D architecture merges two structural characters, i.e., periodic  $\pi$  arrays and ordered one-dimensional channels. The 2D COFs offer a unique platform for constructing periodic columnar  $\pi$  arrays of arenes, porphyrins, phthalocyanines, and thiophenes, which exhibit remarkable light-emitting, semiconducting, photoconductive, charge-transferring, and charge-separating properties.<sup>[2-12]</sup> In addition, 2D COFs provide ordered one-dimensional (1D) channels whose size and shape can be tailored for gas adsorption and guest encapsulations.<sup>[13-45]</sup>

If catalytic sites can be successfully integrated into the frameworks, the highly ordered skeletal alignment and open-channel structure of 2D COFs provide an intriguing motif for exploring well-defined nanoreactors. Two strategies can be used for constructing catalytic COFs. Incorporating building blocks that possess catalytic sites constitute the direct method. However, this technique requires a tedious solvothermal synthesis. Particularly, if the catalytic site is bulky, forming a crystalline porous COF structure becomes difficult. Another methodology for constructing catalytic COFs involves the post-synthetic integration of catalytic sites into a crystalline COF skeleton. This approach can reduce the influence of the bulky catalytic sites on the COF scaffold crystallinity and the undesired effect of harsh solvothermal conditions on the catalytic sites. Using an imine-linked COF as a scaffold, Wang and colleagues reported the use of Pd-imine coordination to prepare a Pd-loaded COF that efficiently catalyzes the Suzuki cross-coupling reaction.<sup>[46]</sup> The construction of a

covalently linked, yet highly active catalyst remains a synthetic challenge in the field.

Our lab have reported a pore surface engineering strategy for the post-synthetic functionalization of COFs that employs click chemistry to covalently link organic units onto the pore walls with the desired density and composition.<sup>[47]</sup> With this powerful surface engineering method, the pore interface and its functionalities, which are critical for gas adsorption, catalysis, and  $\pi$ -electronic properties, can be controlled. This concept has been demonstrated using boronate-linked COFs on which the azide units on the edges undergo a quantitative reaction with ethynyl compounds and integrate various organic units onto the pore walls. Click strategy has also been reported for the high-throughput functionalization of MOFs.<sup>[48-50]</sup> Boronate linkages are not sufficiently robust to withstand aqueous or alcoholic reaction conditions.<sup>[47]</sup> Recently, I explored a novel strategy for engineering the pore surface of stable imine-linked COFs and herein report the pore surface engineering of imine-linked COFs via click chemistry. We demonstrate the utility of this strategy by highlighting the covalent and controlled integration of organocatalytic sites into the pore walls to synthesize organocatalytic COFs that exhibit significantly enhanced activity in asymmetric Michael addition reactions while retaining stereoselectivity in aqueous solutions. The COF catalyst combines a number of striking features, including broad applicability, good recyclability, and high capability to perform catalytic transformation under continuous flow. Our studies on the structure–property relationship provide the basis for exploring the 1D channels of COFs as catalytic reactors.

## 2.2 Results and Discussions

### 2.2.1 Synthesis and Structural Characterization

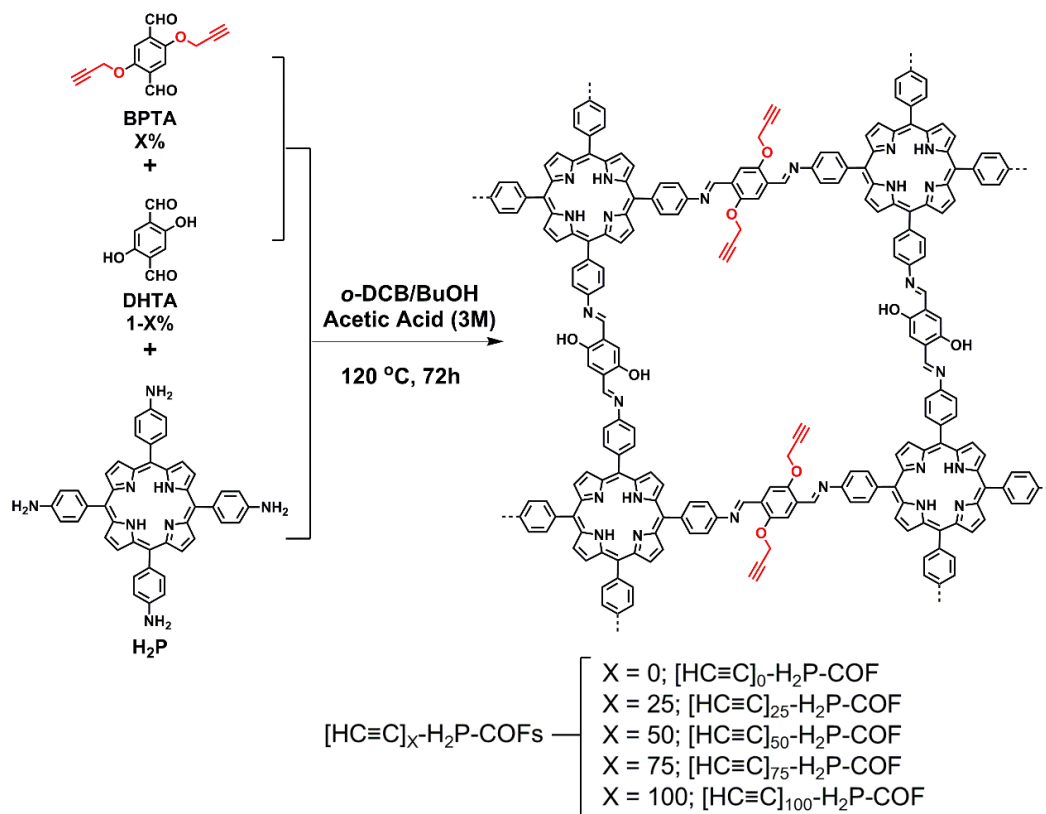


**Figure 1.** Schematic representation of the synthesis of  $[HC\equiv C]_X-H_2P-COFs$  with freebase-porphyrin ( $H_2P$ ) at the vertices and DHTA/BPTA on the edges of the tetragonal framework (the case for  $X = 50$  was exemplified).

The  $[HC\equiv C]_X-H_2P-COFs$  were synthesized by the imine formation reaction of the amino-monomer and aldehyde-monomers in *o*-dichlorobenzene/*n*-butanol co-solvent under solvothermal conditions (**Figure 1**). A three-component reaction system consisting of 5,10,15,20-tetrakis (4'-tetraphenylamino)porphyrin as the vertices and a mixture of 2,5-bis(2-propynyloxy)terephthalaldehyde (BPTA) and 2,5-dihydroxyterephthalaldehyde (DHTA) at varying molar ratios ( $X = [BPTA] / ([BPTA] + [DHTA]) \times 100 = 0, 25, 50, 75, 100$ ) as the edge units was developed to synthesize the COFs, by allowing the integration of ethynyl units of varying

content into the edges (**Figure 1**,  $[\text{HC}\equiv\text{C}]_x\text{-H}_2\text{P-COFs}$ ,  $X = 25, 50, 75,$  and  $100$  ( $X = 0$ :  $\text{H}_2\text{P-COF}$ )). These reactions exhibited similar isolated yields to each other, indicating that the reactivity of BPTA and DHTA is similar under the solvothermal condition (**Table 1**).

To achieve highly crystalline and porous  $[\text{HC}\equiv\text{C}]_x\text{-H}_2\text{P-COFs}$ , we screened and optimized the solvothermal conditions, including the solvent, reaction temperature and time, and the catalyst concentration (**Tables 1**). Single-component solvents, such as dimethylacetamide (DMAc), *m*-cresol, *o*-dichlorobenzene (*o*-DCB), and dioxane, resulted in amorphous and nonporous materials. We thus investigated the synthesis of crystalline and porous COFs *via* two-component solvent systems; a mixture of *o*-DCB and *n*-butanol produced crystalline and porous  $[\text{HC}\equiv\text{C}]_x\text{-H}_2\text{P-COFs}$ . By optimizing the catalyst concentration and reaction time, we developed solvothermal conditions using an *o*-DCB/*n*-butanol solvent mixture (1/1 *v/v*) in the presence of a 0.3 M acetic acid catalyst at 120 °C for 3 days to synthesize  $[\text{HC}\equiv\text{C}]_x\text{-H}_2\text{P-COFs}$ . Different from the pore surface engineering of boronate-linked COFs that utilize azide-functionalized pore walls for the click reaction,<sup>22</sup> the present method explores the ethynyl units as the functional intermediates on the pore walls for the further click reaction with azide derivatives.

**Table 1.** Reaction conditions of preparing  $[\text{HC}\equiv\text{C}]_x\text{-H}_2\text{P-COFs}$ .

X	Solvent	Catalyst: Acetic Acid	Temp. ( °C)	Time (day)	Yield (%)	XRD Intensity (Counts)
50	Mesitylene/Dioxane 0.5 mL/0.5 mL	(6M), 0.1 mL	120	3	60	10010
	Mesitylene/Dioxane 0.5 mL/0.5 mL	(6M), 0.1 mL	120	5	69	3073
	Mesitylene/Dioxane 0.5 mL/0.5 mL	(6M), 0.1 mL	120	15	76	1787

	Mesitylene/Dioxane 0.25 mL/0.75 mL	(6M), 0.1 mL	120	3	60	5705
	Mesitylene/Dioxane 1.0 mL/1.0 mL	(6M), 0.2 mL	120	3	10	No Peak
	<i>o</i> -DCB/BuOH 0.5 mL/0.5 mL	(3M), 0.1 mL	120	3	69	7536
	<i>o</i> -DCB/BuOH 0.5 mL/0.5 mL	(6M), 0.1 mL	120	3	75	4003
	<i>o</i> -DCB/BuOH 0.5 mL/0.5 mL	(6M), 0.1 mL	120	5	80	2305
	<i>o</i> -DCB/BuOH 0.5 mL/0.5 mL	-	120	5	66	1150
	<i>o</i> -DCB/BuOH 0.9 mL/0.1 mL	(6M), 0.1 mL	120	5	82	3231
	DMAc 1mL	-	120	3	79	No Peak
	<i>m</i> -cresol 1mL	-	120	5		No Peak
	<i>m</i> -cresol 1mL	(6M), 0.1 mL	120	5		No Peak
	<i>o</i> -DCB 1mL	(6M), 0.1 mL	120	5		No Peak
	Dioxane 1mL	(6M), 0.1 mL	120	5		No Peak
0	<i>o</i> -DCB/BuOH 0.5 mL/0.5 mL	(3M), 0.1 mL	120	3	80	14666
25	<i>o</i> -DCB/BuOH 0.5 mL/0.5 mL	(3M), 0.1 mL	120	3	72	14095
	<i>o</i> -DCB/BuOH 0.5 mL/0.5 mL	(6M), 0.1 mL	120	5	82	6695
	DMAc 1 mL	(3M), 0.1 mL	120	3	73	4096
	DMAc 1 mL	-	120	1	82	No Peak
75	<i>o</i> -DCB/BuOH 0.5 mL/0.5 mL	(3M), 0.1 mL	120	3	86	2343
100	<i>o</i> -DCB/BuOH 0.5 mL/0.5 mL	(3M), 0.1 mL	120	3	80	1052

The typical synthesis methods for the  $[\text{HC}\equiv\text{C}]_x\text{-H}_2\text{P-COFs}$ : An *o*-DCB/*n*-BuOH (0.5 mL / 0.5 mL) mixture of  $\text{H}_2\text{P}$  (0.022 mmol, 14.9 mg) and DHTA/BPTA (total 0.044 mmol) at different molar ratios of 100/0, 75/25, 50/50, 25/75, and 0/100 in the presence of acetic acid catalyst (3 M, 0.1 mL) in a Pyrex tube (10 mL) was degassed by three freeze–pump–thaw cycles. The tube was sealed off by flame and heated at 120 °C for 3 days.

The precipitate was collected *via* centrifuge, washed with THF for 6 times, and washed with acetone 3 times. The powder was dried at 120 °C under vacuum overnight to give the corresponding COFs in isolated yields of 80%, 72%, 69%, 86%, and 80% for the  $\text{H}_2\text{P-COF}$ ,  $[\text{HC}\equiv\text{C}]_{25}\text{-H}_2\text{P-COF}$ ,  $[\text{HC}\equiv\text{C}]_{50}\text{-H}_2\text{P-COF}$ ,  $[\text{HC}\equiv\text{C}]_{75}\text{-H}_2\text{P-COF}$ , and  $[\text{HC}\equiv\text{C}]_{100}\text{-H}_2\text{P-COF}$ , respectively. The amorphous nonporous polymers 1 and 2 (**Table 6**) were synthesized in DMAc, according to this method under otherwise same conditions.

The X-ray diffraction (XRD) intensity tended to decrease with increasing ethynyl content (**Figure 2**). The  $\text{H}_2\text{P-COF}$  exhibited the highest XRD intensity of  $1.47 \times 10^4$  counts, with  $1.05 \times 10^3$  counts for the  $[\text{HC}\equiv\text{C}]_{100}\text{-H}_2\text{P-COF}$ . This decrease in intensity is caused by the large number of amorphous ethynyl chains on the pore walls. A similar trend was previously reported for boronate-linked COFs upon pore surface engineering with amorphous units<sup>22</sup> and Pd-imine coordinated COFs.<sup>[46]</sup> The presence of ethynyl groups does not create new XRD peaks. Because the  $[\text{HC}\equiv\text{C}]_x\text{-H}_2\text{P-COFs}$  exhibit similar XRD patterns as  $\text{H}_2\text{P-COF}$ ,  $[\text{HC}\equiv\text{C}]_x\text{-H}_2\text{P-COFs}$  possess the same crystalline structure as the  $\text{H}_2\text{P-COF}$ .<sup>[47]</sup>

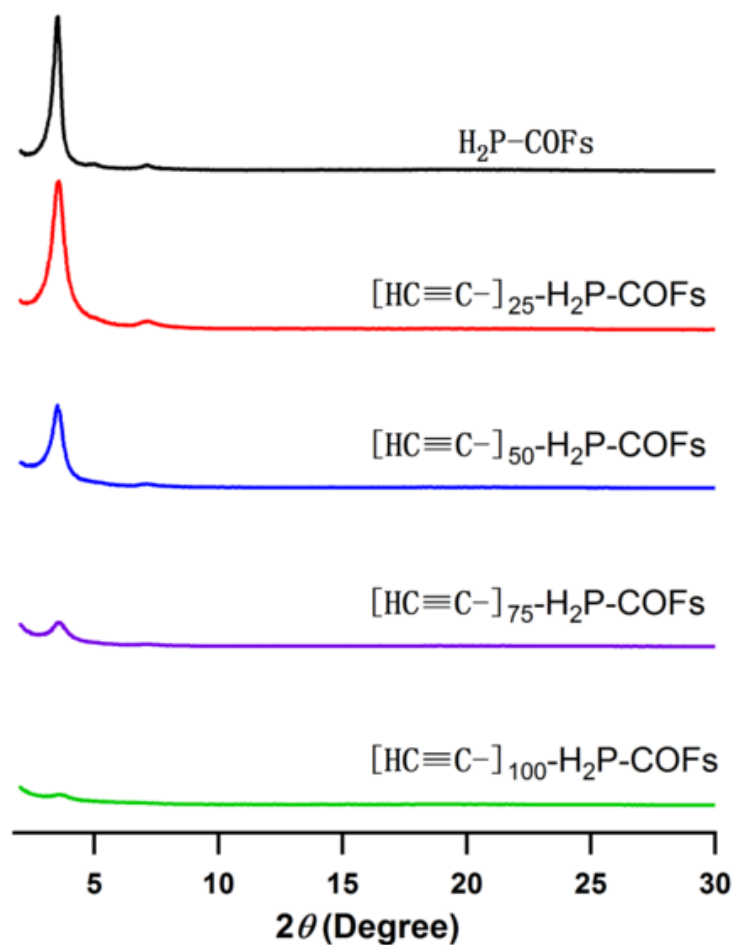


**Figure 2.** XRD patterns of H<sub>2</sub>P-COF (black) and [HC≡C]<sub>x</sub>-H<sub>2</sub>P-COFs

Infrared (IR) spectroscopy provides direct evidence of the presence of ethynyl units in [HC≡C]<sub>x</sub>-H<sub>2</sub>P-COFs with characteristic C≡C and H-C≡C vibration bands at 2120 and 3290 cm<sup>-1</sup>, respectively, which were absent from the H<sub>2</sub>P-COF spectrum (**Figure 3**).<sup>[51]</sup> The intensities of these two bands increased with increasing ethynyl content, indicating the successful integration of ethynyl units at different contents onto the pore walls of [HC≡C]<sub>x</sub>-H<sub>2</sub>P-COFs. A vibration band due to C=N linkages appeared at 1615 cm<sup>-1</sup>, whereas the vibration bands assigned to the C=O unit of the aldehyde residues were attenuated, characteristics that were identical to those of the H<sub>2</sub>P-COF.<sup>[51]</sup> Elemental analysis reveals that the content of ethynyl units is close to the theoretical value (**Table 2**).

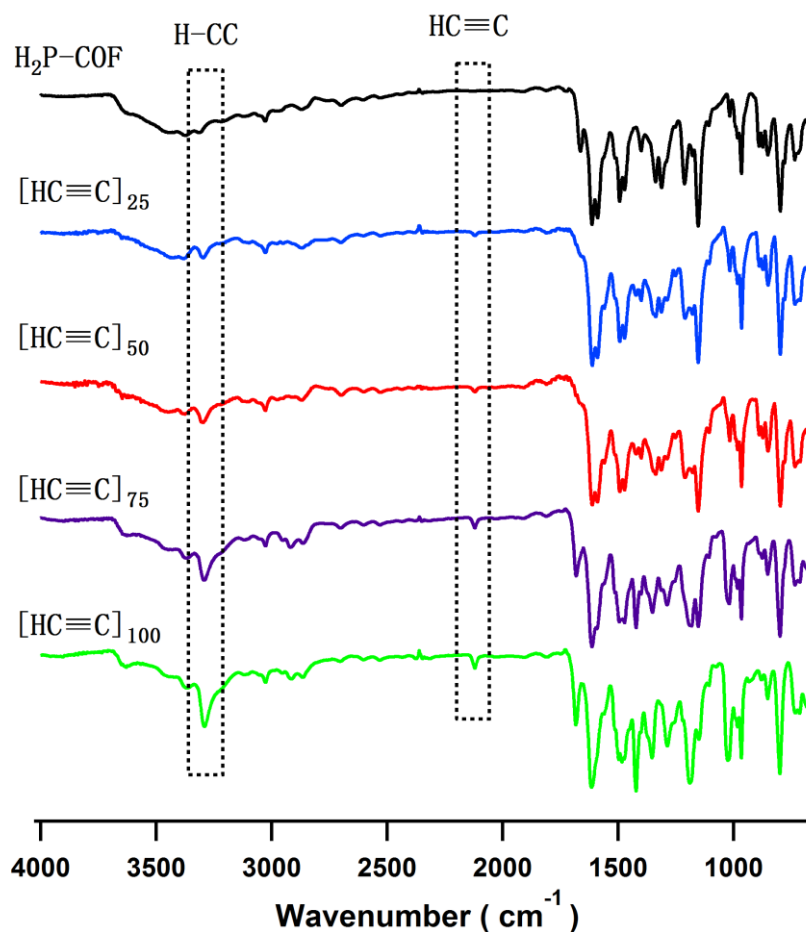


**Figure 3.** IR Spectra of H<sub>2</sub>P-COF and [HC≡C]<sub>x</sub>-H<sub>2</sub>P-COFs

**Table 2.** Elemental analysis of H<sub>2</sub>P-COF (black) and [HC≡C]<sub>x</sub>-H<sub>2</sub>P-COFs

COFs		C (%)	H (%)	N (%)
H <sub>2</sub> P-COF	Calcd.	77.07	4.1	11.98
	Found	73.9	5.23	9.57
[HC≡C] <sub>25</sub> -H <sub>2</sub> P-COF	Calcd.	77.76	4.14	11.52
	Found	75.12	5.76	8.81
[HC≡C] <sub>50</sub> -H <sub>2</sub> P-COF	Calcd.	78.4	4.19	11.08
	Found	75.45	5.29	9.24
[HC≡C] <sub>75</sub> -H <sub>2</sub> P-COF	Calcd.	78.99	4.22	10.68
	Found	74.27	4.8	8.94
[HC≡C] <sub>100</sub> -H <sub>2</sub> P-COF	Calcd.	79.54	4.26	10.31
	Found	75.29	4.83	8.62

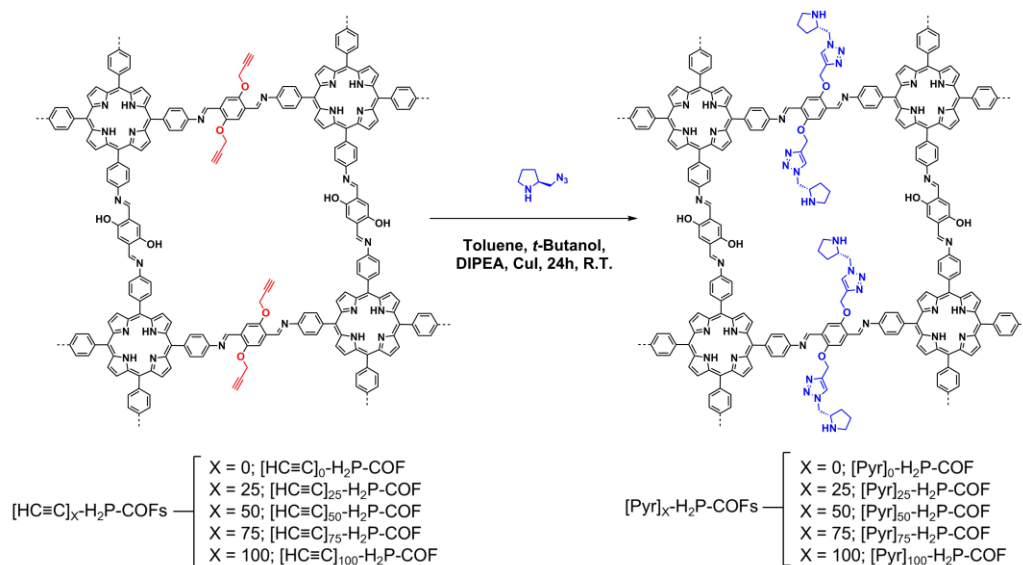


**Figure 4.** The general strategy for the pore surface engineering of the ethynyl-modified COFs *via* click chemistry (the case for  $x = 50$  was exemplified).

### 2.2.2 Preparation of the COF-Catalysts

The three-component reaction system allows the integration of the ethynyl units onto the pore walls with synthetically controlled density. The ethynyl units undergo a quantitative click reaction with azide compounds to construct functional interfaces *via* triazole linkages.<sup>[47]</sup> Pyrrolidine derivatives are well-known organocatalysts for Michael addition reaction, while the derivatives with bulky substituents give high stereoselectivity.<sup>[52-55]</sup> In this study, we utilized the simplest pyrrolidine unit for demonstrating the effectiveness of a click reaction in synthesizing heterogeneous organocatalysts with active sites on the 1D channel walls; the simplest pyrrolidine unit has a relatively low stereoselectivity.

The typical synthesis methods for the  $[\text{Pyr}]_x\text{-H}_2\text{P-COFs}$ : A toluene/*tert*-butanol (0.8 mL / 0.2 mL) mixture of  $[\text{HC}\equiv\text{C}]_{25}\text{-H}_2\text{P-COF}$  (20 mg) in the presence of CuI (2 mg) and DIPEA (40  $\mu\text{L}$ ) in a Pyrex tube (10 mL) was added with (*S*)-2-(azidomethyl)pyrrolidine (toluene solution; 1 M; 21  $\mu\text{L}$ ). The tube was degassed *via* three freeze–pump–thaw cycles and the mixture was stirred at room temperature for 24 h. The precipitate was collected *via* centrifuge, washed with ethanol 5 times, and dried at room temperature under vacuum, to produce  $[\text{Pyr}]_{25}\text{-H}_2\text{P-COF}$ .

H<sub>2</sub>P-COF as a deep brown solid in quantitative yield. The ethynyl groups were quantitatively reacted with the azide units as evident by the IR spectra. The click reaction of [HC≡C]<sub>X</sub>-H<sub>2</sub>P-COFs (X = 50, 75, and 100) with (*S*)-2-(azidomethyl)pyrrolidine were performed according to this method under otherwise same conditions.

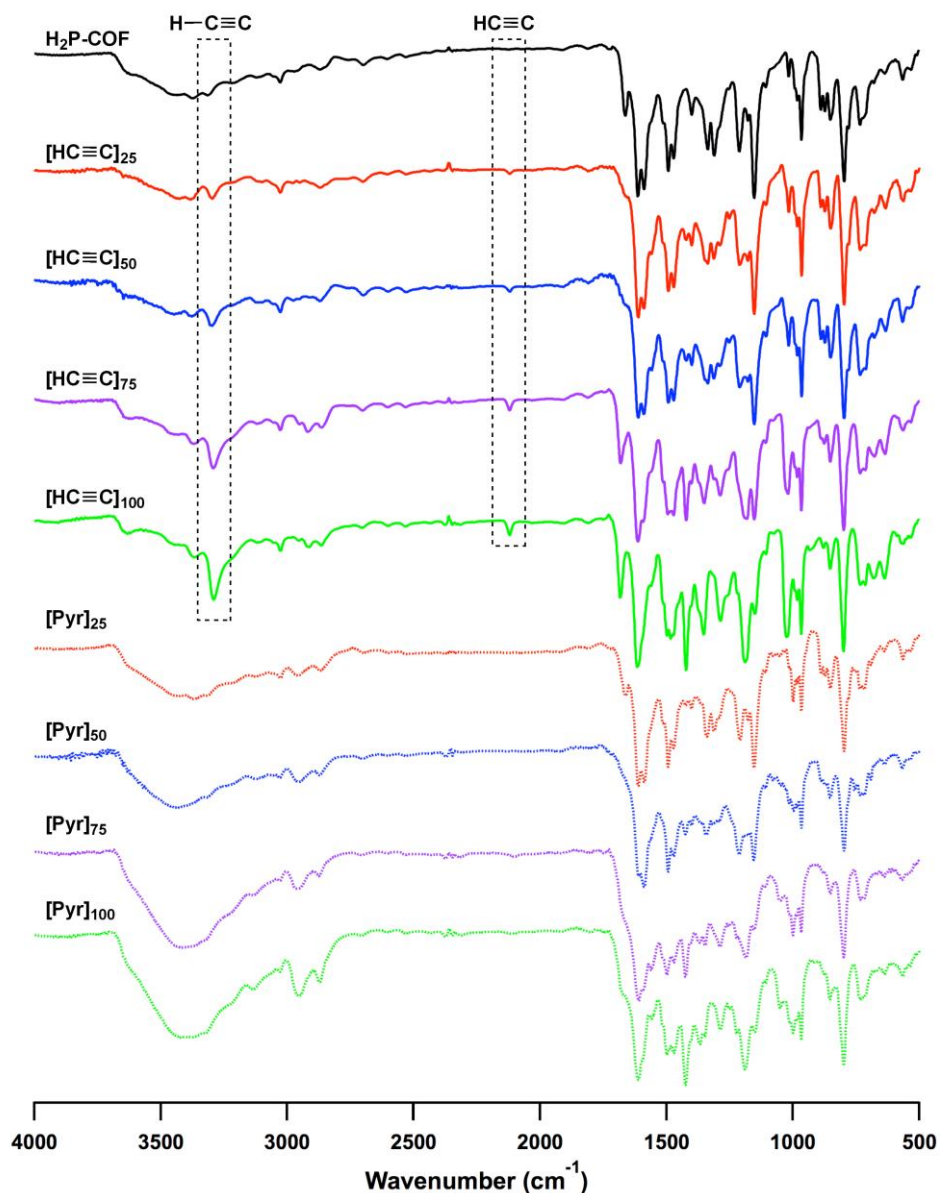


**Figure 5.** FT-IR spectra of H<sub>2</sub>P-COF, [HC≡C]<sub>X</sub>-H<sub>2</sub>P-COFs and [Pyr]<sub>X</sub>-H<sub>2</sub>P-COFs

After the click reaction, a nitrogen rich unit was introduced to the COF pore walls, which cause a significant increase of the nitrogen content; meanwhile, the

experimental content of carbon, hydrogen and nitrogen is quite close to the theoretical value (**Table 3**). Further, IR spectra demonstrated the disappearance of the vibration bands at 2120 and 3290  $\text{cm}^{-1}$  that were attributed to the  $\text{H-C}\equiv\text{C}$  units (**Figure. 5**), indicating all the  $\text{C}\equiv\text{C}$  units are quantitatively transformed. Meanwhile the broad peaks at 2750-3000  $\text{cm}^{-1}$  which corresponding to the characteristic absorption peaks of the aliphatic chain are significantly increased; besides, the strength of these peaks are increasing along with the increase of the catalytic sites content.

**Table 3.** Elemental analysis of  $[\text{Pyr}]_x\text{-H}_2\text{P-COFs}$  and corresponding amorphous polymers.

COFs	Found	75.29	4.83	8.62
$[\text{Pyr}]_{25}\text{-H}_2\text{P-COFs}$	Calcd.	74.3	4.58	15.29
	Found	71.99	4.69	12.51
$[\text{Pyr}]_{50}\text{-H}_2\text{P-COFs}$	Calcd.	72.25	4.95	17.74
	Found	66.53	5.09	13.5
$[\text{Pyr}]_{75}\text{-H}_2\text{P-COFs}$	Calcd.	70.67	5.22	19.62
	Found	63.89	4.86	15.06
$[\text{Pyr}]_{100}\text{-H}_2\text{P-COFs}$	Calcd.	69.42	5.45	21.12
	Found	65.46	5.15	16.82
Amorphous and Nonporous Polymer 1	Calcd.	74.3	4.58	15.29
	Found	67.41	4.65	11.57
Amorphous and Nanporous Polymer 2	Calcd.	72.25	4.95	17.74
	Found	67.19	5.25	13.39

### 2.2.3 PXRD Pattern and Theoretical Calculation

The density of the pyrrolidine units on the pore walls was determined by the ethynyl content of  $[\text{HC}\equiv\text{C}]_x\text{-H}_2\text{P-COFs}$ , since only the ethynyl groups could selectively reacted with the azide units to introduce the catalytic active sites; and

mild reaction condition of the ‘Click reaction’ guarantee the COF network remain stable. Since the isolated yield of the click reaction is almost 100% and the elementary analysis result of the COF-catalyst is quite close to the theoretical value, further, there is no obvious absorption peak of the residue groups (aldehyde- or amino- groups). As shown in **Figure 6**, the pores become smaller and more crowded as the density of pyrrolidine units increases in  $[\text{Pyr}]_x\text{-H}_2\text{P-COF}$ s. This is further supported by the nitrogen sorption results (**Figure 9, Table 5**).

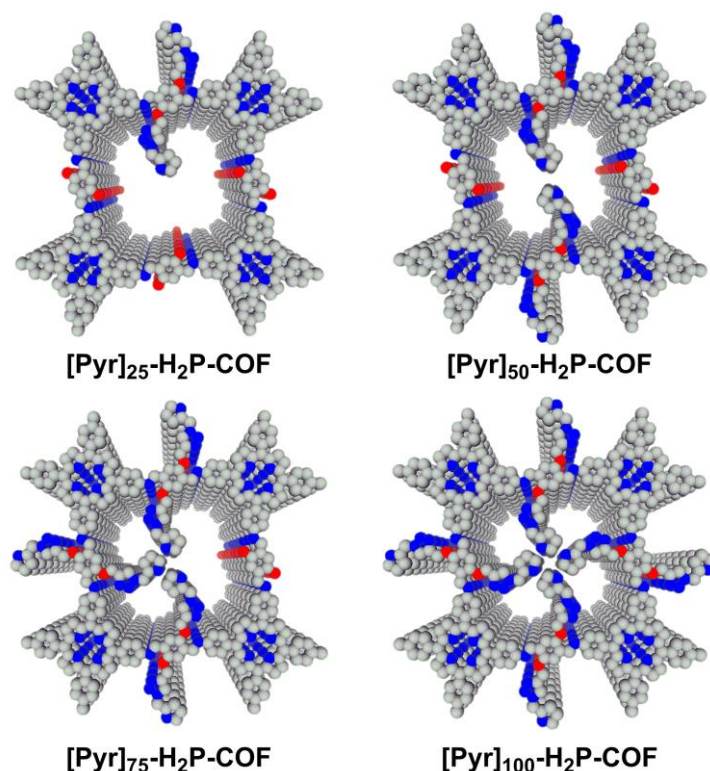


**Figure. 6** The graphical representation of  $[\text{Pyr}]_x\text{-H}_2\text{P-COF}$  with different densities of catalytic sites on the pore walls (gray: carbon, blue: nitrogen, red: oxygen; hydrogen is omitted for clarity).

As more pyrrolidine units were integrated into the pore walls, the XRD intensity decreased (**Figure 7**); a similar phenomenon was observed for  $[\text{HC}\equiv\text{C}]_x\text{-H}_2\text{P-COF}$ s. Similarly, the XRD peak positions remained unaffected, indicating that the crystalline skeleton was retained. For example, both  $[\text{Pyr}]_{50}\text{-H}_2\text{P-COF}$  (**Figure 7B**, blue) and  $\text{H}_2\text{P-COF}$  (**Figure 7A**, black) exhibited peaks

at 3.5, 4.9, 7.0, and 23 °, which are assignable to (100), (110), (200), and (001) facets, respectively. The Pawley refined XRD pattern (**Figure 7**, orange) reproduced the experimental curve (blue), confirming the aforementioned peak assignment, as is evident in their negligible difference (black). The density-functional tight-binding method including Lennard-Jones dispersion was employed to determine the optimal stacking isomer structures and revealed that these COFs adopt 0.8Å-slipped AA stacking structure. (**Table 4**)

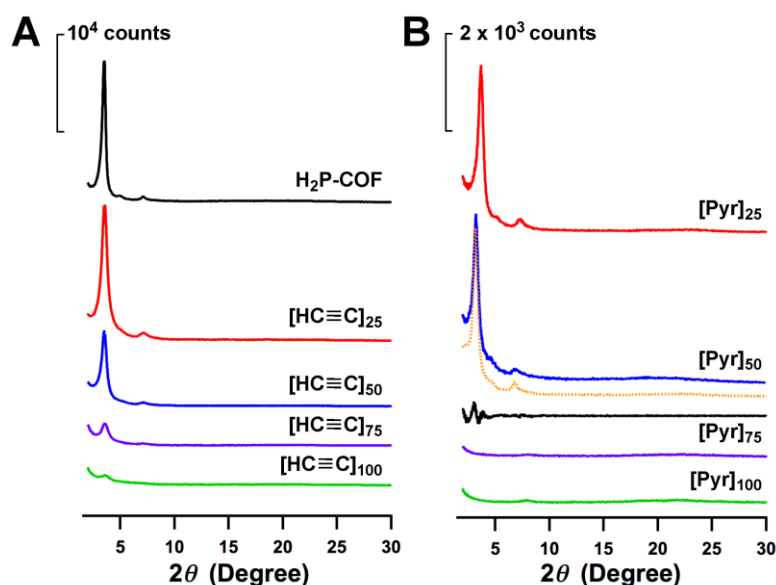


**Figure 7.** Comparison of XRD: **A.** H<sub>2</sub>P-COF (black) and [HC≡C]<sub>x</sub>-H<sub>2</sub>P-COFs, and **B.** [Pyr]<sub>x</sub>-H<sub>2</sub>P-COFs (orange: Pawley refined XRD curve of [Pyr]<sub>50</sub>-H<sub>2</sub>P-COF, black: their difference).

**Table 4.** The total DFTB energies, Lennard-Jones contributions (LJ), and the crystal stacking energies per unit cell for the H<sub>2</sub>P-COF and [Pyr]<sub>25</sub>-H<sub>2</sub>P-COF.

Stacking Mode	<i>c</i> (Å)	Total DFTB Energy (a.u.)	LJ energy (a.u.)	Total crystal stacking energy (kcal mol <sup>-1</sup> )
Monolayer		-149.2124992	0.5816	
AA H <sub>2</sub> P-COF	3.96	-298.6138679	0.9674	59.26

Slipped AA H <sub>2</sub> P-COF (0.8 Å)	3.63	-298.6262435	0.9603	63.14
AB H <sub>2</sub> P-COF	3.22	-298.550363	1.0437	39.33
Slipped AA [Pyr] <sub>25</sub> -H <sub>2</sub> P-COF	4.09	-409.182501	1.2833	92.83

### 2.2.4 Gas Sorption Property

We conducted nitrogen sorption isotherm measurements at 77 K to investigate how the organic groups on the pore walls affect the porosity of the COFs. As the ethynyl content increased, [HC≡C]<sub>x</sub>-H<sub>2</sub>P-COFs exhibited a decrease in the Brunauer–Emmett–Teller (BET) surface area (**Figure 8**). For example, the H<sub>2</sub>P-COF had a BET surface area of 1126 m<sup>2</sup> g<sup>-1</sup>, which decreased to 1092, 859, 324, and 206 m<sup>2</sup> g<sup>-1</sup> for [HC≡C]<sub>25</sub>-H<sub>2</sub>P-COF, [HC≡C]<sub>50</sub>-H<sub>2</sub>P-COF, [HC≡C]<sub>75</sub>-H<sub>2</sub>P-COF, and [HC≡C]<sub>100</sub>-H<sub>2</sub>P-COF, respectively (**Table 5**). The pore size distribution profiles, calculated using nonlocal density functional theory model, revealed that these COFs exhibit one pore type in their skeletons (**Figure 9**). The pore sizes decreased from 2.2 to 2.0, 1.9, 1.5, and 1.5 nm, as the ethynyl content increased from 0 to 25, 50, 75, and 100, respectively.

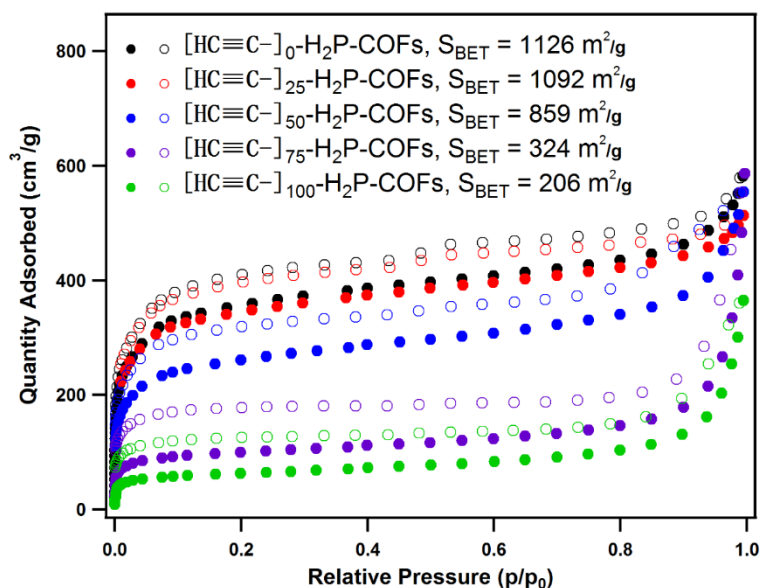


**Figure 8.** Nitrogen sorption isotherm profiles of H<sub>2</sub>P-COF and [HC≡C]<sub>x</sub>-H<sub>2</sub>P-COFs measured at 77 K. The filled circles represent adsorption; the open circles represent desorption.

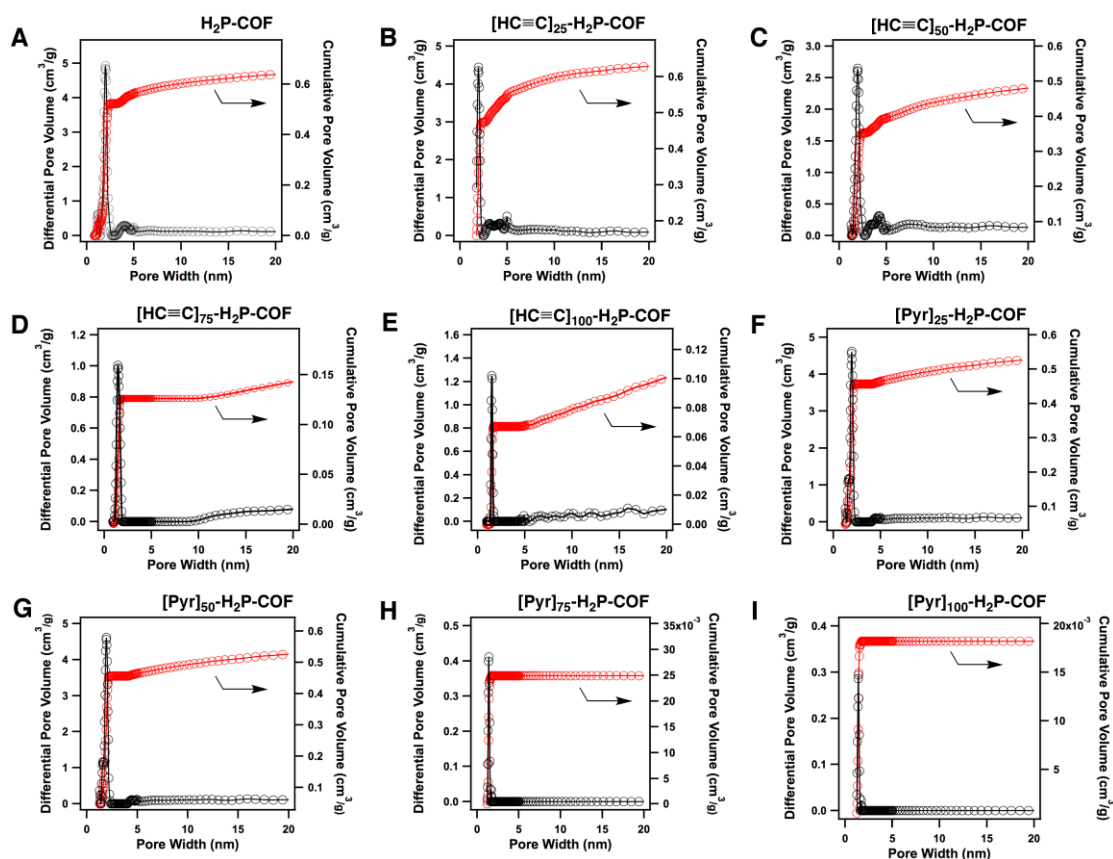


**Figure 9.** (A-I) Pore size distribution (black) and cumulative pore volume (red) profiles of the COFs.

**Table 5.** Pore size and pore volume of the COFs.

COFs/COF	BET Surface Area (m <sup>2</sup> /g)	Pore Size (nm)	Pore Volume (cm <sup>3</sup> /g)
H <sub>2</sub> P-COF	1126	2.2	0.68
[HC≡C] <sub>25</sub> -H <sub>2</sub> P-COF	1092	2	0.66
[HC≡C] <sub>50</sub> -H <sub>2</sub> P-COF	859	1.9	0.52
[HC≡C] <sub>75</sub> -H <sub>2</sub> P-COF	324	1.5	0.16
[HC≡C] <sub>100</sub> -H <sub>2</sub> P-COF	206	1.5	0.14
[Pyr] <sub>25</sub> -H <sub>2</sub> P-COFs	960	1.9	0.56
[Pyr] <sub>50</sub> -H <sub>2</sub> P-COFs	675	1.6	0.42
[Pyr] <sub>75</sub> -H <sub>2</sub> P-COFs	86	1.4	0.025
[Pyr] <sub>100</sub> -H <sub>2</sub> P-COFs	63	1.4	0.018

After the click reactions, much bulky groups were introduced into the pore walls of the COFs. Thus, [Pyr]<sub>x</sub>-H<sub>2</sub>P-COFs exhibited a distinct decrease in their BET surface areas (**Figure 10**). For example, [Pyr]<sub>25</sub>-H<sub>2</sub>P-COF had a surface area of 960 m<sup>2</sup> g<sup>-1</sup>, which decreased to 675, 86, and 63 m<sup>2</sup> g<sup>-1</sup> for [Pyr]<sub>50</sub>-H<sub>2</sub>P-COF, [Pyr]<sub>75</sub>-H<sub>2</sub>P-COF, and [Pyr]<sub>100</sub>-H<sub>2</sub>P-COF, respectively (**Table 5**). The pore sizes decreased from 1.9 to 1.6, 1.4, and 1.4 nm as the pyrrolidine content increased from 25 to 50, 75, and 100, respectively. The pore size distribution profile revealed that only one pore type existed (**Figure 9**), indicating that the pyrrolidine units are homogeneously engineered onto the walls.

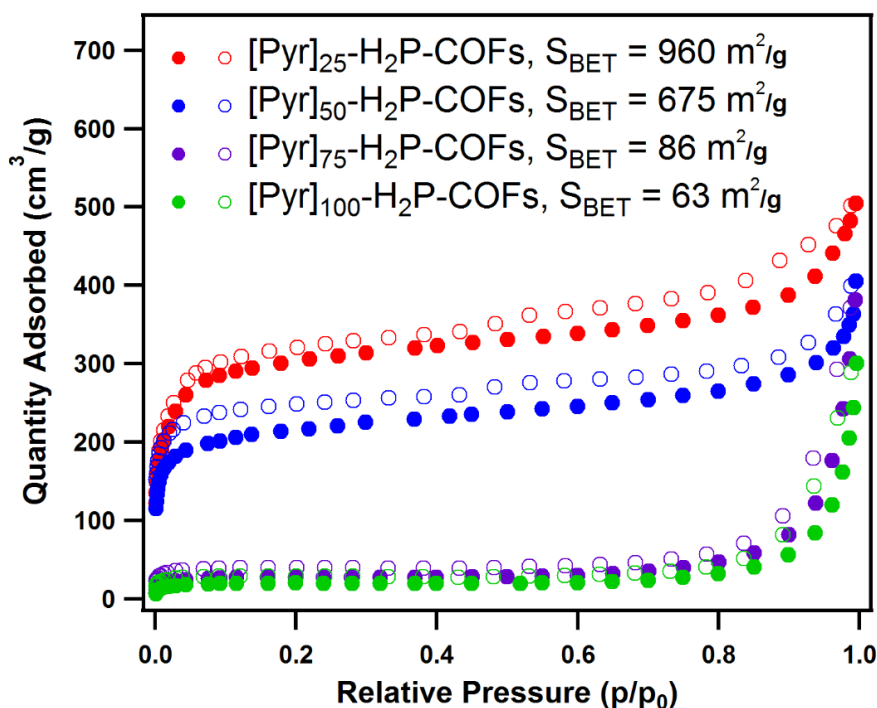


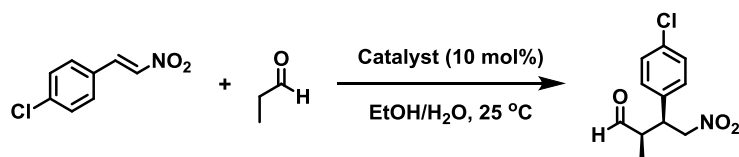
**Figure. 10** Nitrogen sorption isotherm profiles of [Pyr]<sub>x</sub>-H<sub>2</sub>P-COFs measured at 77 K. The filled circles represent adsorption; the open circles represent desorption.

### 2.2.5 Heterogeneous Organocatalysis

Engineering the pore surface covalently integrates the pyrrolidine units onto the pore walls and generates a series of COFs with varying active site densities, surface areas, and pore sizes (**Figure 6 and Table 5**). We investigated the

catalytic activities of [Pyr]<sub>x</sub>-H<sub>2</sub>P-COFs in a Michael addition reaction in aqueous solutions, using (*S*)-4-(phenoxyethyl)-1-(pyrrolidin-2-ylmethyl)-1H-1H-1,2,3-triazole as a control, which has an active structure identical to the pyrrolidine catalytic site of [Pyr]<sub>x</sub>-H<sub>2</sub>P-COFs. **Table 6** summarized the results of the organocatalytic reaction. The pyrrolidine control yields a homogeneous system that required 3.3 h to achieve 100% conversion with ee and dr values of 49% and 60/40, respectively. The stereoselectivity of pyrrolidine derivatives is highly depended on its substitutions; a large substituent gives a high stereoselectivity, while the simplest pyrrolidine unit that we employed in this study yields moderate stereoselectivity.<sup>[52-55]</sup>

**Table 6.** Comparison of the pyrrolidine control, amorphous nonporous polymers, and COFs as catalyst for a Michael addition reaction.



	Time for 100% conversion (h)	dr	ee (%)
	3.3	60/40	49
[Pyr] <sub>25</sub> -H <sub>2</sub> P-COF	1	70/30	49
[Pyr] <sub>50</sub> -H <sub>2</sub> P-COF	2.5	70/30	50
[Pyr] <sub>75</sub> -H <sub>2</sub> P-COF	5	70/30	51
[Pyr] <sub>100</sub> -H <sub>2</sub> P-COF	9	65/35	44
Amorphous Polymer 1	43	70/30	48
Amorphous Polymer 2	65	65/35	46

Remarkably, the activity was significantly enhanced when the pyrrolidine units were integrated to the pore walls of COFs. For example, the reaction time was shortened to only 1 h when [Pyr]<sub>25</sub>-H<sub>2</sub>P-COF was dispersed in the reaction

mixture as a heterogeneous catalyst, yielding ee and dr values of 49% and 70/30, respectively. Similarly, the reaction in the presence of [Pyr]<sub>50</sub>-H<sub>2</sub>P-COF required 2.5 h for 100% conversion and resulted in 50% ee and 70/30 dr. These observations indicate that the organocatalytic COFs have significantly higher catalytic activity than the monomeric catalyst while retaining the stereoselectivity. The 1D channels of the COFs could accommodate the reactant and substrate, which cannot be dissolved in a water/ethanol mixture.

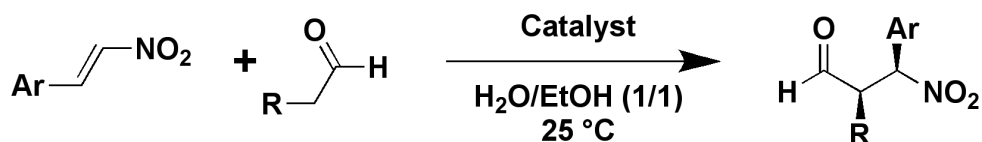
The catalytic activity depends upon the density of the active sites on the pore walls. [Pyr]<sub>75</sub>-H<sub>2</sub>P-COF with 75% active sites on the walls requires 5 h to complete the reaction. When each edge is anchored with catalytic sites, [Pyr]<sub>100</sub>-H<sub>2</sub>P-COF requires 9 h to reach 100% conversion, yielding ee and dr values of 44% and 65/35, respectively. Therefore, highly dense pyrrolidine units on the pore walls cause a steric congestion of the pores and impede the mass transport through the 1D channels. These results indicate that the engineering with the catalytic sites requires a balance between the density and porosity. The ee and dr values of the COF catalysts do not differ significantly from those of the control, indicating that the chiral centers are well retained in the COFs.

To elucidate the effects of crystallinity and porosity, amorphous and nonporous polymers with the same number of catalytic sites as [Pyr]<sub>25</sub>-H<sub>2</sub>P-COF and [Pyr]<sub>50</sub>-H<sub>2</sub>P-COF were utilized for the Michael addition reaction (**Table 6**). Surprisingly, amorphous and nonporous polymer 1, an analogue to [Pyr]<sub>25</sub>-H<sub>2</sub>P-COF, exhibited a rather sluggish reaction, requiring 43 h to reach completion and yielding 48% ee and 70/30 dr. Moreover, amorphous and nonporous polymer 2, an analogue to [Pyr]<sub>50</sub>-H<sub>2</sub>P-COF, exhibited a similarly low activity and required a reaction time of 65 h. Therefore, the crystallinity and porosity of COFs play a vital role in determining their catalytic activities. The amorphous and nonporous polymers can drastically decrease the catalytic activity because most catalytic sites are embedded in the inner portion of the particles that is not accessible to reactants and substrates: only catalytic sites exposed to the particle surface are

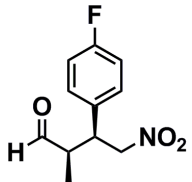
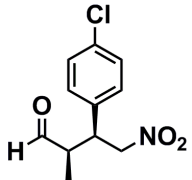
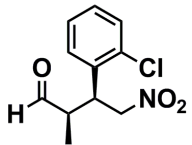
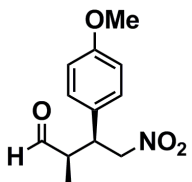
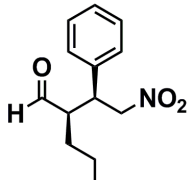
effective and contribute to the reaction. This structural limitation significantly reduces the activity of the amorphous and nonporous polymers, which is lower than the homogenous monomeric catalyst. Remarkably, the crystalline [Pyr]<sub>75</sub>-H<sub>2</sub>P-COF and [Pyr]<sub>100</sub>-H<sub>2</sub>P-COF, although they possess low BET surface areas, are much superior to the amorphous and nonporous polymers 1 and 2, with 7-8 fold increased catalytic activity under the same reaction conditions. Therefore, the development of COFs with high crystallinity and large porosity is critical for achieving high catalytic activity.

Based on these results, I investigated several different substrates to confirm the generality of the reaction system. As indicated in **Table 7**,  $\beta$ -nitrostyrene with different substitution patterns on the phenyl ring, including electron-releasing and electron-withdrawing groups, are tested as Michael acceptors. The catalyst [Pyr]<sub>25</sub>-H<sub>2</sub>P-COF showed good activity and all the addition products were obtained in good yields and with similar diastereo- and enantioselectivities, with no significant dependence on the electronic or steric properties of the substrate.

**Table 7.** Investigating the substrate scope of Michael Addition catalyzed by [Pyr]<sub>25</sub>-H<sub>2</sub>P-COF.

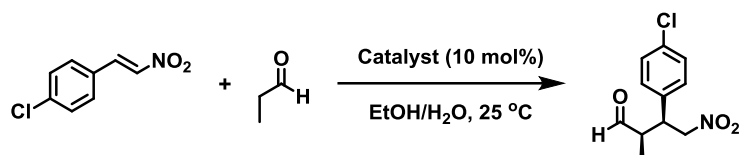


Product	Reaction time to 100% conversion (h)	Yield (%)	dr	ee (%)
	0.75	93	60/40	56

	0.75	94	60/40	46
	1	93	70/30	49
	1.2	94	60/40	57
	1	89	65/35	47
	1.5	88	60/40	46
	3.5	90	75/25	45

The catalyst [Pyr]<sub>x</sub>-H<sub>2</sub>P-COFs could be easily separated from the reaction mixture *via* centrifugation. Thus, [Pyr]<sub>25</sub>-H<sub>2</sub>P-COF can be reused at least four times without loss of the ee and dr values (**Table 8**). The slight decrement in activity could be attributed to the channels becoming blocked upon repetitive use, as evidenced by the decreased BET surface area after recycling (**Figure 11**).

**Table 8.** Recycling experiment of the [Pyr]<sub>25</sub>-H<sub>2</sub>P-COF for the Michael addition reaction.



Catalyst	Reaction time to 100% conversion (h)	Yield (%)	dr	ee (%)	Weight
Fresh	1	93	70/30	49	>99%
Cycle 1	1.5	90	70/30	49	>99%
Cycle 2	2.6	92	70/30	48	>99%
Cycle 3	3.8	88	70/30	48	>99%
Cycle 4	4.6	86	70/30	48	>99%

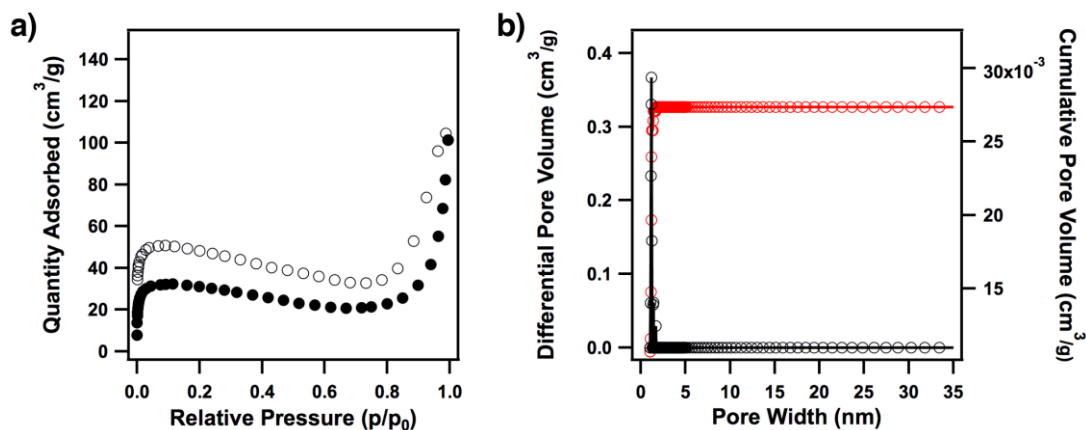


**Figure 11.** a, Nitrogen sorption isotherm curves of the recycled [Pyr]<sub>25</sub>-H<sub>2</sub>P-COF; b, Pore size distribution of the recycled [Pyr]<sub>25</sub>-H<sub>2</sub>P-COF. The BET surface area is 104 m<sup>2</sup>/g.

To utilize the high porosity and activity of the COF catalyst, I further explored the possibility of performing a continuous flow reaction using a columnar setup. I prepared a column consisting of a vertically mounted teflon pipe loaded with silica gel (as a plug to prevent COFs from flowing out) at the bottom and [Pyr]<sub>25</sub>-H<sub>2</sub>P-COF (10 mg, 10-mm bed height) atop the silica gel. The system was assembled with a syringe or pressured flask to flow the reagent solution (**Figure 12**). The column outlet was connected to a receiving flask. After

optimizing the parameters for the continuous-flow process, the device was found to work well at room temperature and yielded an optimal conversion when a solution of *trans*-4-chloro- $\beta$ -nitrostyrene (8.3 mM) and propionaldehyde (83 mM) in a mixture of water/EtOH (1/1 v/v) passed through at a flow rate of  $18 \mu\text{L min}^{-1}$ . The column maintained a 100% conversion and its stereoselectivities (44% ee, 65/35 dr) for more than 48 h under flow conditions.

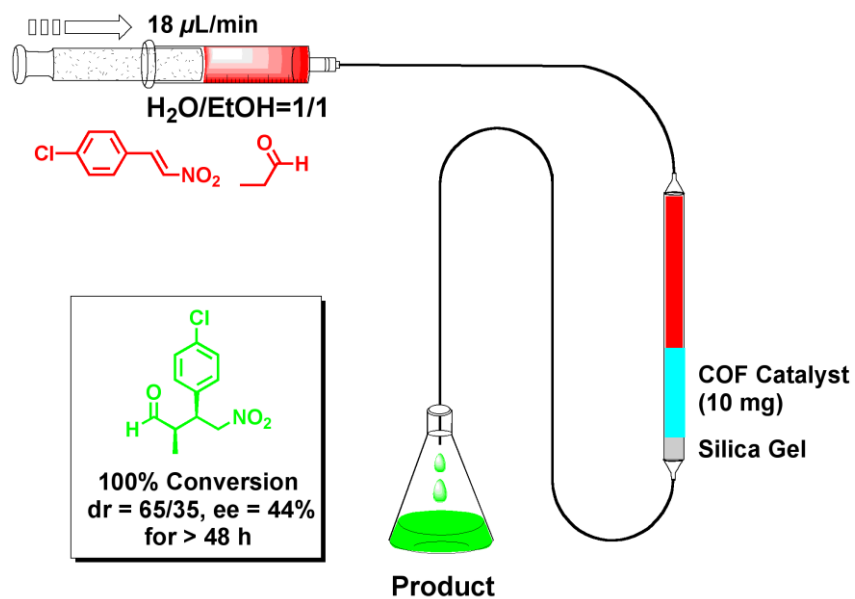


**Figure 12.** Representative Chart for the flow reaction system based on the organocatalytic COF column.

## 2.3 Conclusion

A pore surface engineering strategy for the controlled functionalization of imine-linked COFs was demonstrated using a three-component condensation system in conjunction with click chemistry. This method allows the molecular design of COF skeletons, controls the density and composition of the functional groups, and offers a general principle for designing catalytic COFs. Engineering pyrrolidine units onto the pore walls creates aqueous organocatalytic COFs, which combine a number of striking catalytic features, including significantly enhanced activity, good recyclability, and high capability to perform transformation under continuous flow while retaining stereoselectivity. The present work opens a way to precisely organized and synthetically controlled nanoreactors – a highly desired and long-pursued structure for heterogeneous catalysts.

## 2.4 Experimental Section

### 2.4.1 Methods

Thin-layer chromatography (TLC) plates were visualized by exposure to ultraviolet light and/or developed with iodine vapor. Flash column chromatography was carried out with silica gel (200-300 mesh).  $^1\text{H}$  nuclear magnetic resonance (NMR) spectra were recorded on JEOL models JNM-LA400 NMR spectrometers, where chemical shifts ( $\delta$  in ppm) were determined with a residual proton of the solvent as standard. Fourier transform infrared (IR) spectra were recorded on a JASCO model FT-IR-6100 infrared spectrometer. Matrix-assisted laser desorption ionization time-of-flight mass (MALDI-TOF MS) spectra were recorded on an Applied Biosystems BioSpectrometry model Voyager-DE-STR spectrometer in reflector or linear mode. X-ray diffraction (XRD) data were recorded on a Rigaku model RINT Ultima III diffractometer by depositing powder on glass substrate, from  $2\theta = 1.5^\circ$  up to  $60^\circ$  with  $0.02^\circ$  increment. Nitrogen sorption isotherms were measured at 77 K with a Micromeritics Instrument Corporation model 3Flex surface characterization analyzer. The Brunauer-Emmett-Teller (BET) method was utilized to calculate the specific surface areas. By using the non-local density functional theory (NLDF) model, the pore volume was derived from the sorption curve. Elemental analysis was performed on a Yanako model CHN CORDER MT-6 elemental analyzer. High performance liquid chromatography were performed on a JASCO model HPLC model with Daicel chiral AD-H and OD-H columns with *i*-PrOH/*n*-hexane as the eluent.

The molecular structure and electronic properties of monolayer and stacked H<sub>2</sub>P-COF isomers were determined using the density-functional tight-binding (DFTB) method including Lennard-Jones (LJ) dispersion. The corresponding LJ and crystal stacking energies as well as the HOMO-LUMO energy gaps were computed. The calculations were carried out with the DFTB+ program package version 1.2.<sup>[56]</sup> DFTB is an approximate density functional theory method based on the tight binding approach and utilizes an optimized minimal LCAO Slater-type all-valence basis set in combination with a two-center approximation for Hamiltonian matrix elements. The

Coulombic interaction between partial atomic charges was determined using the self-consistent charge (SCC) formalism. Lennard-Jones type dispersion was employed in all calculations to describe van der Waals (vdW) and  $\pi$ -stacking interactions. The lattice dimensions were optimized simultaneously with the geometry. Standard DFTB parameters for X–Y element pair (X, Y = C, O, H and N) interactions were employed from the mio-0-1 set.<sup>[57]</sup> The optimal single layer 2D model system consisted of 110 atoms for the monomer. The monomer had an optimal lattice parameter of  $a = b = 25.5$  Å. Using the optimized monomer, three different stacking configurations: perfect AA, AA slip-stacked by 0.8 Å in the  $a$  and  $b$  directions, and AB were optimized. The third dimension of the lattice,  $c$  was initialized at 3.5 Å for all structures.

Orientation of catalyst groups is beginning with the optimized H<sub>2</sub>P-COF, the hydroxyl- hydrogen atoms of the central phenyl group were replaced with the triazole-pyrrolidine group. The triazole-pyrrolidine group is conformationally flexible, and so in order to determine its orientation within the COF, a Genetic Algorithm (GA) previously optimized for the determination of molecular conformers was employed.<sup>S3</sup> The optimum structures and corresponding electronic properties of stacked isomers of [Pyr]<sub>50</sub>-H<sub>2</sub>P-COF were calculated using density-functional tight-binding (DFTB) method including Lennard-Jones (LJ) dispersion. For the monolayer structures, the optimized lattice constant is,  $a = b = 25.5$  Å. To avoid H-H overlap with the porphyrin ring, the adjacent phenyl groups rotate to an almost perpendicular orientation, with a dihedral angle of 74 ° and the central ring tilts in the opposing direction by 38 °. Using the optimal monolayer structure, three stacked configurations; AA, slipped-AA, and AB were generated and optimized. The interlayer stacking distances, and the corresponding LJ and crystal stacking energies per monolayer of each structure are shown in Table 4.

## 2.4.2 Coordinates and Atomic Net Charges

slipped-AA structure of [Pyr]<sub>50</sub>-H<sub>2</sub>P-COF

C	8.09354273	12.04914696	4.86244234	3.9075992
C	7.37172051	10.85030007	5.18861027	4.14821349
C	8.29017408	9.851878	5.4339699	4.15070222

C	9.60515893	10.41820841	5.3175066	3.89998983
N	9.43157111	11.74567936	4.99384226	5.06202971
C	7.54838818	13.27839792	4.39957989	4.04317447
C	10.85039952	9.7426499	5.44998632	4.04906216
C	12.11706362	10.37601037	5.52090114	3.83255051
C	13.35787783	9.64501166	5.76910388	4.14565765
C	14.35769004	10.56870662	5.79899862	4.15327045
C	13.73715307	11.87159247	5.57738283	3.83023426
N	12.38317979	11.7169657	5.42656135	5.41743353
C	14.46485548	13.08472071	5.49361555	4.0456166
C	13.88208866	14.35903825	5.2576291	3.90124724
C	14.53231097	15.63059857	5.40415773	4.14546142
C	13.6093612	16.61272442	5.11872614	4.15032404
C	12.37481121	15.97043461	4.75703979	3.90388214
N	12.58420072	14.61675746	4.88767979	5.05460468
C	11.17765877	16.5937932	4.31576431	4.04963613
C	9.9637841	15.90571731	4.03687356	3.83431695
C	8.81713083	16.52639456	3.38106206	4.14631417
C	7.80135697	15.61678335	3.41858282	4.14871493
C	8.32519802	14.42778914	4.08720342	3.83674802
N	9.64797936	14.62132333	4.39624137	5.41645765
C	6.061737	13.36805021	4.28403585	3.9853624
C	11.19258211	18.08220121	4.21509183	3.97336019
C	10.83887596	8.24669681	5.4519804	3.97330169
C	15.95480505	13.03827674	5.53581393	3.98953267
C	5.3608203	14.37240205	4.99077848	4.08679238
C	3.97098557	14.45125233	4.93922512	4.12615727
C	3.21803431	13.50042573	4.21090995	3.82821906
C	3.91284964	12.50792078	3.47915428	4.13434718
C	5.30904676	12.45685513	3.50952256	4.08983188
C	10.19357443	7.48434946	6.44842115	4.09263843
C	10.13153435	6.09385955	6.35347477	4.12114893
C	10.75406557	5.41086804	5.28307513	3.83104084
C	11.46364352	6.16690967	4.32161511	4.12499702
C	11.48734278	7.55844957	4.40270639	4.08440832
C	16.69092435	12.50784662	6.61760463	4.09085355
C	18.08258722	12.42005671	6.5601715	4.13063785
C	18.78542977	12.9086354	5.43573344	3.82869435
C	18.05366536	13.46304435	4.36085247	4.13904099
C	16.66442955	13.51221403	4.41175687	4.09171845
C	12.16550757	18.76579988	3.4543336	4.0933243
C	12.20966956	20.15753315	3.42906709	4.11200535
C	11.28221396	20.92643879	4.16989292	3.82796065

C	10.30779505	20.24776563	4.94114089	4.12654966
C	10.26718682	18.8536332	4.95404892	4.08552401
N	20.16652729	12.72191271	5.34065353	5.24571842
C	20.95483517	13.60844064	4.8328401	3.87542037
C	26.62089687	12.69100333	4.20087303	3.88038987
N	27.47777489	13.65551199	4.16406858	5.25250804
N	10.54691331	4.02790163	5.18365288	5.29609234
C	11.37315894	3.20110103	4.62677761	3.87726215
C	11.08776972	1.76932861	4.5165803	4.07800952
C	9.86539622	1.15253698	4.93196339	3.72668755
C	9.71609713	-0.24139324	4.86577136	4.18230152
C	10.74417806	-1.08887682	4.39079058	4.0788284
C	11.93888586	-0.46603073	3.91041194	3.72838625
C	12.09190555	0.92722355	3.98445176	4.17661725
C	10.52096956	-2.5344699	4.43248381	3.88069254
N	11.45235311	-3.38475352	4.13499945	5.29724057
O	8.79238652	1.85441984	5.41328051	6.39838658
O	12.97976236	-1.16501079	3.35759259	6.39986713
H	6.28343879	10.73909667	5.22710343	0.89653005
H	8.05074892	8.81241297	5.67902999	0.89892982
H	10.20248097	12.41451867	4.82032898	0.77286758
H	13.46677735	8.56465712	5.90909889	0.90882082
H	15.42394033	10.36993548	5.95250837	0.9141361
H	15.56591766	15.79181979	5.72707228	0.89615756
H	13.78600773	17.69140583	5.18025809	0.8971418
H	11.87656739	13.88944834	4.68656277	0.77174335
H	8.79901649	17.51420239	2.90540942	0.90760652
H	6.79805939	15.74341172	2.99367555	0.91331971
H	5.91719624	15.10211682	5.599388	0.91929822
H	3.44603476	15.2361448	5.50368096	0.91558514
H	3.36063877	11.79564907	2.84754686	0.92124489
H	5.82633632	11.70184393	2.89611091	0.92299299
H	9.72860332	7.98645586	7.31112443	0.9217567
H	9.60806606	5.51714659	7.13098314	0.91900561
H	11.95998728	5.67324843	3.4725076	0.92270955
H	11.99890794	8.1296027	3.61206865	0.92076802
H	16.1659888	12.16264523	7.52204325	0.92397922
H	18.64167746	12.00304593	7.41112578	0.9206911
H	18.57635789	13.83151237	3.46687513	0.90889236
H	16.11220805	13.91599024	3.55127296	0.91614323
H	12.90408907	18.19848064	2.8696187	0.9193806
H	12.96406451	20.66746543	2.81078465	0.91994861
H	9.5901821	20.80338369	5.56384492	0.92222973

H	9.51756847	18.34815165	5.58277991	0.91880111
H	20.59748433	14.64161159	4.56300749	0.95945295
H	26.93623413	11.61436205	4.30888871	0.96291714
H	12.37461567	3.52880951	4.23411387	0.95347264
H	8.77256145	-0.68067079	5.22317831	0.9078898
H	13.03409699	1.36617866	3.6239878	0.90409018
H	9.48680182	-2.85658756	4.73722644	0.95728886
H	8.97766398	2.82535944	5.41471261	0.66725982
H	12.78498614	-2.13464024	3.34808402	0.66801911
C	7.3571386	14.05638273	0.19844095	3.9021351
C	6.72872428	12.77819454	0.01808753	4.14565739
C	7.64775362	11.80408565	0.34210511	4.15136626
C	8.8604394	12.45626915	0.75478737	3.90413921
N	8.64151471	13.80897086	0.62253106	5.05471666
C	6.7624626	15.32441175	-0.04879333	4.04476521
C	10.05196154	11.83674501	1.22143353	4.05040052
C	11.26456236	12.52656557	1.49751078	3.83461691
C	12.42778751	11.90996757	2.12988271	4.14716543
C	13.44139808	12.81923727	2.06023637	4.1487129
C	12.89832988	14.00630405	1.40296916	3.83696995
N	11.56935797	13.81078675	1.12875096	5.41607286
C	13.66428944	15.15457035	1.06333712	4.04195452
C	13.10823382	16.38556182	0.62044335	3.90773797
C	13.82199043	17.58755588	0.28842045	4.14763952
C	12.89782093	18.58851953	0.0789835	4.15169032
C	11.58596555	18.01928586	0.21638123	3.90001506
N	11.7674076	16.6894044	0.5241783	5.06214989
C	10.33795982	18.69350806	0.10632983	4.04936361
C	9.07176381	18.06082906	0.02788227	3.83239945
C	7.82818841	18.78836762	-0.21970941	4.1435967
C	6.83398827	17.86035526	-0.28169949	4.15022759
C	7.46370462	16.55544684	-0.07927486	3.8300482
N	8.81299787	16.71817179	0.09725356	5.41709819
C	5.27863643	15.34467806	-0.18246018	3.99032209
C	10.34959878	20.18754378	0.11812657	3.97348508
C	10.03983348	10.35006596	1.33332059	3.97248535
C	15.15175069	15.05571615	1.12057326	3.9890547
C	4.5045815	14.84169931	0.8843484	4.09503519
C	3.11428366	14.88177097	0.84757569	4.13924261
C	2.44911064	15.47032718	-0.25199896	3.82943658
C	3.21768316	15.96952181	-1.32845113	4.13458756
C	4.60972806	15.88543458	-1.30233671	4.09124159
C	9.04435837	9.67388326	2.07122447	4.09395043

C	8.99581015	8.28285937	2.10571919	4.11216179
C	9.94126866	7.5059344	1.39668428	3.82837128
C	10.94813666	8.17675154	0.66037765	4.12646398
C	10.99231251	9.57052312	0.63724184	4.08562329
C	15.94064432	15.96602421	1.85840676	4.08994059
C	17.33606063	15.90955651	1.82099731	4.13824121
C	17.98705549	14.90730289	1.06415506	3.82524081
C	17.20152409	13.95171103	0.38035988	4.12608985
C	15.81193741	14.04194596	0.38855635	4.08624034
C	10.99844183	20.95446555	-0.8724044	4.09158822
C	11.06153723	22.34343005	-0.76817915	4.12153699
C	10.43295565	23.01739922	0.30388609	3.8317093
C	9.72401547	22.25726839	1.2621842	4.12734441
C	9.70049745	20.86611768	1.17298589	4.08494823
N	19.37643004	14.7440192	1.04172921	5.24469512
C	20.21113277	15.704235	0.83409581	3.8817301
C	25.88838118	14.81128326	0.24042172	3.8716217
N	26.71940048	15.678438	-0.23041109	5.24652444
N	9.7689987	6.11582049	1.437579	5.29825596
C	10.69010343	5.25433498	1.14015054	3.88096577
C	10.44811031	3.81209565	1.17244045	4.07853083
C	9.23557313	3.19928537	1.62027438	3.72871615
C	9.07711645	1.80656105	1.55057516	4.17725702
C	10.09037705	0.95645427	1.04938807	4.07824429
C	11.3254963	1.56396485	0.65803066	3.7261107
C	11.48082852	2.9570239	0.72306979	4.1820156
C	9.80317179	-0.47458689	0.94085903	3.8776798
N	10.64854864	-1.30387833	0.41920743	5.29455335
O	8.18140354	3.90796939	2.13480631	6.40062648
O	12.40769762	0.85861679	0.20457164	6.39718481
H	5.7124141	12.60646863	-0.35097108	0.89587306
H	7.48526167	10.72396491	0.26767869	0.89726655
H	9.33322777	14.54194526	0.85497473	0.77237294
H	12.46903476	10.92358126	2.60666744	0.90851087
H	14.45586538	12.68748999	2.45489909	0.91297648
H	14.90871786	17.69993072	0.22084613	0.89592337
H	13.13246174	19.63087552	-0.15828195	0.89888566
H	11.00162436	16.01748005	0.7067674	0.77321877
H	7.71654622	19.86964664	-0.35341343	0.91047156
H	5.77010167	18.07039976	-0.4457364	0.91655256
H	5.00716081	14.43209571	1.77214314	0.91705339
H	2.53720366	14.49459484	1.6990179	0.91047455
H	2.70890598	16.40200893	-2.20280617	0.91687563

H	5.1888643	16.24943985	-2.16509204	0.92144968
H	8.29077922	10.24765308	2.63003206	0.92025728
H	8.22113618	7.77933904	2.703805	0.9205608
H	11.6897319	7.61548075	0.07180619	0.92168926
H	11.76637126	10.06672644	0.03097383	0.91836335
H	15.45444399	16.72431278	2.49301666	0.92416084
H	17.92499872	16.62570506	2.41394491	0.92188896
H	17.69926263	13.16263802	-0.20177806	0.91252317
H	15.22320563	13.31593228	-0.19355733	0.91961206
H	11.46299648	20.45775811	-1.73833154	0.92065867
H	11.58681111	22.92625882	-1.53971005	0.9180853
H	9.22646431	22.74801011	2.11232856	0.92353188
H	9.18657725	20.28848684	1.95761548	0.92006636
H	19.86822494	16.7571179	0.62531415	0.96190552
H	26.2142851	13.77331542	0.5320742	0.96262187
H	11.73079241	5.56252886	0.84450803	0.95662051
H	8.12372561	1.37377166	1.88861536	0.90530969
H	12.43589628	3.38878534	0.38826785	0.90681609
H	8.78765431	-0.80026221	1.29846624	0.9543348
H	8.37804773	4.87736294	2.13474368	0.66810457
H	12.22575972	-0.11265173	0.20492024	0.66719358
C	22.37733642	13.34835673	4.60206081	4.04310074
C	22.92016298	12.03064291	4.61333362	3.73868931
C	24.29865553	11.8366361	4.42025207	4.20204776
C	25.17290599	12.93247559	4.21874605	4.05549875
C	24.61225955	14.24262202	4.13494257	3.73465424
C	23.23343955	14.43432403	4.32600527	4.19990999
H	24.7313891	10.82608134	4.46473596	0.91466339
H	22.79256304	15.44082601	4.29319905	0.91421864
O	25.49000735	15.2748767	3.86484317	6.27237173
O	22.008929	11.01628519	4.85862023	6.27866954
C	24.97139893	16.63642342	3.78174692	3.85914713
C	26.07224813	17.49884813	3.26394987	3.95602794
C	27.39956135	17.14693147	2.98794891	4.14327675
N	27.95691862	18.28484863	2.49164365	4.77646263
N	27.06202946	19.27494375	2.47310292	5.15948986
N	25.90620841	18.81186971	2.93906797	5.22299929
C	29.3152296	18.48860343	2.04501265	4.08590985
C	30.31161239	18.42977772	3.22742942	3.90285935
C	29.97837687	19.40023561	4.37871904	4.12581691
C	31.28863718	20.11543451	4.71628688	4.11323266
C	32.36379735	19.3803222	3.92412343	3.97447937
N	31.64711736	18.81992145	2.79202568	5.32715202

C	22.36273129	9.63193551	4.56460563	3.85814877
C	21.20725207	8.77782661	4.97547009	3.95261218
C	20.31410306	8.95881969	6.04336624	4.15277184
N	19.53069439	7.84322409	6.0239488	4.78721008
N	19.8984918	7.03208012	5.02836887	5.16345557
N	20.91719496	7.58705243	4.38213793	5.20222031
C	18.48007194	7.4717609	6.94452324	4.06192654
C	17.09169632	8.0663664	6.56063748	3.9091364
C	16.42609428	7.35506426	5.3659685	4.14115482
C	15.46879758	6.3404816	5.98467612	4.11854146
C	15.26606779	6.78192004	7.44116015	3.97928727
N	16.16772402	7.90771068	7.68448629	5.34000261
H	24.08813525	16.67579134	3.09712576	0.95707048
H	24.62699188	16.97079004	4.79472649	0.95976108
H	23.28187545	9.33879687	5.13694537	0.96518491
H	22.58996639	9.51858942	3.47898365	0.94570832
H	20.18817321	9.77329634	6.76516621	0.8934874
H	27.95100548	16.21081137	3.11572754	0.88838755
H	18.43258055	6.36461445	6.9947589	0.91986386
H	18.75840853	7.82871773	7.95949448	0.93524029
H	29.57679302	17.70887321	1.29447976	0.93520865
H	29.36968859	19.47564062	1.5168228	0.90829236
H	17.2432408	9.15779722	6.35548145	0.96355696
H	17.16191039	6.87469459	4.69450843	0.93514898
H	15.87652489	8.09320522	4.74220904	0.9286094
H	14.51085467	6.29031988	5.43244624	0.9433609
H	15.89764467	5.32031627	5.94205836	0.94487431
H	14.21621836	7.08266269	7.64772137	0.95848085
H	15.48310473	5.93898469	8.14438029	0.9676846
H	30.3077554	17.36589019	3.62534159	0.9794403
H	29.57575687	18.84828333	5.2490097	0.94283226
H	29.19399725	20.12617781	4.09204161	0.93383448
H	32.84966646	18.59026199	4.56002258	0.9730473
H	33.18736714	20.05194215	3.5846427	0.96794809
H	31.50138027	20.11527568	5.80176754	0.94693793
H	31.23894012	21.17989778	4.41179249	0.94651347
H	32.16012492	18.06934778	2.29563461	0.81390951
H	15.65250449	8.78073573	7.89466614	0.81690811
C	21.65855796	15.47733884	0.76406212	4.05278843
C	22.23618855	14.18160995	0.90458412	3.74051468
C	23.61965704	14.0061809	0.74489396	4.19952547
C	24.46116579	15.08350194	0.40524238	4.04903364
C	23.88904392	16.38229513	0.26240236	3.73130335

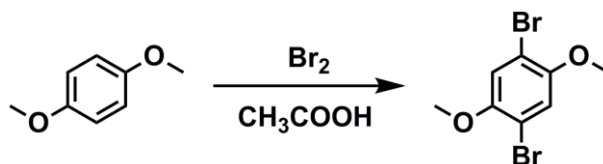
C	22.50894228	16.56721545	0.45903615	4.20731671
H	24.08273491	13.01710749	0.86814298	0.91487722
H	22.05651058	17.56373873	0.34798243	0.91430538
O	24.77328569	17.38152975	-0.07462799	6.2679388
O	21.38367072	13.13191486	1.20087179	6.27353913
C	24.3293083	18.76697388	-0.16512482	3.85616062
C	25.51503055	19.55269667	-0.61889736	3.94535796
C	26.84729308	19.12521466	-0.70712932	4.13815665
N	27.5211523	20.20727914	-1.18164086	4.78315836
N	26.68387876	21.23007171	-1.38188325	5.16849152
N	25.45778109	20.84649412	-1.04056132	5.21375424
C	28.9260026	20.30553502	-1.50515099	4.0546546
C	29.58841535	21.51604497	-0.80726389	3.90990935
C	31.01768933	21.77799452	-1.30381231	4.12419064
C	31.7416002	22.34190993	-0.08831594	4.11800594
C	31.05490784	21.66774269	1.09758874	3.9880826
N	29.70503184	21.31263924	0.64307773	5.33332129
C	21.92321482	11.78051634	1.06838924	3.85915982
C	20.83356023	10.81485821	1.37580047	3.96090948
C	19.7264578	10.98202733	2.21680753	4.14415186
N	19.10013178	9.77454336	2.19391659	4.77524518
N	19.75711212	8.91889303	1.40815382	5.15082814
N	20.81920294	9.53673281	0.90287585	5.22070036
C	17.89756515	9.38411614	2.88489793	4.05826444
C	16.63378501	10.09485296	2.33218704	3.91685476
C	16.42191114	9.88566403	0.8142826	4.12852219
C	14.96482229	9.4587027	0.66591597	4.1221058
C	14.6141132	8.85256423	2.0245847	3.97783473
N	15.43976703	9.56109655	2.9998317	5.34165273
H	23.48224059	18.85959517	-0.89027451	0.96126656
H	23.96261994	19.11222961	0.8345146	0.94915428
H	22.77689904	11.63957405	1.78338381	0.96653012
H	22.31824263	11.6265172	0.03564616	0.95424897
H	19.36409613	11.84118492	2.78622197	0.88866963
H	27.32628666	18.17285568	-0.45764855	0.88876082
H	17.79919049	8.28413684	2.7961608	0.91732858
H	18.00875191	9.61815564	3.96848698	0.93756762
H	29.42108973	19.35529854	-1.21465488	0.93620264
H	29.04224572	20.39840037	-2.61133819	0.93722612
H	16.72561694	11.18876645	2.56396553	0.96042298
H	17.09965041	9.10388349	0.41882491	0.93258594
H	16.6491121	10.80529749	0.24432957	0.94040989
H	14.32056645	10.33623264	0.45627379	0.94052594

H	14.81145299	8.75003503	-0.16922325	0.94478047
H	13.5404601	8.95133799	2.28434616	0.95781829
H	14.83866481	7.75542692	2.04331842	0.96924179
H	28.94306763	22.41447368	-1.01625454	0.95403602
H	31.03563583	22.46406719	-2.17105566	0.94200828
H	31.49707227	20.83615953	-1.64194162	0.94183715
H	31.00833804	22.32318078	1.99367092	0.9616205
H	31.61277883	20.74826504	1.41537148	0.95300844
H	31.61712514	23.4428943	-0.03925364	0.94565391
H	32.83103844	22.15436984	-0.11776772	0.93990945
H	28.96364534	21.81717507	1.16299444	0.81101428
H	14.90468319	10.31737614	3.46535711	0.8110463

### 2.4.3 Materials and Synthetic Procedures

Dehydrated *N,N*-dimethylformide (DMF), *N,N*-dimethylacetamide (DMAc), dehydrated tetrahydrofuran (THF), and *o*-dichlorobenzene (*o*-DCB) were purchased from Kanto Chemicals. Pyrrole, *p*-nitrobenzaldehyde, hydrobromic acid, *p*-toluenesulfonyl chloride, trifluoroacetic acid, toluene, dioxane, mesitylene, 1-butanol, ethanol, and acetic acid were purchased from Wako Chemicals. Propionic acid, propargyl bromide, 1,4-dimethoxybenzene, *N*-(*tert*-butoxycarbonyl)-L-prolinol, *tert*-butyl alcohol, propionaldehyde, valeraldehyde and benzoic acid were purchased from TCI. *trans-beta*-Nitrostyrene, *N,N*-diisopropylethylamine, *trans*-4-chloro-*beta*-nitrostyrene, *trans*-4-bromo-*beta*-nitrostyrene, *trans*-4-fluoro-*beta*-nitrostyrene, *trans*-2-chloro-*beta*-nitrostyrene, and *trans*-4-methoxy-*beta*-nitrostyrene were purchased from Sigma-Aldrich Co.

#### Synthesis of 1,4-dibromo-2,5-dimethoxybenzene



1,4-Dimethoxybenzene (40.0 g, 0.290 mol) was dissolved in acetic acid (80 mL), and bromine (100 g, 2.0 equiv) in acetic acid (30 mL) was slowly added at room temperature. The reaction was stirred for 2 h, and during this time the desired dibromide crystallized out. The reaction mixture was cooled to 0 °C, which induced crystallization. The white crystals were collected by filtration and then washed with cooled methanol.

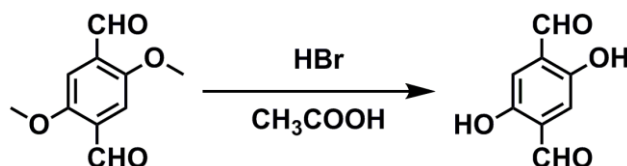
The mother liquid was diluted with water (0.8 L) and extracted with ethyl acetate (0.5 L), washed with 2 M NaOH (0.5 L), dried ( $\text{Na}_2\text{SO}_4$ ), filtered, and concentrated in vacuo to give a second crop. The combined crude product was recrystallized from MeOH to afford the 1,4-dibromo-2,5-dimethoxybenzene as a white crystalline crystals, yield: 87%.  $^1\text{H}$  NMR (400 MHz,  $\text{CDCl}_3$ ):  $\delta = 7.10$  (s, 2H, ArH), 3.84 (s, 6H,  $\text{OCH}_3$ ) ppm.

#### Synthesis of 2,5-dimethoxyterephthalaldehyde (DMTA)



*n*-Butyllithium 1.6 M in hexane (250 mL) was dropwise added to a solution of 1,4-dibromo-2,5-dimethoxybenzene (23.6 g, 80 mmol) in dry THF (dehydration with sodium, 140 mL) at  $-78\text{ }^\circ\text{C}$  under a argon atmosphere and stirred for 2 h at the same temperature. To this solution was added a further portion of dry THF (100 mL). To the reaction mixture was added 80 mL of DMF and the solution was stirred for 4h and hydrolysed with 200 mL of 3 M hydrochloric acid. The reaction mixture was allowed to warm to room temperature. The yellow precipitate was filtered by suction. After drying in vacuo, yellow crystals of the 2,5-dimethoxyterephthalaldehyde were obtained, yield: 50%.  $^1\text{H}$  NMR (400 MHz,  $\text{CDCl}_3$ ):  $\delta = 10.49$  (s, 2H, CHO), 7.45 (s, 2H, ArH), 3.94 (s, 6H,  $\text{OCH}_3$ ) ppm.

#### Synthesis of 2,5-dihydroxyterephthalaldehyde (DHTA)



100 mL of HBr (50% in water) added to a solution of 2,5-dimethoxyterephthalaldehyde (1.8 g, 9.3 mmol) in acetic acid (100 mL), then stirred and refluxed for 30 h (monitored by TLC). After reaction, the black precipitate was collected by filtration, washed with water to remove residual acid and then dried under vacuum at room temperature overnight. The filtrate was combined and extracted with chloroform for 5 times, evaporation of the solvent gave out dark yellow solid. Then

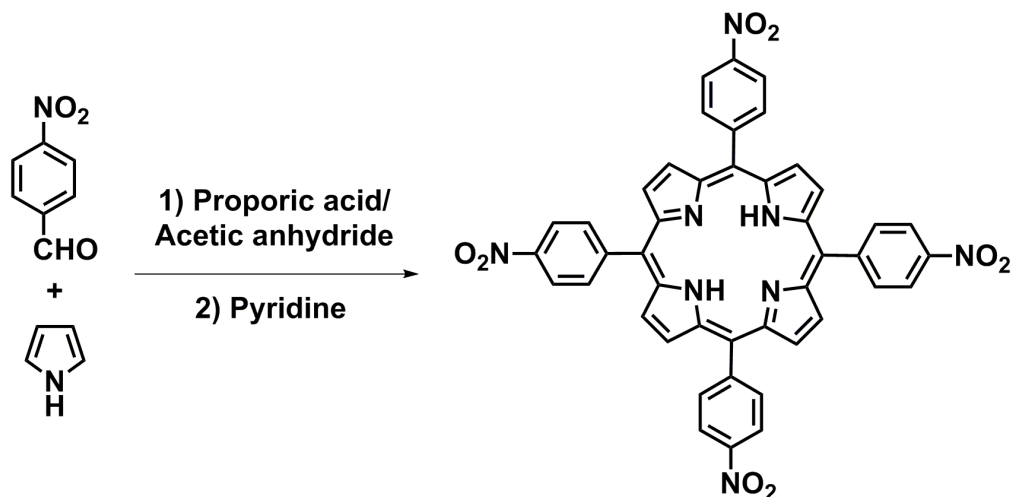
combine the black precipitate and the dark yellow solid, extracted with dichloromethane using Soxhlet extractor for two days. Evaporate the solution part gave out golden yellow solid, yield: 60%.  $^1\text{H}$  NMR (400 MHz,  $\text{CDCl}_3$ ):  $\delta = 10.22$  (s, 2H, CHO), 9.95 (s, 2H, OH), 7.23 (s, 2H, ArH) ppm.

#### Synthesis of 2,5-bis(2-propynyloxy)terephthalaldehyde (BPTA)



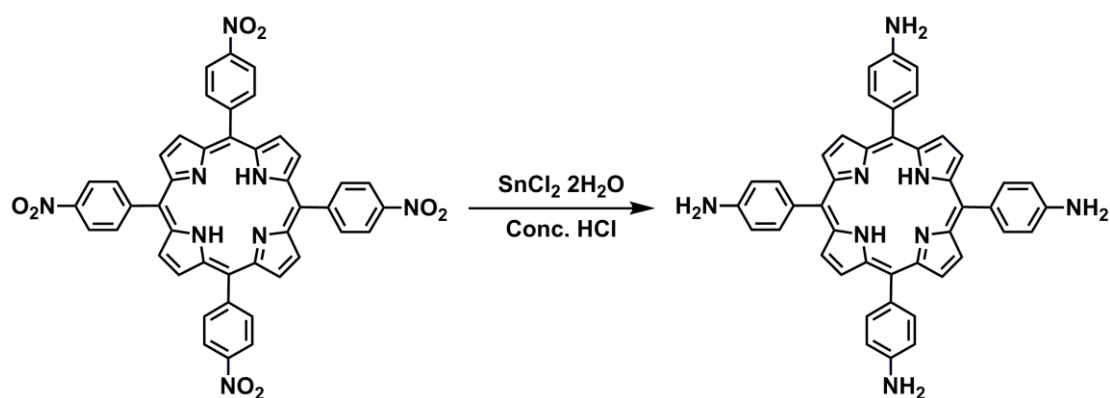
A flask was charged with 2,5-dihydroxyterephthalaldehyde (0.8 g, 4.8 mmol), anhydrous potassium carbonate (dried at 150 °C overnight, 1.32 g, 9.6 mmol) and 18-crown-6 (recrystallized in acetonitrile and dried under vacuum, 10 mg), degassed under vacuum to remove residual air for 0.5h and then filled with argon. 40 mL of DMF was injected and stirred at room temperature for 1h and then inject propargyl bromide (80% in toluene, 1.1 mL, 10 mmol). The reaction system was degassed by being subjected to three freeze–pump–thaw cycles and then stirred at room temperature (monitored by TLC). After reaction, the solution was poured into ice water and collected the white solid by filtration. Wash the precipitate with cold water (3 times) and cooled methanol (1 time), then collected and dried at vacuum. The product was purified by column chromatography (silica gel,  $\text{CH}_2\text{Cl}_2$ ), yield: 84%.  $^1\text{H}$  NMR (400 MHz,  $\text{CDCl}_3$ ):  $\delta = 10.49$  (s, 2H, CHO), 7.59 (s, 2H, ArH), 4.84 (d,  $J = 2.4$  Hz, 4H, CH<sub>2</sub>), 2.56 (t,  $J = 2.4$  Hz, 2H, CH) ppm.

#### Synthesis of 5,10,15,20-tetrakis(4-nitrophenyl)porphyrin



4-Nitrobenzaldehyde (11.0 g, 72.8 mmol) and acetic anhydride (12 mL, 127 mmol) was dissolved in propionic acid (300 mL). The solution was then refluxed, to which pyrrole (5.0 mL, 72 mmol) was dropwise added. After refluxing for 30 min, the resulting mixture was cooled to give a precipitate which was collected by filtration, washed with H<sub>2</sub>O (6 times) and methanol (3 times), and dried under vacuum. The resulting powder was dissolved in pyridine (80 mL) which was refluxed for 1 h. After cooling, the precipitate was collected by filtration and washed with acetone to give 5,10,15,20-tetrakis(4-nitrophenyl)porphyrin as a purple crystal, yield: 13%. The product was directly used for next step.

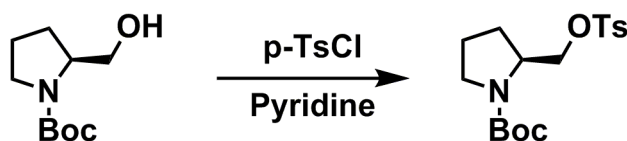
#### Synthesis of 5,10,15,20-Tetrakis(4-tetraaminophenyl)porphyrin (H<sub>2</sub>P)



5,10,15,20-tetrakis(4'-nitrophenyl)porphyrin (1.92 g, 2.41 mmol) was dissolved in hot HCl (240 mL) at 70 °C, to which was added SnCl<sub>2</sub>·2H<sub>2</sub>O (8.72 g, 38.6 mmol, 16 equiv). The resulting mixture was stirred at 70 °C for 2.5h and then cooled to 0 °C. After neutralization with aqueous NH<sub>3</sub>, the resulting gray product was collected by

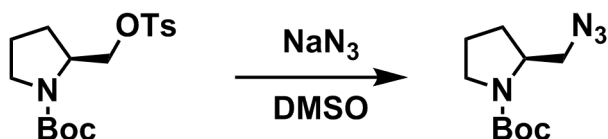
filtration, and then dried under vacuum. The crude product was dissolved in THF, and reflux for 0.5 h, then cooled to room temperature. Concentration in vacuum after filtration give out product as purple solid which was further recrystallized in acetone result purple crystals, yield: 92%.  $^1\text{H}$  NMR (400 MHz, DMSO):  $\delta$  = 8.84 (s, 8H, porphyrin-H), 7.81 (d,  $J$  = 8.8 Hz, 8H, ArH), 6.95 (d,  $J$  = 8.8 Hz, 8H, ArH), 5.53 (s, 8H,  $\text{NH}_2$ ) ppm.

#### Synthesis of *tert*-butyl (*S*)-2-((tosyloxy)methyl)pyrrolidine-1-carboxylate



In a 25 mL round-bottom flask, (*S*)-1-(*tert*-Butoxycarbonyl)-2-pyrrolidinemethanol (1.21g, 6 mmol) was dissolved in 6 mL of pyridine, and cooled down to 0 °C. Then *p*-toluenesulfonyl chloride (1.38g, 7.2 mmol) was added and the mixture was stirred at 0 °C for 24 h. After this time, the reaction mixture was diluted with 400 mL of diethyl ether and washed with 1M HCl (100 mL, 3 times), saturated  $\text{NaHCO}_3$  (100 mL, 2times) and water (100 mL, 6 times). The organic layer was dried with sodium sulfate, filtered and concentrated under reduced pressure, yielding yellow oil. The crude product was purified by flash chromatography through deactivated silica (2.5%  $\text{Et}_3\text{N}$  v/v) eluting with hexane-ethyl acetate 3:1. After evaporation of the solvents, the title product was obtained as colorless oil, yield: 94%.  $^1\text{H}$  NMR (400 MHz,  $\text{CDCl}_3$ ):  $\delta$  = 7.76 (d,  $J$  = 8 Hz, 2H, ArH), 7.33 (br, 2H, ArH), 4.13-3.80 (m, 3H, CH,  $\text{CH}_2$ ), 3.75-3.68 (m, 2H,  $\text{CH}_2$ ), 3.38-3.21 (m, 2H,  $\text{CH}_2$ ), 2.43 (s, 3H,  $\text{CH}_3$ ), 1.98-1.73 (m, 4H,  $\text{CH}_2$ ), 1.35 (s, 9H,  $\text{CH}_3$ ) ppm.

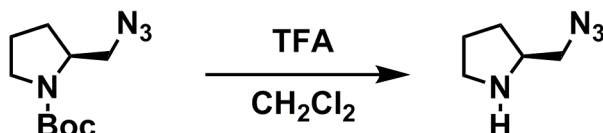
#### Synthesis of *tert*-butyl (*S*)-2-(azidomethyl)pyrrolidine-1-carboxylate



*tert*-butyl (*S*)-2-((tosyloxy)methyl)pyrrolidine-1-carboxylate (1.45 g, 4 mmol) was dissolved in DMSO (40 mL) and sodium azide (1.6 g, 24 mmol) was added and the resulting mixture was heated to 65 °C for 19 h. Then, it was allowed to cool to room

temperature, diluted with diethyl ether (300 mL), washed with H<sub>2</sub>O (100 mL, 5 times) and brine (50 mL, 2 times) and dried over Na<sub>2</sub>SO<sub>4</sub>. After removal of the solvent under reduced pressure, the title product was obtained as a colourless oil, yield: 88%. <sup>1</sup>H NMR (400 MHz, CDCl<sub>3</sub>):  $\delta$  = 3.98-3.82 (br, 1H, CH), 3.62-3.32 (br, 4H, CH<sub>2</sub>), 2.04-1.76 (br, 4H, CH<sub>2</sub>), 1.46 (s, 9H, CH<sub>3</sub>) ppm.

#### Synthesis of (*S*)-2-(azidomethyl)pyrrolidine



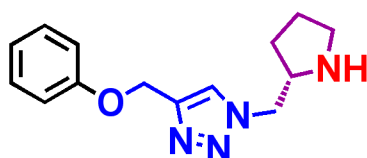
To a solution of *tert*-butyl (*S*)-2-(azidomethyl)pyrrolidine-1-carboxylate (0.68g, 3 mmol) in CH<sub>2</sub>Cl<sub>2</sub> (7.5 mL) was added dropwise trifluoroacetic acid (7.5 mL) at 0 °C. The mixture was warmed to room temperature and stirred overnight. After removal of the organic solvents under vacuo, the residue was dissolved in CH<sub>2</sub>Cl<sub>2</sub> (7.5 mL) and then treated with saturated NaHCO<sub>3</sub> solution (20 mL) for 4h at room temperature. The aqueous layer was extracted (10 mL, 3 times) and the combined extracts were dried over anhydrous Na<sub>2</sub>SO<sub>4</sub>. Concentration in vacuo after filtration gave out azide product as yellow oil, yield: 70%. NMR (400 MHz, CDCl<sub>3</sub>):  $\delta$  = 3.34-3.25 (m, 3H, CH<sub>2</sub>, CH), 3.00-2.89 (m, 2H, CH<sub>2</sub>), 1.90-1.72 (m, 3H, CH<sub>2</sub>), 1.38-1.47(m, 1H, CH<sub>2</sub>) ppm.

**[HC≡C]<sub>x</sub>-H<sub>2</sub>P-COFs.** An *o*-DCB/BuOH (0.5 mL / 0.5 mL) mixture of H<sub>2</sub>P (0.022 mmol, 14.9 mg) and DHTA/BPTA (total 0.044 mmol) at different molar ratios of 100/0, 75/25, 50/50, 25/75, and 0/100 in the presence of acetic acid catalyst (3 M, 0.1 mL) in a Pyrex tube (10 mL) was degassed by three freeze–pump–thaw cycles. The tube was sealed off by flame and heated at 120 °C for 3 days.

The precipitate was collected *via* centrifuge, washed with THF for 6 times, and washed with acetone 3 times. The powder was dried at 120 °C under vacuum overnight to give the corresponding COFs in isolated yields of 80%, 72%, 69%, 86%, and 80% for the H<sub>2</sub>P-COF, [HC≡C]<sub>25</sub>-H<sub>2</sub>P-COF, [HC≡C]<sub>50</sub>-H<sub>2</sub>P-COF, [HC≡C]<sub>75</sub>-H<sub>2</sub>P-COF, and [HC≡C]<sub>100</sub>-H<sub>2</sub>P-COF, respectively. The amorphous nonporous polymers 1 and 2 were synthesized in DMAc, according to this method under otherwise same conditions. The

ethynyl contents in the COFs as estimated by considering the elemental analysis results together with particle size and remained edges units were close to the theoretical results.

**[Pyr]<sub>x</sub>-H<sub>2</sub>P-COFs.** A toluene/*tert*-butanol (0.8 mL / 0.2 mL) mixture of [HC≡C]<sub>25</sub>-H<sub>2</sub>P-COF (20 mg) in the presence of CuI (2 mg) and DIPEA (40 μL) in a Pyrex tube (10 mL) was added with (*S*)-2-(azidomethyl)pyrrolidine (toluene solution; 1 M; 21 μL). The tube was degassed *via* three freeze–pump–thaw cycles and the mixture was stirred at room temperature for 24 h. The precipitate was collected *via* centrifuge, washed with ethanol 5 times, and dried at room temperature under vacuum, to produce [Pyr]<sub>25</sub>-H<sub>2</sub>P-COF as a deep brown solid in quantitative yield. The ethynyl groups were quantitatively reacted with the azide units as evident by the IR spectra. The click reaction of [HC≡C]<sub>x</sub>-H<sub>2</sub>P-COFs (X = 50, 75, and 100) with (*S*)-2-(azidomethyl)pyrrolidine were performed according to this method under otherwise same conditions.



**Control: (*S*)-4-(Phenoxymethyl)-1-(pyrrolidin-2-ylmethyl)-1H-1,2,3-triazole**

**(*S*)-4-(Phenoxymethyl)-1-(pyrrolidin-2-ylmethyl)-1H-1,2,3-triazole.** The click reaction to synthesize this monomeric catalyst control was prepared according to the above procedure for [Pyr]<sub>x</sub>-H<sub>2</sub>P-COF, using phenyl propargyl ether (toluene solution; 1M, 80 μL) in place of [HC≡C]<sub>x</sub>-H<sub>2</sub>P-COFs as a reactant.

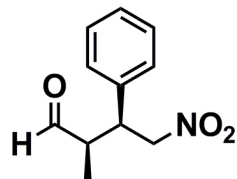
**Michael addition reaction.** To an EtOH/H<sub>2</sub>O (1/1 *v/v* 0.5 mL) suspension of [Pyr]<sub>25</sub>-H<sub>2</sub>P-COF was added with aldehyde (1.0 mmol), nitrostyrene (0.1 mmol), and benzoic acid (0.1 mmol). The mixture was stirred at room temperature for a period to reach 100% conversion. After addition of EtOH, the organic layer was removed *via* centrifuge. The catalyst was washed with EtOH twice and with ethyl acetate 3 times, the organic layer was then combined and concentrated under reduced pressure. <sup>1</sup>H-NMR spectra were utilized to calculate diastereomeric ratio (dr). The enantiomeric excess (ee) was determined by HPLC on a chiral phase chiralpak AD-H or OD-H column.

**Recycle procedure of [Pyr]<sub>25</sub>-H<sub>2</sub>P-COF.** The COF catalyst was recovered *via* centrifuge, washed with ethyl acetate and a mixture of triethylamine/ethanol solution (5% v) to remove the product and reactants and simply dried before reuse.

#### 2.4.4 Characterization of Products

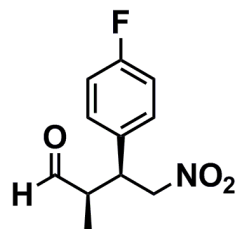
All Michael addition products are known compounds.

(2R,3S)-2-Methyl-4-nitro-3-phenylbutanal<sup>[58]</sup>



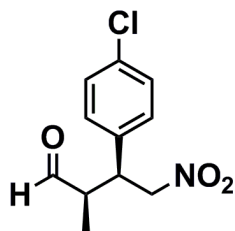
Major diastereomer: <sup>1</sup>H NMR (400 MHz, CDCl<sub>3</sub>):  $\delta$  = 9.71 (d,  $J$  = 2 Hz, 1H), 7.35-7.28 (m, 3H), 7.20-7.16 (m, 2H), 4.82-4.64 (m, 2H), 3.85-3.77 (m, 1H), 2.82-2.74 (m, 1H), 0.99 (d,  $J$  = 7.2 Hz, 3H). HPLC conditions: The enantiomeric excess was determined by HPLC (Chiralcel OD-H), hexane : *i*-PrOH = 90 : 10, UV = 214 nm, 1.0 mL min<sup>-1</sup>, syn:  $t_R$  = 22.4 min (major) and  $t_R$  = 17.6 min (minor).

(2R,3S)-3-(4-Fluorophenyl)-2-methyl-4-nitrobutanal<sup>[59]</sup>



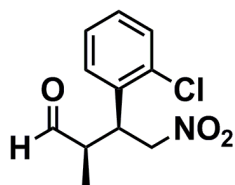
Major diastereomer: <sup>1</sup>H NMR (400 MHz, CDCl<sub>3</sub>):  $\delta$  = 9.70 (d,  $J$  = 1.6 Hz, 1H), 7.20-7.12 (m, 2H), 7.05-7.00 (m, 2H), 4.80-4.60 (m, 2H), 3.83-3.76 (m, 1H), 2.81-2.72 (m, 1H), 1.00 (d,  $J$  = 7.2 Hz, 3H). HPLC conditions: The enantiomeric excess was determined by HPLC (Chiralcel AD-H), hexane : *i*-PrOH = 98 : 2, UV = 214 nm, 1.0 mL min<sup>-1</sup>, syn:  $t_R$  = 33.9 min (major) and  $t_R$  = 47.0 min (minor).

(2R, 3S)-3-(4-Chlorophenyl)-2-methyl-4-nitrobutanal<sup>[55]</sup>



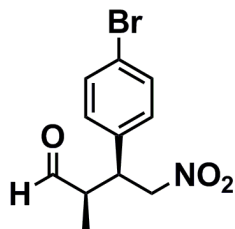
Major diastereomer:  $^1\text{H NMR}$  (400 MHz,  $\text{CDCl}_3$ ):  $\delta = 9.68$  (d,  $J = 1.2$  Hz, 1H), 7.33-7.29 (m, 2H), 7.16-7.09 (m, 2H), 4.80-4.60 (m, 2H), 3.81-3.75 (m, 1H), 2.81-2.72 (m, 1H), 1.00 (d,  $J = 7.2$  Hz, 3H). HPLC conditions: The enantiomeric excess was determined by HPLC (Chiralcel AD-H), hexane : *i*-PrOH = 98 : 2, UV = 214 nm, 1.0 ml min $^{-1}$ , syn:  $t_R = 41.1$  min (major) and  $t_R = 60.5$  min (minor).

(2R,3S)-3-(2-Chlorophenyl)-2-methyl-4-nitrobutanal<sup>[54]</sup>



Major diastereomer:  $^1\text{H NMR}$  (400 MHz,  $\text{CDCl}_3$ ):  $\delta = 9.73$  (d,  $J = 1.6$  Hz, 1H), 7.42-7.39 (m, 1H), 7.26-7.18 (m, 3H), 4.86-4.74 (m, 2H), 4.35-4.28 (m, 1H), 3.04-2.93 (m, 1H), 1.02 (d,  $J = 7.2$  Hz, 3H). HPLC conditions: The enantiomeric excess was determined by HPLC (Chiralcel AD-H), hexane : *i*-PrOH = 98 : 2, UV = 214 nm, 1.0 mL min $^{-1}$ , syn:  $t_R = 20.83$  min (major) and  $t_R = 38.0$  min (minor).

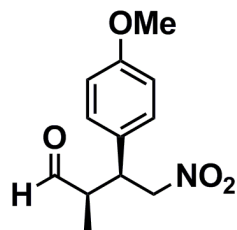
(2R,3S)-3-(4-Bromophenyl)-2-methyl-4-nitrobutanal<sup>[53]</sup>



Major diastereomer:  $^1\text{H NMR}$  (400 MHz,  $\text{CDCl}_3$ ):  $\delta = 9.68$  (d,  $J = 1.2$  Hz, 1H), 7.48-7.45 (m, 2H), 7.10-7.04 (m, 2H), 4.80-4.60 (m, 2H), 3.82-3.74 (m, 1H), 2.81-2.70 (m, 1H), 0.99 (d,  $J = 7.2$  Hz, 3H). HPLC conditions: The enantiomeric excess was

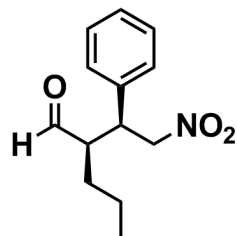
determined by HPLC (Chiralcel AD-H), hexane : *i*-PrOH = 98 : 2, UV = 214 nm, 1.0 ml min<sup>-1</sup>, syn:  $t_R = 24.16$  min (major) and  $t_R = 33.93$  min (minor).

(2R,3S)-3-(4-Methoxyphenyl)-2-methyl-4-nitrobutanal<sup>[55]</sup>



Major diastereomer: <sup>1</sup>H NMR (400 MHz, CDCl<sub>3</sub>):  $\delta = 9.69$  (d,  $J = 1.2$  Hz, 1H), 7.12-7.04 (m, 2H), 6.86-6.83 (m, 2H), 4.77-4.59 (m, 2H), 3.77 (s, 3H), 3.78-3.69 (m, 1H), 2.78-2.68 (m, 1H), 0.99 (d,  $J = 7.6$  Hz, 3H). HPLC conditions: The enantiomeric excess was determined by HPLC (Chiralcel OD-H), hexane : *i*-PrOH = 80 : 20, UV = 214 nm, 1.0 mL min<sup>-1</sup>, syn:  $t_R = 23.17$  min (major) and  $t_R = 20.77$  min (minor).

(R)-2-((S)-2-Nitro-1-phenylethyl)pentanal<sup>[54]</sup>



Major diastereomer: <sup>1</sup>H NMR (400 MHz, CDCl<sub>3</sub>):  $\delta = 9.69$  (d,  $J = 3.6$  Hz, 1H), 7.34-7.28 (m, 3H), 7.17-7.15 (m, 2H), 4.70-4.60 (m, 2H), 3.79-3.73 (m, 1H), 2.72-2.66 (m, 1H), 1.48-1.13 (m, 4H), 0.79 (t,  $J = 7.2$  Hz, 3H). HPLC conditions: The enantiomeric excess was determined by HPLC (Chiralcel OD-H), hexane : *i*-PrOH = 90 : 10, UV = 214 nm, 1.0 mL min<sup>-1</sup>, syn:  $t_R = 23.29$  min (major) and  $t_R = 20.45$  min (minor).

## 2.5 References

- [1] Cote, A. P.; Benin, A. I.; Ockwig, N. W.; O'Keeffe, M.; Matzger, A. J.; Yaghi, O. M., *Science* **2005**, 310, 1166-1170.
- [2] Wan, S.; Guo, J.; Kim, J.; Ihee, H.; Jiang, D., *Angew. Chem. Int. Ed.* **2008**, 47, 8826-8830.
- [3] Wan, S.; Guo, J.; Kim, J.; Ihee, H.; Jiang, D., *Angew. Chem. Int. Ed.* **2009**, 48, 5439-5442.
- [4] Ding, X.; Guo, J.; Feng, X.; Honsho, Y.; Guo, J.; Seki, S.; Maitarad, P.; Saeki, A.; Nagase, S.; Jiang, D., *Angew. Chem. Int. Ed.* **2011**, 50, 1289-1293.
- [5] Feng, X.; Chen, L.; Dong, Y.; Jiang, D., *Chem. Commun.* **2011**, 47, 1979-1981.
- [6] Ding, X.; Feng, X.; Saeki, A.; Seki, S.; Nagai, A.; Jiang, D., *Chem. Commun.* **2012**, 48, 8952-8954.
- [7] Feng, X.; Liu, L.; Honsho, Y.; Saeki, A.; Seki, S.; Irle, S.; Dong, Y.; Nagai, A.; Jiang, D., *Angew. Chem. Int. Ed.* **2012**, 51, 2618-2622.
- [8] Feng, X.; Dong, Y.; Jiang, D., *CrystEngComm* **2013**, 15, 1508.
- [9] Jin, S.; Ding, X.; Feng, X.; Supur, M.; Furukawa, K.; Takahashi, S.; Addicoat, M.; El-Khouly, M. E.; Nakamura, T.; Irle, S.; Fukuzumi, S.; Nagai, A.; Jiang, D., *Angew. Chem. Int. Ed.* **2013**, 52, 2017-2021.
- [10] Jin, S.; Furukawa, K.; Addicoat, M.; Chen, L.; Takahashi, S.; Irle, S.; Nakamura, T.; Jiang, D., *Chem. Sci.* **2013**, 4, 4505.
- [11] Chen, L.; Furukawa, K.; Gao, J.; Nagai, A.; Nakamura, T.; Dong, Y.; Jiang, D., *J. Am. Chem. Soc.* **2014**, 136, 9806-9809.
- [12] Jin, S.; Sakurai, T.; Kowalczyk, T.; Dalapati, S.; Xu, F.; Wei, H.; Chen, X.; Gao, J.; Seki, S.; Irle, S.; Jiang, D., *Chem. Eur. J.* **2014**, 20, 14608-14613.
- [13] Choi, Y. J.; Lee, J. W.; Choi, J. H.; Kang, J. K., *Appl. Phys. Lett.* **2008**, 92, 173102.
- [14] Garberoglio, G.; Vallauri, R., *Microporous Mesoporous Mater.* **2008**, 116, 540-547.
- [15] Han, S. S.; Furukawa, H.; Yaghi, O. M.; Goddard, W. A., 3rd, *J. Am. Chem. Soc.* **2008**, 130, 11580-11581.
- [16] Klontzas, E.; Tylianakis, E.; Froudakis, G. E., *J. Phys. Chem. C* **2008**, 112, 9095-9098.
- [17] Makhseed, S.; Samuel, J., *Chem. Commun.* **2008**, 4342-4344.
- [18] Cao, D.; Lan, J.; Wang, W.; Smit, B., *Angew. Chem. Int. Ed.* **2009**, 48, 4730-4733.
- [19] Furukawa, H.; Yaghi, O. M., *J. Am. Chem. Soc.* **2009**, 131, 8875-8883.
- [20] Han, S. S.; Mendoza-Cortes, J. L.; Goddard, W. A., 3rd, *Chem. Soc. Rev.* **2009**, 38, 1460-1476.
- [21] Assfour, B.; Seifert, G., *Microporous Mesoporous Mater.* **2010**, 133, 59-65.

- [22] Assfour, B.; Seifert, G., *Chem. Phys. Lett.* **2010**, 489, 86-91.
- [23] Li, F.; Zhao, J.; Johansson, B.; Sun, L., *Int. J. Hydrogen Energy* **2010**, 35, 266-271.
- [24] Zou, X.; Zhou, G.; Duan, W.; Choi, K.; Ihm, J., *J. Phys. Chem. C* **2010**, 114, 13402-13407.
- [25] Tyliaakis, E.; Klontzas, E.; Froudakis, G. E., *Nanoscale* **2011**, 3, 856-869.
- [26] Ganz, E.; Dornfeld, M., *J. Phys. Chem. C* **2012**, 116, 3661-3666.
- [27] Guo, J.-H.; Zhang, H.; Gong, M.; Cheng, X.-L., *Struct. Chem.* **2012**, 24, 691-703.
- [28] Guo, J.-H.; Zhang, H.; Liu, Z.-P.; Cheng, X.-L., *J. Phys. Chem. C* **2012**, 116, 15908-15917.
- [29] Kalidindi, S. B.; Oh, H.; Hirscher, M.; Esken, D.; Wiktor, C.; Turner, S.; Van Tendeloo, G.; Fischer, R. A., *Chem. Eur. J.* **2012**, 18, 10848-10856.
- [30] Kim, D.; Jung, D. H.; Kim, K.-H.; Guk, H.; Han, S. S.; Choi, K.; Choi, S.-H., *J. Phys. Chem. C* **2012**, 116, 1479-1484.
- [31] Yang, Z.; Cao, D., *J. Phys. Chem. C* **2012**, 116, 12591-12598.
- [32] Gao, T.-F.; Zhang, H., *Struct. Chem.* **2013**, 25, 503-513.
- [33] Guo, J. H.; Zhang, H.; Miyamoto, Y., *Phys. Chem. Chem. Phys.* **2013**, 15, 8199-8207.
- [34] Guo, J. H.; Zhang, H.; Tang, Y.; Cheng, X., *Phys. Chem. Chem. Phys.* **2013**, 15, 2873-2881.
- [35] Kalidindi, S. B.; Fischer, R. A., *Phys. Status Solidi* **2013**, 250, 1119-1127.
- [36] Kandambeth, S.; Shinde, D. B.; Panda, M. K.; Lukose, B.; Heine, T.; Banerjee, R., *Angew. Chem. Int. Ed.* **2013**, 52, 13052-13056.
- [37] Koenig, A. R. V.; Desgranges, C.; Delhommelle, J., *Mol. Simul.* **2013**, 40, 71-79.
- [38] Oh, H.; Kalidindi, S. B.; Um, Y.; Bureekaew, S.; Schmid, R.; Fischer, R. A.; Hirscher, M., *Angew. Chem. Int. Ed.* **2013**, 52, 13219-13222.
- [39] Das, G.; Balaji Shinde, D.; Kandambeth, S.; Biswal, B. P.; Banerjee, R., *Chem. Commun.* **2014**, 50, 12615-12618.
- [40] Li, L.-L.; Gao, T.-F.; Zhang, R.-Y.; Zhang, H., *Chin. Phys. Lett.* **2014**, 31, 097101.
- [41] Li, X.-D.; Guo, J.-H.; Zhang, H.; Cheng, X.-L.; Liu, X.-Y., *R. Soc. Chem. Adv.* **2014**, 4, 24526.
- [42] Li, X.-D.; Zang, H.-P.; Wang, J.-T.; Wang, J.-F.; Zhang, H., *J. Mater. Chem. A* **2014**, 2, 18554-18561.
- [43] Stegbauer, L.; Schwinghammer, K.; Lotsch, B. V., *Chem. Sci.* **2014**, 5, 2789.
- [44] Thote, J.; Aiyappa, H. B.; Deshpande, A.; Diaz Diaz, D.; Kurungot, S.; Banerjee, R., *Chem. Eur. J.* **2014**, 20, 15961-15965.
- [45] Doonan, C. J.; Tranchemontagne, D. J.; Glover, T. G.; Hunt, J. R.; Yaghi, O. M., *Nature Chem.* **2010**, 2, 235-238.

- [46] Ding, S. Y.; Gao, J.; Wang, Q.; Zhang, Y.; Song, W. G.; Su, C. Y.; Wang, W., *J. Am. Chem. Soc.* **2011**, 133, 19816-19822.
- [47] Nagai, A.; Guo, Z.; Feng, X.; Jin, S.; Chen, X.; Ding, X.; Jiang, D., *Nature Commun.* **2011**, 2, 536.
- [48] Gadzikwa, T.; Farha, O. K.; Malliakas, C. D.; Kanatzidis, M. G.; Hupp, J. T.; Nguyen, S. T., *J. Am. Chem. Soc.* **2009**, 131, 13613-13615.
- [49] Lee, J.; Farha, O. K.; Roberts, J.; Scheidt, K. A.; Nguyen, S. T.; Hupp, J. T., *Chem. Soc. Rev.* **2009**, 38, 1450-1459.
- [50] Kaur, P.; Hupp, J. T.; Nguyen, S. T., *Acs Catalysis* **2011**, 1, 819-835.
- [51] Chen, X.; Addicoat, M.; Irle, S.; Nagai, A.; Jiang, D., *J. Am. Chem. Soc.* **2013**, 135, 546-549.
- [52] MacMillan, D. W., *Nature* **2008**, 455, 304-308.
- [53] Hayashi, Y.; Gotoh, H.; Hayashi, T.; Shoji, M., *Angew. Chem. Int. Ed.* **2005**, 44, 4212-4215.
- [54] Wang, C. A.; Zhang, Z. K.; Yue, T.; Sun, Y. L.; Wang, L.; Wang, W. D.; Zhang, Y.; Liu, C.; Wang, W., *Chem. Eur. J.* **2012**, 18, 6718-6723.
- [55] Zhao, L.; Shen, J.; Liu, D.; Liu, Y.; Zhang, W., *Org. Biomol. Chem.* **2012**, 10, 2840-2846.
- [56] Aradi, B.; Hourahine, B.; Frauenheim, T., *J. Phys. Chem. A* **2007**, 111, 5678-5684.
- [57] <http://www.dftb.org>
- [58] Betancort, J. M.; Barbas, C. F., 3rd, *Org. Lett.* **2001**, 3, 3737-3740.
- [59] Husmann, R.; Jorres, M.; Raabe, G.; Bolm, C., *Chem. Eur. J.* **2010**, 16, 12549-12552.

**Chapter 3.**  
**Construction of High Crystalline Meso-  
Porous Imine-based Covalent Organic  
Frameworks**

*Preparing Manuscript*

Hong Xu, Hao Wei, Jia Gao and Donglin Jiang

## **Abstract**

A synthetic discovery for the novel mesoporous imine COF which combines high crystallinity, porosity and excellent stabilities was described. The high crystalline structure feature endows this COF highly ordered one-dimensional nano-channel arrays with a channel size of 3.3nm, extremely high surface area which is up to the theoretical values; meanwhile, benefit from the high crystallinity, such COF material possess an exceptional chemical stability. This discovery makes a breakthrough in the field of crystalline frameworks, providing an efficient solution to the contradiction of high performance with high stability.

### 3.1 Introduction

Covalent organic frameworks (COFs) are a class of crystalline porous polymers that enable the atomically precise integration of building blocks into periodicities.<sup>[1]</sup> They have attracted intensive research interest in the past decade, because of their high surface area, highly order crystalline structure together with tunable chemical and physical properties. As predesignable porous materials, COFs have been emerged as new candidates for gas adsorption and storage.<sup>[2-34]</sup> Meanwhile, because of their unique topology and stacking layer structures, 2D COFs possess highly ordered columnar arrays throughout their building blocks, which are difficult to achieve in traditional linear polymers, supramoleculars or porous materials. Under this notion, various  $\pi$ -electronic two-dimensional frameworks have been developed, which shows unique semiconducting, photo-conducting, and charge transfer properties.<sup>[35-45]</sup> On the other hand, highly ordered skeletal alignment, high surface area together with open-channel structure of the 2D COFs provides an intriguing motif for exploring well-defined nanoreactors, thus, exhibit a high potential to develop high-performance heterogeneous catalysts.<sup>[46]</sup>

Despite the great potential in the field of gas storage, photo-electricity and heterogeneous catalysis; essentially, COFs are designed and synthesized under the principle of dynamic covalent chemistry (DCC)<sup>[47-48]</sup>, in which chemical reactions were carried out reversibly under the conditions of thermodynamic control. The reversible nature of the reactions could introduce the mechanisms of "error checking" and "proof-reading" during synthetic process. Synthesis of covalent linked polymers has generally been dominated by kinetically controlled reactions, which irreversibly form covalent bonds. In contrast, dynamic covalent chemistry leads to the reversible formation of covalent bonds, which can be formed, broken, and reformed. Therefore, unlike conventional covalent bond formation, DCC is thermodynamically controlled and offers reversible reaction systems with "error checking" and "proof-reading" characteristics, leading to the formation of the most thermodynamically stable structures. By utilizing DCC concept for the construction of COF materials, the

polymer skeleton formation occurs alongside the crystallization process, while the self-healing feedback reduces the incidence of structural defects and assists in the formation of ordered structure. Reactions involved in COF formation is reversible, which makes COF a crystalline material but less stable, compare with conventional covalent linked polymers.

The first class of COFs are boroxine<sup>[1, 40, 49]</sup> or boronate-ester based COF,<sup>[1, 35, 42, 44, 49-60]</sup> which shows high crystallinity and porosity because of the high reversibility of the boroxine or boronate-ester formation reactions. However, all of them are not stable in the presence of water or other protonic solvents. Utilizing less reversible formation reactions, the second class of COFs, including imine-<sup>[40, 61]</sup> hydrazone-<sup>[15, 62-63]</sup>, triazine-<sup>[64-66]</sup> phenazine-<sup>[67]</sup> and azine-<sup>[68]</sup>linked COFs, has been developed, which showed improved stability compared with the first class of COFs. However, almost all of them suffer from low crystallinity and poor surface area which largely limit their practical applications. As a result, the reversible problem makes the high performance seem to be incompatible to stabilities in COF system.

In this Chapter, we will challenge this contradiction by a synthetic discovery of highly crystallized imine-COF which owns a chemical robust nature but shows high crystallinity. The high crystalline structure endows extremely high surface area and also benefits the chemical stability, the novel COF exhibits remarkable stability under harsh conditions, such as strong acid or base conditions.

## 3.2 Results and Discussions

### 3.2.1 Synthesis and Structural Characterization

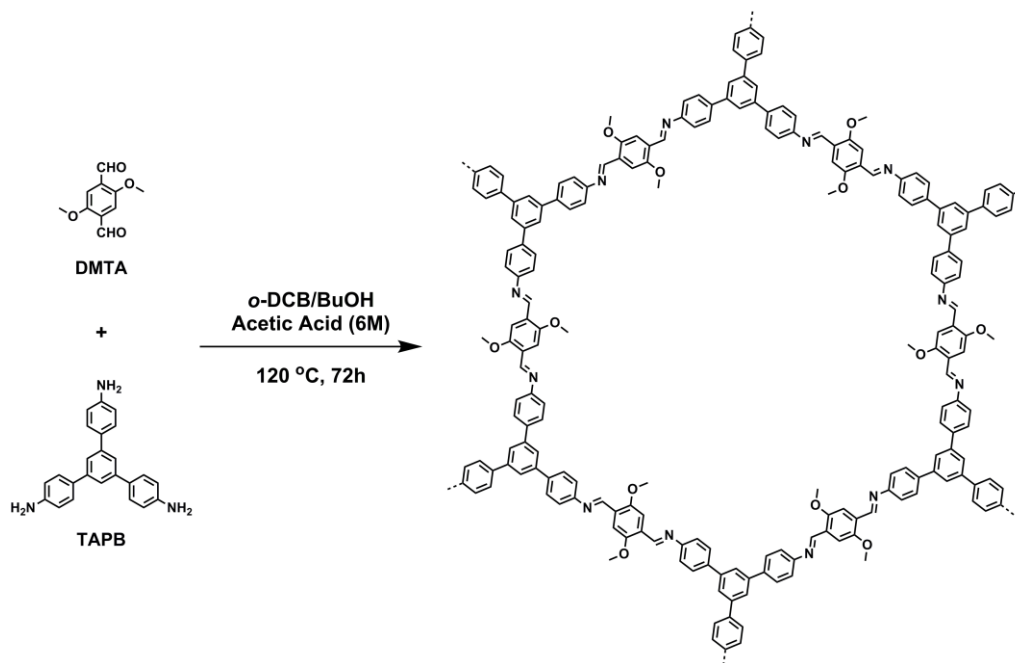


**Figure 1.** Synthesis of TPB-DMTP-COF via condensation of 2,5-dimethoxy terephthalaldehyde (DMTA) and 1,3,5-tri(4-aminophenyl) benzene (TAPB).

**Figure 1** shows the structure of a 2D imine COF with a pore size of 3.3nm. We selected C3-symmetric 1,3,5-tri(4-aminophenyl) benzene (TAPB) and C2-symmetric 2,5-dimethoxyterephthalaldehyde (DMTA) as building blocks for the topological ring fusion reaction and prepared the crystalline imine-linked mesoporous COF in isolated yields of 81% under solvothermal conditions. The TPB-DMTP-COF was purified by being washed with tetrahydrofuran (THF), and then soaked in THF for 1 day to remove trapped guest molecules, after that dried under vacuum at 120 °C for 8h.

The introduction of the methoxy- group in DMTA could largely enhance the crystallinity of the mesoporous 2D COF. Utilizing different co-solvent system, such as *o*-DCB/*n*-BuOH or mesitylene/1,4-dioxane with various volume ratio could give out high crystalline COF (**Figure 2a**), even ultrasonic-treating monomer solution at room temperature could lead to COF with a moderate

crystallinity (**Figure 2b**). Generally, the ultrasonic treatment is considered to be a harsh conditions to COFs which will destroy the crystals into disordered fragments or oligomers. However, the TPB-DMTP-COF seems to have a high trend to crystallize, it could form crystalline COF in such local heating but ‘disorder-inducing’ conditions.

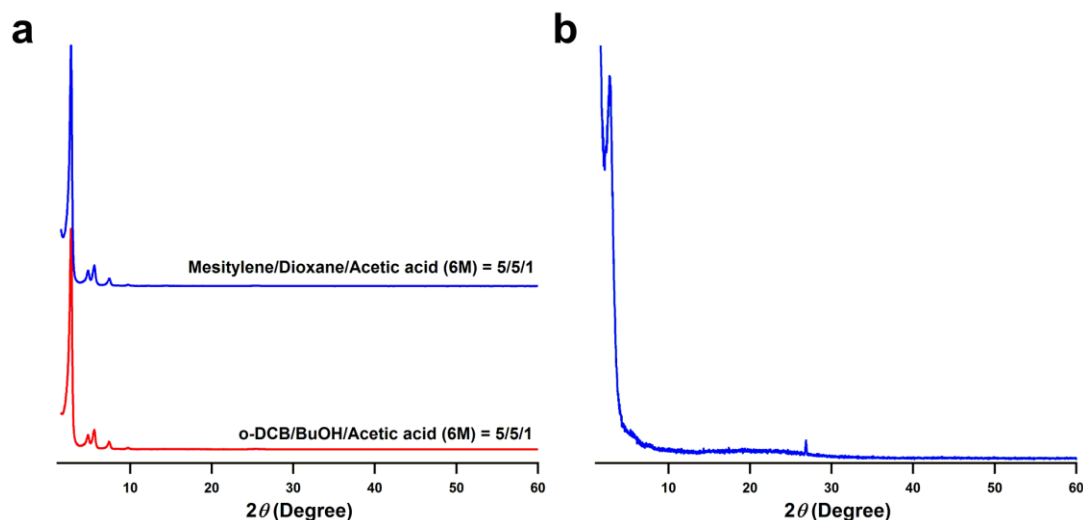


**Figure 2.** PXRD of TPB-DMTP-COF **a.** synthesized in Mesitylene/Dioxane co-solvents and o-DCB/BuOH co-solvents under solvothermal conditions; **b.** synthesized in o-DCB/BuOH co-solvents via ultrasonic treatment.

To investigate the reason of high crystallinity of TPB-DMTP-COF, I further synthesized two analogues, change the substituent group from methoxyl- group in the 2,5-dimethoxyterephthalaldehyde monomer into methyl- group (2,5-dimethylterephthalaldehyde, mark the corresponding COF as COF-Me) and non-substituent (terephthalaldehyde, mark the corresponding COF as COF-Non), and synthesize these two COFs in similar conditions. However, I found that these two COFs showed much lower crystallinity compared to TPB-DMTP-COF, although many solvothermal conditions were carefully optimized. The best results from these three COF were summarized in **Figure 3**, the significant difference in crystallinity suggests that these two COFs have much lower crystallinity than TPB-DMTP-COF; and the non- substituent case has the worst crystallinity, just about  $5 \times 10^3$  cps in intensity which almost could not considered

to be a COF because the amorphous part take the major in such materials. These three COFs own same topological design and skeletons, just slightly difference in the substituent groups in the linker monomers, however, it lead to significant difference in the crystallinity, in Section 3.2.2 I will simulate the crystalline structure of these COFs and explain the reason for this phenomenon.

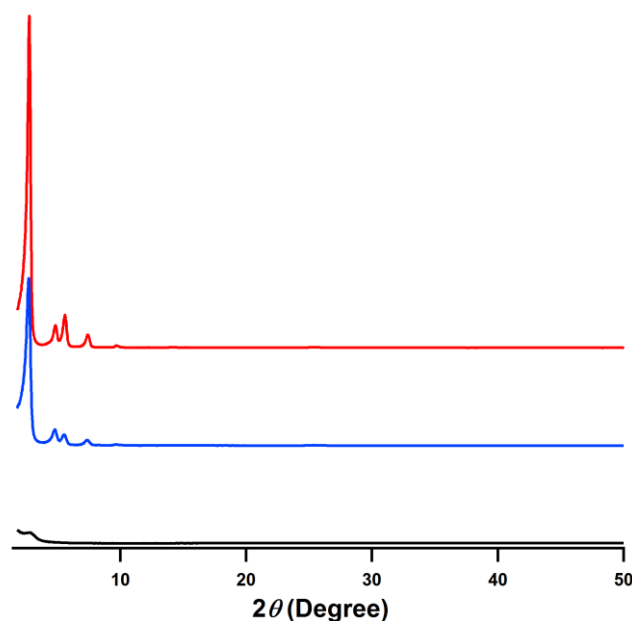


**Figure 3.** The effect of the substituent groups to crystallinity: red, TPB-DMTP-COF, intensity of the main peak ( $2.76^\circ$ ) is about  $135 \times 10^3$  cps; Blue, COF-Me, intensity of the main peak ( $2.76^\circ$ ) is about  $68 \times 10^3$  cps; TPB-DMTP-COF (methoxyl- substituted COF), intensity of the main peak ( $2.76^\circ$ ) is about  $5 \times 10^3$  cps.

### 3.2.2 PXRD Pattern and Theoretical Calculation

We investigated the crystal structure of TPB-DMTP-COF by using X-ray diffraction (XRD) measurements in conjunction with computational structural simulations. The TPB-DMTP-COF exhibited clearly six diffraction peaks with the main one at  $2.76^\circ$  together with other five peaks at  $4.82$ ,  $5.60$ ,  $7.42$ ,  $9.70$ , and  $25.2^\circ$ , which were assigned to the 100, 110, 200, 210, 300, and 001 facets, respectively (**Figure 4a**, blue curve). A significant feature is that TPB-DMTP-COF has much more XRD peaks than conversional imine-linked COFs and exhibits an exceptional intensity of its main

signal as high as  $135 \times 10^3$  cps, which is much higher than other COFs. Pawley refinement (green curve) confirmed the diffraction assignments and gave a good match to the observed XRD pattern, as evidenced by their negligible difference (orange curve). Crystalline structure simulations using the Reflex Plus module of the Materials Studio version 4.4 suite of programs produced unit-cell parameters of  $a = b = 37.2 \text{ \AA}$ ,  $c = 3.5 \text{ \AA}$ ,  $\alpha = \beta = 90^\circ$ , and  $\gamma = 120^\circ$ . The lattice structures were built using a slipped AA stacking mode of the P3 space group, in which optimal atomic coordinates lead to adjacent sheets lying on top of each other with an offset of  $0.3\text{-\AA}$  along the a and b directions (**Figure 4b**), and a staggered AB-stacking mode, where the sheets are offset by  $\frac{1}{2}, \frac{1}{2}$  (**Figure 4c**). The simulated XRD pattern of the  $0.3\text{-\AA}$  slipped AA-stacking mode (**Figure 4a**, blue curve) matched the experimental peak positions and intensities well, whereas the staggered AB-stacking mode (**Figure 4a**, red curve) did not reproduce with the experimental data (black curve). Especially, the peaks in the range of  $12\text{-}16^\circ$  calculated for the staggered AB-stacking mode rules out its possibility because these peaks are absent in the experimental data.

To investigate the big different in crystallinity of such two similar COF, we computed the London Dispersion Energies, Electronic Energies and Crystal Stacking Energies (**Table 1**) using the Dispersion-Corrected Self-Consistent-Charge Density-Functional-Based Tight-Binding method (SCC-DFTB)<sup>[69]</sup>. TPB-DMTP-COF and its non-substituent analogue COF-Non showed London dispersion energies of  $-97.63 \text{ kcal mol}^{-1}$  and  $-107.13 \text{ kcal mol}^{-1}$ , respectively. On the other hand, the electronic energy of TPB-DMTP-COF is  $0.267 \text{ kcal mol}^{-1}$ , much lower than COF-Non ( $3.548 \text{ kcal mol}^{-1}$ ), which indicates the repulsive Coulomb force between the layers in COF-Non is much higher than TPB-DMTP-COF. As a result, TPB-DMTP-COF reveals a much high crystal stacking energy ( $-106.86 \text{ kcal mol}^{-1}$ ) than COF-Non ( $-94.08 \text{ kcal mol}^{-1}$ ), which endows TPB-DMTP-COF extremely high crystallinity than its non-substituent analogue.

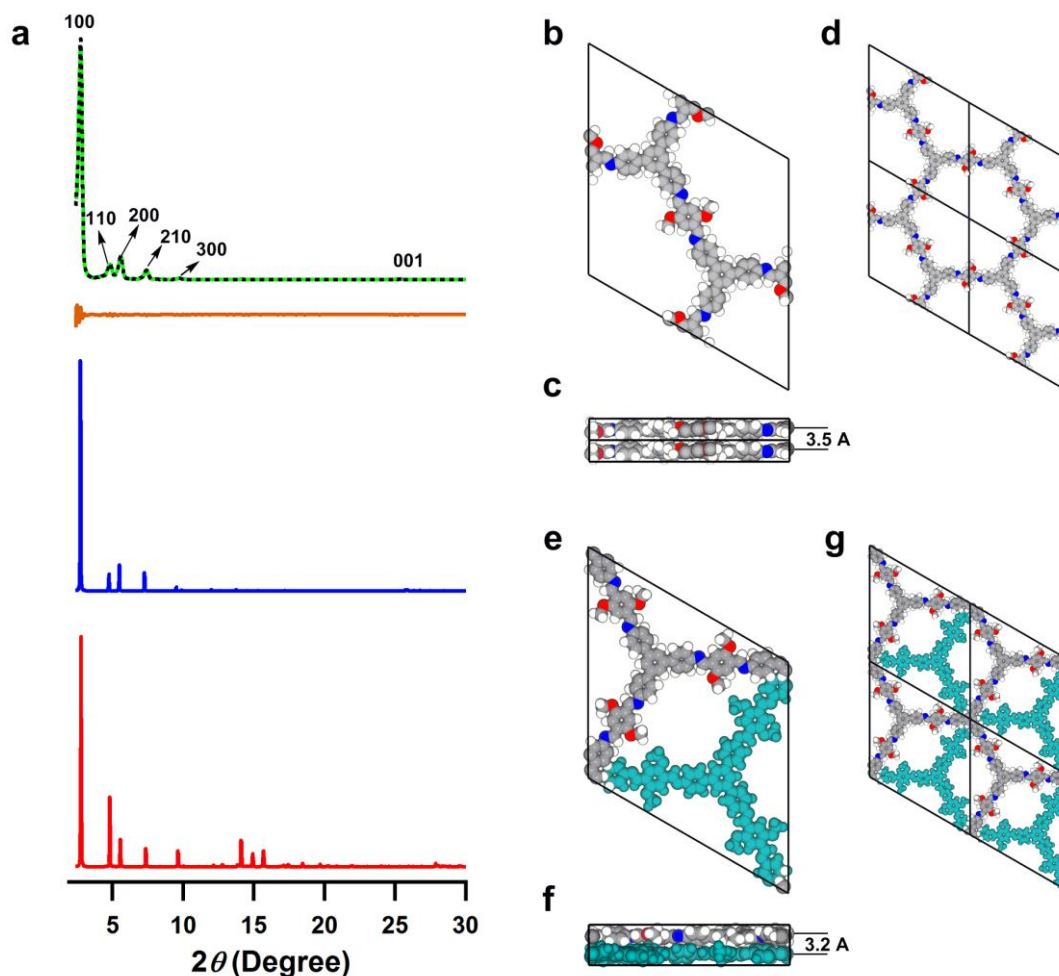


**Figure 4.** **a.** XRD patterns of experimentally observed (black), Pawley refinement (green), and their difference curve (orange), and simulated patterns of AA (blue) and staggered AB modes (red); **b-d.** Views of the unit cell derived from the AA mode along **b** the z and **c** y axes and **d** the structure of a single pore; **e-g.** Views of the unit cell along **e** the z and **f** y axes, and **g** the  $2 \times 2$  pore structure of the staggered AB mode.

**Table 1.** Crystal Stacking Energies per Layer for TPB-DMTP-COF and COF-Non

	$E_{\text{stack}}$	$E_L$	$E_e$	$E_c$
COF-Non	-94.084	-97.632	3.548	-87.04
TPB-DMTP-COF	-106.862	-107.129	0.267	-87.04

$E_{\text{stack}}$  = stacking energy,  $E_L$  = London dispersion energy,  $E_e$  = electronic energy,  $E_c$  = condensation energy. Energies are per unit cell and are given in [ $\text{kcal mol}^{-1}$ ].

### 3.2.3 Gas Sorption Property

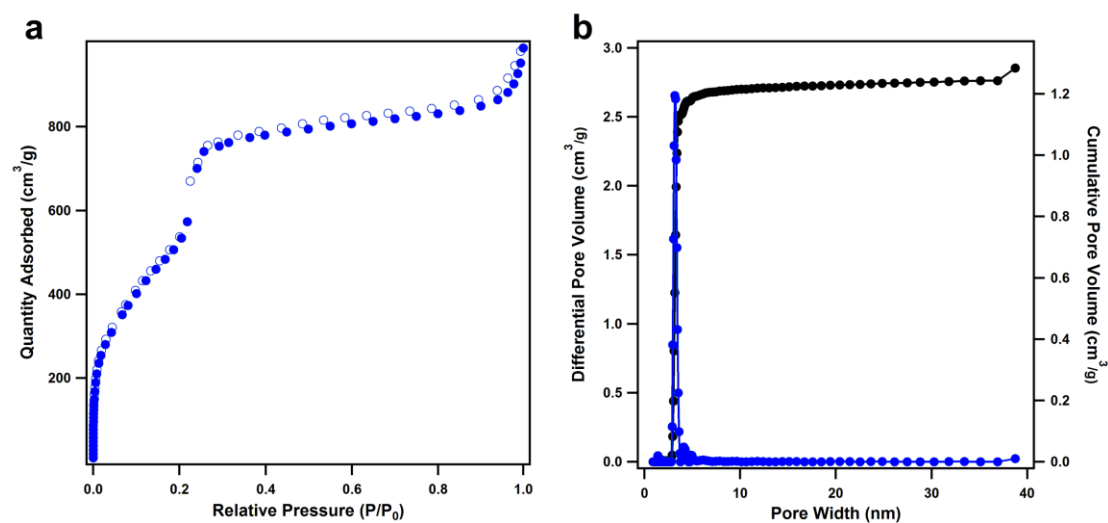


**Figure 5.** **a.** Nitrogen adsorption (filled circles) and desorption (open circles) isotherm curves at 77K; **b.** Pore size distribution profile calculated by NLDFT method.

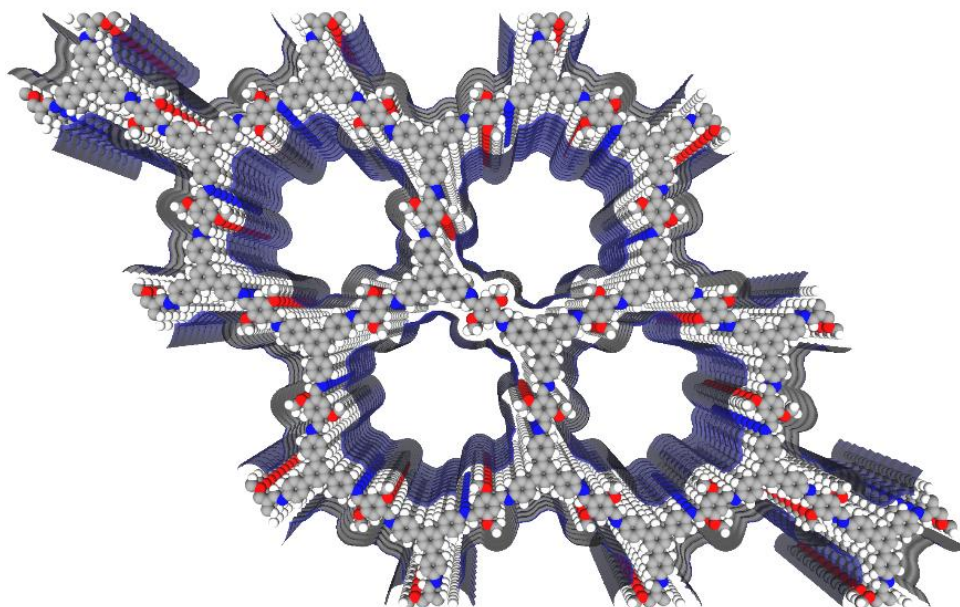


**Figure 6.** Accessible surface area simulated by the crystalline structure of TPB-DMTP-COF (gray: carbon, blue: nitrogen, red: oxygen; hydrogen: white, the blue shadow: accessible surface).

Nitrogen sorption isotherms measured at 77 K exhibited a rapid uptake at low pressure of  $P/P_0 < 0.1$ , followed by a sharp step between  $P/P_0 = 0.15-0.25$  (**Figure 5a**).

This sorption profile is best described as a type-IV isotherm, which is characteristic of mesoporous materials. The Brunauer–Emmett–Teller (BET) surface area is evaluated to be  $2104 \text{ m}^2 \text{ g}^{-1}$  and Langmuir surface area is  $3335 \text{ m}^2 \text{ g}^{-1}$ . The pore size and volume were evaluated to be  $3.26 \text{ nm}$  and  $1.28 \text{ cm}^3 \text{ g}^{-1}$ , respectively (**Table 2**). We simulated the theoretical BET surface area according to the crystalline  $0.3\text{-}\text{\AA}$  slipped AA stacking mode, which yields an accessible BET surface area of  $2098 \text{ m}^2 \text{ g}^{-1}$ . The experimental BET surface area is nearly identical to the theoretical one, which indicates that TPB-DMTP-COF has a perfect structural ordering, in which the ordered one-dimensional open channels are fully accessible to guest molecules.<sup>[70]</sup>

**Table 2.** Surface area, pore size, and pore volume of the COFs

COFs	BET Surface Area ( $\text{m}^2 \text{ g}^{-1}$ )	Langmuir Surface Area ( $\text{m}^2 \text{ g}^{-1}$ )	Pore Size (nm)	Pore Volume ( $\text{cm}^3 \text{ g}^{-1}$ )
TPB-DMTP-COF	2105	3336	3.26	1.28
TPB-DMTP-COF (HCl, 12 M)	2074	3299	3.26	1.23
TPB-DMTP-COF (H <sub>2</sub> O, 100 °C)	2081	3321	3.25	1.27
TPB-DMTP-COF (NaOH, 14 M)	2020	3126	3.25	1.18

### 3.2.4 Chemical Stability

To investigate the chemical stability, we dispersed the TPB-DMTP-COF samples in various different solvents, including DMF, DMSO, THF, MeOH, cyclohexanone, water (100 and 25 °C), aqueous HCl (12 M) and NaOH (14 M) solutions for 1 week. Figure 2f presents the residue weigh percentage of the COF samples. In water and all the organic solvents examined at 25 °C, there is nearly no weight loss (< 0.1 wt%). Remarkably, under the ultra-harsh conditions such as strong acid (12 M HCl) and base (14 M NaOH), the residue weight percentage is as high as 85 wt% and 92 wt %, respectively. Even keeping in the boiling water for one week, the TPB-DMTP-COF could keep 72 wt % of the original weight. To confirm whether the crystalline structure

of the COF samples is retained, XRD measurements were conducted. Figure 2g revealed that the TPB-DMTP-COF keeps the original crystalline structure, without showing any changes in peak intensities and positions. The porosities of the COF samples are also unaffected. Indeed, nitrogen sorption isotherm curves measurements at 77 K suggest that the COF samples have similar sorption curves to the original ones (Figure 7b), and possess similar surface areas, pore sizes, and pore volumes (Table 2). Infrared spectra confirmed that the chemical bonds of the TPB-DMTP-COF are well reserved (Figure 7d). These results unambiguously proved that the TPB-DMTP-COF is a stable crystalline porous framework.<sup>[14, 68, 71-73]</sup> The stability of all COFs thus far reported is summarized in Table 3. It is clear that these COFs upon treatment with solvents cause deterioration in crystallinity together with irreversible loss of porosity.

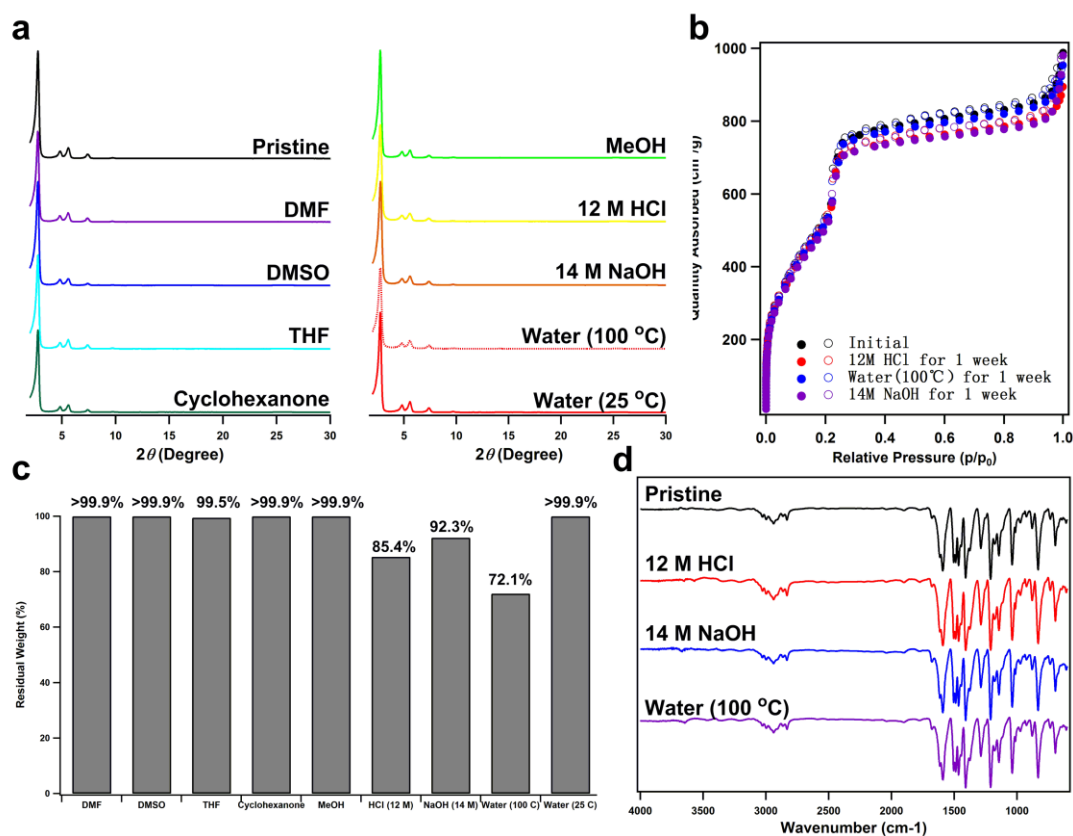


**Figure 7.** **a.** XRD patterns; **b.** Nitrogen sorption isotherm curves; **c.** Residual weight; **d.** FT-IR spectra of TPB-DMTP-COF after being treated in common organic solvents, strong acid/base and boiling water for 1 week.

To gain insights to the stability of the TPB-DMTP-COF, we investigated crystal stacking energy of COF and condensation energy of monolayer, by using the dispersion-corrected self-consistent-charge density-functional-based tight-binding method (SCC-DFTB).<sup>[69]</sup> The TPB-DMTP-COF exhibited a high crystal stacking energy of  $-107.13 \text{ kcal mol}^{-1}$ , which is comparable to the condensation energy of  $-87.04 \text{ kcal mol}^{-1}$  (**Table 1**). From the thermodynamics point of view, the crystal stacking energy offers additional stabilization energy to the crystalline COF system than the common amorphous imine compound; decomposing an idea COF crystal requires to overcome the crystal stacking energy together with the condensation energy. As a result, the highly ordered crystalline structure renders the TPB-DMTP-COF exceptional stability.

### 3.3 Conclusion

In summary, we have developed a mesoporous COF that satisfies the requirements on stability, crystallinity, and porosity for functional exploration. The intense main peak ( $135 \times 10^3$  cps) together with five detailed minor peaks suggests that this COF material has a highly ordered crystalline structure; besides, the experimental BET surface area is nearly identical to the theoretical surface area, which indicates its high crystallinity nature, since only the ideal structure could offer efficient access to guest molecules and result a theoretical porosity. The highly ordered crystalline structure benefits the porosity and also endow this COF with an exceptional stability: this COF could perfectly maintain its crystallinity and porosity in different organic solvents and strong acid (12 M HCl), strong base (14 M NaOH), and even at heating conditions (boiling water) for 1 week. This discovery makes a breakthrough in the field of crystalline frameworks, providing an efficient solution to the contradiction of high performance with high stability.

### 3.4 Experimental Sections

#### 3.4.1 Materials and Methods

Flash column chromatography was carried out with silica gel (200-300 mesh).  $^1\text{H}$  nuclear magnetic resonance (NMR) spectra were recorded on JEOL models JNM-LA400 NMR spectrometers, where chemical shifts ( $\delta$  in ppm) were determined with a residual proton of the solvent as standard. Fourier transform infrared (IR) spectra were recorded on a JASCO model FT-IR-6100 infrared spectrometer. X-ray diffraction (XRD) data were recorded on a Rigaku model RINT Ultima III diffractometer by depositing powder on glass substrate, from  $2\theta = 1.5^\circ$  up to  $60^\circ$  with  $0.02^\circ$  increment. Nitrogen sorption isotherms were measured at 77 K with a Micromeritics Instrument Corporation model 3Flex surface characterization analyzer. The Brunauer-Emmett-Teller (BET) method was utilized to calculate the specific surface areas. By using the non-local density functional theory (NLDFIT) model, the pore volume was derived from the sorption curve. Elemental analysis was performed on a Yanako model CHN CORDER MT-6 elemental analyzer. High performance liquid chromatography were performed on a JASCO model HPLC model with Daicel chiral AD-H columns with *i*-PrOH/*n*-hexane as the eluent.

The crystalline structure of COF were determined using the density-functional tight-binding (DFTB) method including Lennard-Jones (LJ) dispersion. The calculations were carried out with the DFTB+ program package version 1.2.<sup>[74]</sup> DFTB is an approximate density functional theory method based on the tight binding approach and utilizes an optimized minimal LCAO Slater-type all-valence basis set in combination with a two-center approximation for Hamiltonian matrix elements. The Coulombic interaction between partial atomic charges was determined using the self-consistent charge (SCC) formalism. Lennard-Jones type dispersion was employed in all calculations to describe van der Waals (vdW) and  $\pi$ -stacking interactions. The lattice dimensions were optimized simultaneously with the geometry. Standard DFTB parameters for X–Y element pair (X, Y = C, O, H and N) interactions were employed from the mio-0-1 set. The monolayer formation energy (condensation energy,  $E_c$ ) is

calculated from the total energies of the monolayer and of the individual building blocks.<sup>[75]</sup> The accessible surface areas were calculated from the Monte Carlo integration technique using a nitrogen-size probe molecule (diameter = 3.68 Å) roll over the framework surface with a grid interval of 0.25 Å.<sup>[70]</sup>

Dehydrated N,N-dimethylformide (DMF), N,N-dimethylacetamide (DMAc), dehydrated tetrahydrofuran (THF), and o-dichlorobenzene (o-DCB) were purchased from Kanto Chemicals. Hydrobromic acid, p-toluenesulonyl chloride, trifluoroacetic acid, toluene, dioxane, mesitylene, 1-butanol, ethanol, and acetic acid were purchased from Wako Chemicals. Propargyl bromide, 1,4-dimethoxybenzene, N-(tert-butoxycarbonyl)-L-prolinol, tert-butyl alcohol, 1,3,5-tri(4-aminophenyl) benzene and benzoic acid were purchased from TCI. trans-beta-Nitrostyrene, N,N-diisopropylethylamine, trans-4-chloro-beta-nitrostyrene, trans-2-chloro-beta-nitrostyrene, trans-4-bromo-beta-nitrostyrene, trans-4-methyl-beta-nitrostyrene, and trans-4-methoxy-beta-nitrostyrene were purchased from Sigma-Aldrich Co.

1,4-dibromo-2,5-dimethoxybenzene, 2,5-dimethoxyterephthalaldehyde (DMTA) were synthesized according to the procedures described in **Chapter 2, Section 2.4.3**.

**TPB-DMTP-COF** An o-DCB/BuOH (0.5 mL / 0.5 mL) mixture of TAPB (0.080 mmol, 28.1 mg) and DMTA (0.120 mmol, 23.3 mg) in the presence of acetic acid catalyst (6 M, 0.1 mL) in a Pyrex tube (14 ML) was degassed by three freeze–pump–thaw cycles. The tube was sealed off by flame and heated at 120 °C for 3 days. The precipitate was collected via centrifuge, washed with THF for 6 times and then soaked in THF for 1 day to remove trapped guest molecules. The powder was collected and dried at 120 °C under vacuum overnight to give the TPB-DMTP-COF in isolated yield of 81%.

### 3.4.2 Crystallographic Information of Modeled COFs

#### **TPB-DMTP-COF-AA**

Space group *P3*

$a = 37.1669 \text{ \AA}$ ;  $c = 3.4614 \text{ \AA}$

$\alpha = 90^\circ$ ;  $\gamma = 120^\circ$ .

C1	C	0.30797	0.68424	0.52716
C2	C	0.28952	0.64079	0.52711
H3	H	0.28776	0.69824	0.52713
C4	C	0.69212	0.31586	0.52427
C5	C	0.71047	0.35931	0.52422
H6	H	0.71241	0.30195	0.52411
C7	C	0.38618	0.63003	0.52658
C8	C	0.42754	0.65226	0.39523
C9	C	0.45288	0.63474	0.39531
C10	C	0.43832	0.59366	0.52518
C11	C	0.39669	0.57143	0.6579
C12	C	0.37158	0.58913	0.65807
H13	H	0.4402	0.68445	0.28956
H14	H	0.4851	0.65324	0.28881
H15	H	0.38396	0.53928	0.76509
H16	H	0.33929	0.57067	0.76487
C17	C	0.55023	0.46091	0.54309
N18	N	0.53459	0.42089	0.51267
C19	C	0.4492	0.53855	0.50022
N20	N	0.46498	0.5786	0.52777
H21	H	0.58455	0.48239	0.57744
H22	H	0.41485	0.51711	0.46859
C23	C	0.61363	0.36976	0.52341
C24	C	0.5725	0.34768	0.38605
C25	C	0.54716	0.36519	0.38367
C26	C	0.56137	0.40599	0.5201
C27	C	0.60279	0.42807	0.65868
C28	C	0.62797	0.41045	0.65952
H29	H	0.56008	0.31568	0.27606
H30	H	0.51512	0.34682	0.27255
H31	H	0.61533	0.46011	0.76837
H32	H	0.6601	0.42882	0.77018
C33	C	0.52468	0.48054	0.53329
C34	C	0.48124	0.45671	0.48544
C35	C	0.45658	0.47519	0.47412
C36	C	0.4747	0.51885	0.5089
C37	C	0.51813	0.54262	0.5559
C38	C	0.54281	0.5242	0.56913
H39	H	0.46697	0.42273	0.45641
O40	O	0.41227	0.45189	0.4265
H41	H	0.53289	0.57676	0.58625
O42	O	0.58701	0.54729	0.62517
C43	C	0.39507	0.40677	0.41333

C44	C	0.60509	0.59259	0.63416
H45	H	0.40355	0.39537	0.68058
H46	H	0.40543	0.39723	0.1454
H47	H	0.36076	0.39282	0.40295
H48	H	0.62414	0.60612	0.36515
H49	H	0.62555	0.6047	0.89557
H50	H	0.58056	0.60156	0.64985

**TPB-DMTP-COF-AB**Space group *P*-3 $a = 36.6669 \text{ \AA}$ ;  $c = 6.400 \text{ \AA}$  $\alpha = 90^\circ$ ;  $\gamma = 120^\circ$ .

C1	C	-0.02536	1.01757	0.28511
C2	C	-0.04381	0.97412	0.28508
H3	H	-0.04557	1.03158	0.28509
C4	C	0.35879	0.6492	0.28354
C5	C	0.37713	0.69264	0.28352
H6	H	0.37907	0.63528	0.28346
C7	C	0.05285	0.96336	0.28479
C8	C	0.0942	0.98559	0.21462
C9	C	0.11954	0.96807	0.21466
C10	C	0.10499	0.92699	0.28403
C11	C	0.06336	0.90477	0.35495
C12	C	0.03825	0.92247	0.35504
H13	H	0.10686	1.01777	0.15817
H14	H	0.15175	0.98656	0.15776
H15	H	0.05064	0.87262	0.41222
H16	H	0.00597	0.90402	0.41211
C17	C	0.21689	0.79424	0.29372
N18	N	0.20125	0.75422	0.27727
C19	C	0.11587	0.87188	0.27054
N20	N	0.13164	0.91194	0.28544
H21	H	0.25122	0.81572	0.3123
H22	H	0.08151	0.85044	0.25343
C23	C	0.2803	0.70309	0.28308
C24	C	0.23917	0.68102	0.20965
C25	C	0.21384	0.69854	0.20837
C26	C	0.22804	0.73933	0.28129
C27	C	0.26945	0.7614	0.35537
C28	C	0.29462	0.74377	0.35583
H29	H	0.22676	0.64902	0.15086

H30	H	0.1818	0.68017	0.14896
H31	H	0.28198	0.79343	0.414
H32	H	0.32676	0.76213	0.41498
C33	C	0.19135	0.81387	0.28843
C34	C	0.14791	0.79004	0.26255
C35	C	0.12325	0.80852	0.25642
C36	C	0.14137	0.85218	0.27523
C37	C	0.1848	0.87596	0.30065
C38	C	0.20947	0.85753	0.30781
H39	H	0.13364	0.75607	0.24684
O40	O	0.07894	0.78522	0.23067
H41	H	0.19956	0.9101	0.31707
O42	O	0.25368	0.88062	0.33811
C43	C	0.06174	0.74011	0.22355
C44	C	0.27176	0.92592	0.34297
H45	H	0.07022	0.7287	0.36808
H46	H	0.0721	0.73056	0.07864
H47	H	0.02743	0.72616	0.21793
H48	H	0.2908	0.93945	0.19749
H49	H	0.29222	0.93804	0.48436
H50	H	0.24723	0.93489	0.35146

**Me-COF-AA**Space group  $P3$  $a = 37.137991 \text{ \AA}$ ;  $c = 3.464297 \text{ \AA}$  $\alpha = 90^\circ$ ;  $\gamma = 120^\circ$ .

C1	C	0.30797	0.68424	0.52716
C2	C	0.28952	0.64079	0.52711
H3	H	0.28776	0.69824	0.52713
C4	C	0.69212	0.31586	0.52427
C5	C	0.71047	0.35931	0.52422
H6	H	0.71241	0.30195	0.52411
C7	C	0.38618	0.63003	0.52658
C8	C	0.42754	0.65226	0.39523
C9	C	0.45288	0.63474	0.39531
C10	C	0.43832	0.59366	0.52518
C11	C	0.39669	0.57143	0.6579
C12	C	0.37158	0.58913	0.65807
H13	H	0.4402	0.68445	0.28956
H14	H	0.4851	0.65324	0.28881
H15	H	0.38396	0.53928	0.76509

H16	H	0.33929	0.57067	0.76487
C17	C	0.55023	0.46091	0.54309
N18	N	0.53459	0.42089	0.51267
C19	C	0.4492	0.53855	0.50022
N20	N	0.46498	0.5786	0.52777
H21	H	0.58455	0.48239	0.57744
H22	H	0.41485	0.51711	0.46859
C23	C	0.61363	0.36976	0.52341
C24	C	0.5725	0.34768	0.38605
C25	C	0.54716	0.36519	0.38367
C26	C	0.56137	0.40599	0.5201
C27	C	0.60279	0.42807	0.65868
C28	C	0.62797	0.41045	0.65952
H29	H	0.56008	0.31568	0.27606
H30	H	0.51512	0.34682	0.27255
H31	H	0.61533	0.46011	0.76837
H32	H	0.6601	0.42882	0.77018
C33	C	0.52468	0.48054	0.53329
C34	C	0.48124	0.45671	0.48544
C35	C	0.45658	0.47519	0.47412
C36	C	0.4747	0.51885	0.5089
C37	C	0.51813	0.54262	0.5559
C38	C	0.54281	0.5242	0.56913
H39	H	0.46697	0.42273	0.45641
H40	H	0.53289	0.57676	0.58625
C41	C	0.42151	0.45515	0.43661
C42	C	0.57782	0.54449	0.6091
H43	H	0.41148	0.42142	0.50488
H44	H	0.41279	0.45759	0.12588
H45	H	0.40521	0.46642	0.64156
H46	H	0.59261	0.56047	0.32439
H47	H	0.59138	0.52433	0.70337
H48	H	0.58447	0.56897	0.8395

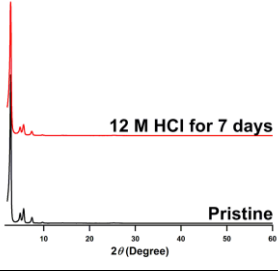
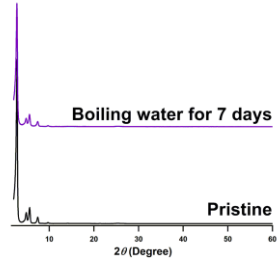
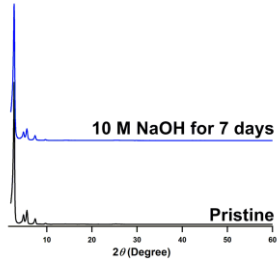
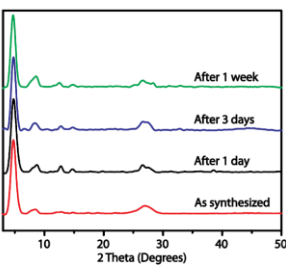
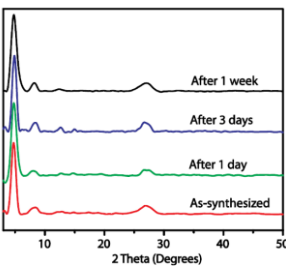
**COF-AA**Space group  $P3$  $a = 37.1967 \text{ \AA}; c = 3.475149 \text{ \AA}$  $\alpha = 90^\circ; \gamma = 120^\circ.$ 

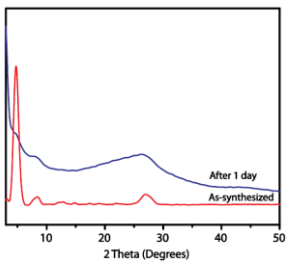
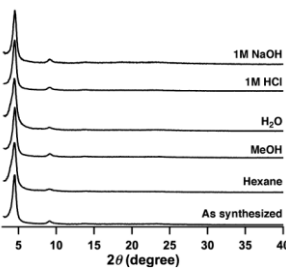
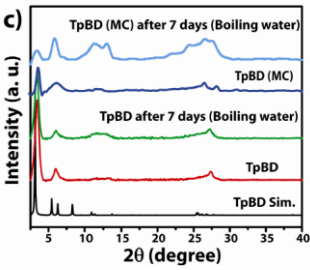
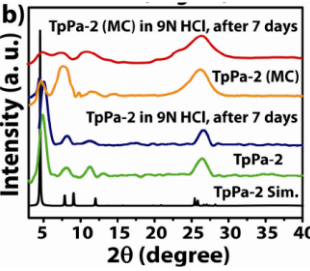
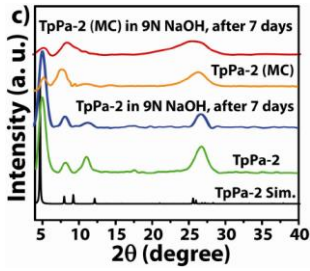
C1	C	0.30797	0.68424	0.52716
C2	C	0.28952	0.64079	0.52711
H3	H	0.28776	0.69824	0.52713

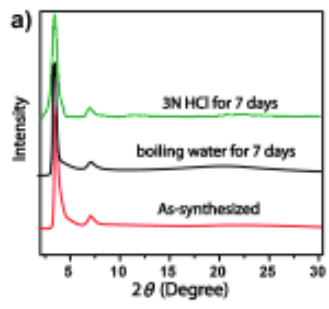
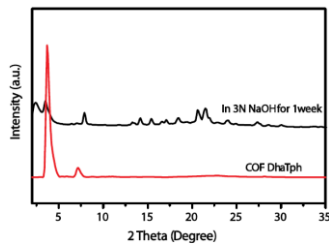
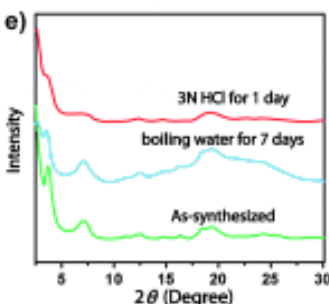
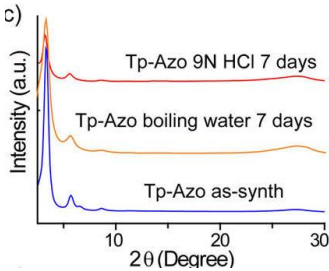
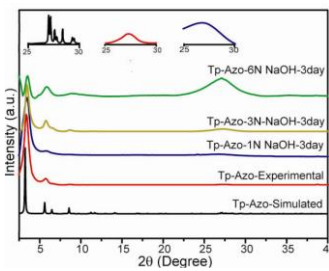
C4	C	0.69212	0.31586	0.52427
C5	C	0.71047	0.35931	0.52422
H6	H	0.71241	0.30195	0.52411
C7	C	0.38618	0.63003	0.52658
C8	C	0.42754	0.65226	0.39523
C9	C	0.45288	0.63474	0.39531
C10	C	0.43832	0.59366	0.52518
C11	C	0.39669	0.57143	0.6579
C12	C	0.37158	0.58913	0.65807
H13	H	0.4402	0.68445	0.28956
H14	H	0.4851	0.65324	0.28881
H15	H	0.38396	0.53928	0.76509
H16	H	0.33929	0.57067	0.76487
C17	C	0.55023	0.46091	0.54309
N18	N	0.53459	0.42089	0.51267
C19	C	0.4492	0.53855	0.50022
N20	N	0.46498	0.5786	0.52777
H21	H	0.58455	0.48239	0.57744
H22	H	0.41485	0.51711	0.46859
C23	C	0.61363	0.36976	0.52341
C24	C	0.5725	0.34768	0.38605
C25	C	0.54716	0.36519	0.38367
C26	C	0.56137	0.40599	0.5201
C27	C	0.60279	0.42807	0.65868
C28	C	0.62797	0.41045	0.65952
H29	H	0.56008	0.31568	0.27606
H30	H	0.51512	0.34682	0.27255
H31	H	0.61533	0.46011	0.76837
H32	H	0.6601	0.42882	0.77018
C33	C	0.52468	0.48054	0.53329
C34	C	0.48124	0.45671	0.48544
C35	C	0.45658	0.47519	0.47412
C36	C	0.4747	0.51885	0.5089
C37	C	0.51813	0.54262	0.5559
C38	C	0.54281	0.5242	0.56913
H39	H	0.46697	0.42273	0.45641
H40	H	0.53289	0.57676	0.58625
H41	H	0.42151	0.45515	0.43661
H42	H	0.57782	0.54449	0.6091

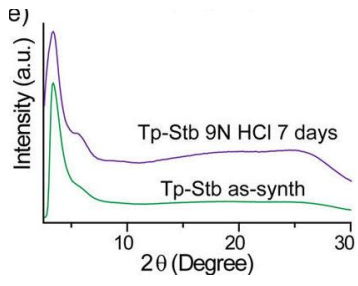
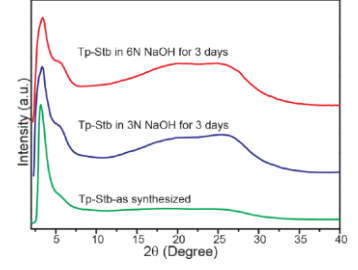
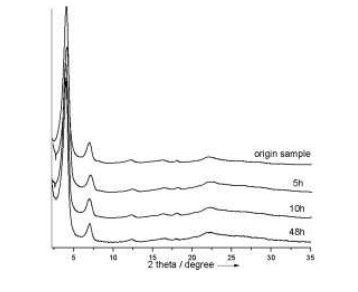
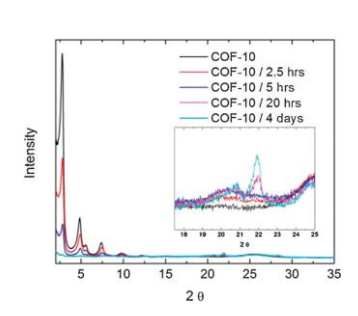
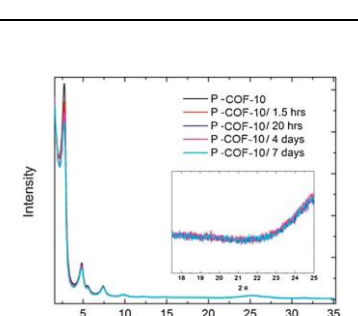
### 3.4.3 Stability in Different COF Systems

**Table 3.** Stability in different COFs

Name	Conditions	PXRD	Surface Area	Reference
TPB-DMTP-COF	12 M HCl (7 days)		Pristine: 2105 m <sup>2</sup> g <sup>-1</sup> ; 7days later: 2074 m <sup>2</sup> g <sup>-1</sup> .	This Paper
	Boiling water (7 days)		Pristine: 2105 m <sup>2</sup> g <sup>-1</sup> ; 7days later: 2081 m <sup>2</sup> g <sup>-1</sup> .	
	14 M NaOH (7 days)		Pristine: 2105 m <sup>2</sup> g <sup>-1</sup> ; 7days later: 2020 m <sup>2</sup> g <sup>-1</sup> .	
TpPa-1	Boiling water. (7 days)		Pristine: 535 m <sup>2</sup> g <sup>-1</sup> ; 7days later: 520 m <sup>2</sup> g <sup>-1</sup> .	J. Am. Chem. Soc. <b>134</b> , 19524- 19527, (2012).
	9 M HCl (7 days)		Pristine: 535 m <sup>2</sup> g <sup>-1</sup> ; 7days later: 512 m <sup>2</sup> g <sup>-1</sup> .	

	9 M NaOH (1 day)		Pristine: $535 \text{ m}^2 \text{ g}^{-1}$ ; 7days later: $324 \text{ m}^2 \text{ g}^{-1}$ .	J. Am. Chem. Soc. <b>134</b> , 19524- 19527, (2012).
Py-Azine COF	1M NaOH (1 day); 1M HCl (1 day); H <sub>2</sub> O (1 day); MeOH (1 day); Hexane (1 day).		Pristine: $1210 \text{ m}^2 \text{ g}^{-1}$ .	J. Am. Chem. Soc. <b>135</b> , 17310- 17313, (2013).
TpBD TpBD(MC)	Boiling water. (7 days)		Pristine: $537 \text{ m}^2 \text{ g}^{-1}$ ; $35 \text{ m}^2 \text{ g}^{-1}$ .	
TpPa-2 TpPa-2(MC)	9 M HCl (7 days)		Pristine: $339 \text{ m}^2 \text{ g}^{-1}$ ; $56 \text{ m}^2 \text{ g}^{-1}$ .	J. Am. Chem. Soc. <b>135</b> , 5328- 5331, (2013).
TpPa-2 TpPa-2(MC)	9 M NaOH (7 days)		Pristine: $339 \text{ m}^2 \text{ g}^{-1}$ ; $56 \text{ m}^2 \text{ g}^{-1}$ .	

DhaTph	3 M HCl Boiling water. (7 days)		Pristine: 1305 m <sup>2</sup> g <sup>-1</sup> ; 7days later: 570 m <sup>2</sup> g <sup>-1</sup> (3M HCl); 1252 m <sup>2</sup> g <sup>-1</sup> (Boiling water)	Angew. Chem. Int. Ed. <b>52</b> , 13052- 13056, (2013).
	3 M NaOH (7 days)		70% weight loss, the surface area information is not mentioned.	Angew. Chem. Int. Ed. <b>52</b> ,
DmaTph	3 M HCl (1 day) Boiling water. (7 days)		Pristine: 431 m <sup>2</sup> g <sup>-1</sup> ;	13052- 13056, (2013).
Tp-Azo	9 M HCl (7 days) Boiling water. (7 days)		Pristine: 1328 m <sup>2</sup> g <sup>-1</sup> .	J. Am. Chem. Soc. <b>136</b> , 6570- 6573,
	1, 3 and 6 M NaOH (3 days)		Pristine: 1328 m <sup>2</sup> g <sup>-1</sup> .	(2014).

Tp-Stb	9 M HCl (7 days)		Pristine: 422 m <sup>2</sup> g <sup>-1</sup> .	J. Am. Chem. Soc. <b>136</b> , 6570- 6573, (2014).
	3 and 6 M NaOH (3 days)		Pristine: 422 m <sup>2</sup> g <sup>-1</sup> .	
CTV-COF-1	Water for 5h, 10h and 48h.		Pristine: 1245 m <sup>2</sup> g <sup>-1</sup> ; 997 m <sup>2</sup> g <sup>-1</sup> .	Chem. Commun. <b>50</b> , 788- 791, (2014).
COF-10	Under 50% R.H atmosphere for 2.5h, 5h, 20h and 4days.		Pristine: 1200 m <sup>2</sup> g <sup>-1</sup> ; 30 m <sup>2</sup> g <sup>-1</sup> .	Chem. Commun. <b>48</b> , 4606- 4608,
Pyridine modified COF-10	Under 50% R.H atmosphere for 1.5h, 20h, 4days and 7days.		Pristine: 1200 m <sup>2</sup> g <sup>-1</sup> ; 950 m <sup>2</sup> g <sup>-1</sup> .	(2012).

### 3.5 References

- [1] Cote, A. P.; Benin, A. I.; Ockwig, N. W.; O'Keeffe, M.; Matzger, A. J.; Yaghi, O. M., *Science* **2005**, *310*, 1166-1170.
- [2] Garberoglio, G.; Vallauri, R., *Microporous Mesoporous Mater.* **2008**, *116*, 540-547.
- [3] Koenig, A. R. V.; Desgranges, C.; Delhommelle, J., *Mol. Simul.* **2013**, *40*, 71-79.
- [4] Assfour, B.; Seifert, G., *Microporous Mesoporous Mater.* **2010**, *133*, 59-65.
- [5] Guo, J.-H.; Zhang, H.; Gong, M.; Cheng, X.-L., *Struct. Chem.* **2012**, *24*, 691-703.
- [6] Zou, X.; Zhou, G.; Duan, W.; Choi, K.; Ihm, J., *J. Phys. Chem. C* **2010**, *114*, 13402-13407.
- [7] Thote, J.; Aiyappa, H. B.; Deshpande, A.; Diaz Diaz, D.; Kurungot, S.; Banerjee, R., *Chem. Eur. J.* **2014**, *20*, 15961-15965.
- [8] Kalidindi, S. B.; Fischer, R. A., *Phys. Status Solidi* **2013**, *250*, 1119-1127.
- [9] Han, S. S.; Furukawa, H.; Yaghi, O. M.; Goddard, W. A., 3rd, *J. Am. Chem. Soc.* **2008**, *130*, 11580-11581.
- [10] Oh, H.; Kalidindi, S. B.; Um, Y.; Bureekaew, S.; Schmid, R.; Fischer, R. A.; Hirscher, M., *Angew. Chem. Int. Ed.* **2013**, *52*, 13219-13222.
- [11] Li, X.-D.; Guo, J.-H.; Zhang, H.; Cheng, X.-L.; Liu, X.-Y., *R. Soc. Chem. Adv.* **2014**, *4*, 24526.
- [12] Li, X.-D.; Zang, H.-P.; Wang, J.-T.; Wang, J.-F.; Zhang, H., *J. Mater. Chem. A* **2014**, *2*, 18554-18561.
- [13] Yang, Z.; Cao, D., *J. Phys. Chem. C* **2012**, *116*, 12591-12598.
- [14] Kandambeth, S.; Shinde, D. B.; Panda, M. K.; Lukose, B.; Heine, T.; Banerjee, R., *Angew. Chem. Int. Ed.* **2013**, *52*, 13052-13056.
- [15] Stegbauer, L.; Schwinghammer, K.; Lotsch, B. V., *Chem. Sci.* **2014**, *5*, 2789.
- [16] Makhseed, S.; Samuel, J., *Chem. Commun.* **2008**, 4342-4344.
- [17] Assfour, B.; Seifert, G., *Chem. Phys. Lett.* **2010**, *489*, 86-91.
- [18] Guo, J. H.; Zhang, H.; Tang, Y.; Cheng, X., *Phys. Chem. Chem. Phys.* **2013**, *15*, 2873-2881.
- [19] Klontzas, E.; Tylianakis, E.; Froudakis, G. E., *J. Phys. Chem. C* **2008**, *112*, 9095-9098.
- [20] Choi, Y. J.; Lee, J. W.; Choi, J. H.; Kang, J. K., *Appl. Phys. Lett.* **2008**, *92*, 173102.
- [21] Li, F.; Zhao, J.; Johansson, B.; Sun, L., *Int. J. Hydrogen Energy* **2010**, *35*, 266-271.
- [22] Cao, D.; Lan, J.; Wang, W.; Smit, B., *Angew. Chem. Int. Ed.* **2009**, *48*, 4730-4733.

- [23] Das, G.; Balaji Shinde, D.; Kandambeth, S.; Biswal, B. P.; Banerjee, R., *Chem. Commun.* **2014**, *50*, 12615-12618.
- [24] Kalidindi, S. B.; Oh, H.; Hirscher, M.; Esken, D.; Wiktor, C.; Turner, S.; Van Tendeloo, G.; Fischer, R. A., *Chem. Eur. J.* **2012**, *18*, 10848-10856.
- [25] Li, L.-L.; Gao, T.-F.; Zhang, R.-Y.; Zhang, H., *Chin. Phys. Lett.* **2014**, *31*, 097101.
- [26] Guo, J.-H.; Zhang, H.; Liu, Z.-P.; Cheng, X.-L., *J. Phys. Chem. C* **2012**, *116*, 15908-15917.
- [27] Gao, T.-F.; Zhang, H., *Struct. Chem.* **2013**, *25*, 503-513.
- [28] Tylisanakis, E.; Klontzas, E.; Froudakis, G. E., *Nanoscale* **2011**, *3*, 856-869.
- [29] Guo, J. H.; Zhang, H.; Miyamoto, Y., *Phys. Chem. Chem. Phys.* **2013**, *15*, 8199-8207.
- [30] Kim, D.; Jung, D. H.; Kim, K.-H.; Guk, H.; Han, S. S.; Choi, K.; Choi, S.-H., *J. Phys. Chem. C* **2012**, *116*, 1479-1484.
- [31] Han, S. S.; Mendoza-Cortes, J. L.; Goddard, W. A., 3rd, *Chem. Soc. Rev.* **2009**, *38*, 1460-1476.
- [32] Ganz, E.; Dornfeld, M., *J. Phys. Chem. C* **2012**, *116*, 3661-3666.
- [33] Furukawa, H.; Yaghi, O. M., *J. Am. Chem. Soc.* **2009**, *131*, 8875-8883.
- [34] Doonan, C. J.; Tranchemontagne, D. J.; Glover, T. G.; Hunt, J. R.; Yaghi, O. M., *Nature Chem.* **2010**, *2*, 235-238.
- [35] Wan, S.; Guo, J.; Kim, J.; Ihee, H.; Jiang, D., *Angew. Chem. Int. Ed.* **2008**, *47*, 8826-8830.
- [36] Jin, S.; Ding, X.; Feng, X.; Supur, M.; Furukawa, K.; Takahashi, S.; Addicoat, M.; El-Khouly, M. E.; Nakamura, T.; Irle, S.; Fukuzumi, S.; Nagai, A.; Jiang, D., *Angew. Chem. Int. Ed.* **2013**, *52*, 2017-2021.
- [37] Ding, X.; Feng, X.; Saeki, A.; Seki, S.; Nagai, A.; Jiang, D., *Chem. Commun.* **2012**, *48*, 8952-8954.
- [38] Feng, X.; Liu, L.; Honsho, Y.; Saeki, A.; Seki, S.; Irle, S.; Dong, Y.; Nagai, A.; Jiang, D., *Angew. Chem. Int. Ed.* **2012**, *51*, 2618-2622.
- [39] Jin, S.; Furukawa, K.; Addicoat, M.; Chen, L.; Takahashi, S.; Irle, S.; Nakamura, T.; Jiang, D., *Chem. Sci.* **2013**, *4*, 4505.
- [40] Wan, S.; Guo, J.; Kim, J.; Ihee, H.; Jiang, D., *Angew. Chem. Int. Ed.* **2009**, *48*, 5439-5442.
- [41] Chen, L.; Furukawa, K.; Gao, J.; Nagai, A.; Nakamura, T.; Dong, Y.; Jiang, D., *J. Am. Chem. Soc.* **2014**, *136*, 9806-9809.
- [42] Feng, X.; Chen, L.; Dong, Y.; Jiang, D., *Chem. Commun.* **2011**, *47*, 1979-1981.
- [43] Feng, X.; Dong, Y.; Jiang, D., *CrystEngComm* **2013**, *15*, 1508.

- [44] Ding, X.; Guo, J.; Feng, X.; Honsho, Y.; Guo, J.; Seki, S.; Maitarad, P.; Saeki, A.; Nagase, S.; Jiang, D., *Angew. Chem. Int. Ed.* **2011**, *50*, 1289-1293.
- [45] Jin, S.; Sakurai, T.; Kowalczyk, T.; Dalapati, S.; Xu, F.; Wei, H.; Chen, X.; Gao, J.; Seki, S.; Irle, S.; Jiang, D., *Chem. Eur. J.* **2014**, *20*, 14608-14613.
- [46] Ding, S. Y.; Gao, J.; Wang, Q.; Zhang, Y.; Song, W. G.; Su, C. Y.; Wang, W., *J. Am. Chem. Soc.* **2011**, *133*, 19816-19822.
- [47] Rowan, S. J.; Cantrill, S. J.; Cousins, G. R.; Sanders, J. K.; Stoddart, J. F., *Angew. Chem. Int. Ed.* **2002**, *41*, 898-952.
- [48] Belowich, M. E.; Stoddart, J. F., *Chem. Soc. Rev.* **2012**, *41*, 2003-2024.
- [49] El-Kaderi, H. M.; Hunt, J. R.; Mendoza-Cortes, J. L.; Cote, A. P.; Taylor, R. E.; O'Keeffe, M.; Yaghi, O. M., *Science* **2007**, *316*, 268-272.
- [50] Tilford, R. W.; Gemmill, W. R.; zur Loye, H. C.; Lavigne, J. J., *Chem. Mater.* **2006**, *18*, 5296-5301.
- [51] Cote, A. P.; El-Kaderi, H. M.; Furukawa, H.; Hunt, J. R.; Yaghi, O. M., *J. Am. Chem. Soc.* **2007**, *129*, 12914-12915.
- [52] Hunt, J. R.; Doonan, C. J.; LeVangie, J. D.; Cote, A. P.; Yaghi, O. M., *J. Am. Chem. Soc.* **2008**, *130*, 11872-11873.
- [53] Tilford, R. W.; Mugavero, S. J., 3rd; Pellechia, P. J.; Lavigne, J. J., *Adv. Mater.* **2008**, *20*, 2741-2746.
- [54] Spitler, E. L.; Dichtel, W. R., *Nature Chem.* **2010**, *2*, 672-677.
- [55] Ding, X.; Chen, L.; Honsho, Y.; Feng, X.; Saengsawang, O.; Guo, J.; Saeki, A.; Seki, S.; Irle, S.; Nagase, S.; Parasuk, V.; Jiang, D., *J. Am. Chem. Soc.* **2011**, *133*, 14510-14513.
- [56] Dogru, M.; Sonnauer, A.; Gavryushin, A.; Knochel, P.; Bein, T., *Chem. Commun.* **2011**, *47*, 1707-1709.
- [57] Nagai, A.; Guo, Z.; Feng, X.; Jin, S.; Chen, X.; Ding, X.; Jiang, D., *Nature Commun.* **2011**, *2*, 536.
- [58] Spitler, E. L.; Koo, B. T.; Novotney, J. L.; Colson, J. W.; Uribe-Romo, F. J.; Gutierrez, G. D.; Clancy, P.; Dichtel, W. R., *J. Am. Chem. Soc.* **2011**, *133*, 19416-19421.
- [59] Wan, S.; Gándara, F.; Asano, A.; Furukawa, H.; Saeki, A.; Dey, S. K.; Liao, L.; Ambrogio, M. W.; Botros, Y. Y.; Duan, X.; Seki, S.; Stoddart, J. F.; Yaghi, O. M., *Chem. Mater.* **2011**, *23*, 4094-4097.
- [60] Bunck, D. N.; Dichtel, W. R., *Angew. Chem. Int. Ed.* **2012**, *51*, 1885-1889.
- [61] Uribe-Romo, F. J.; Hunt, J. R.; Furukawa, H.; Klock, C.; O'Keeffe, M.; Yaghi, O. M., *J. Am. Chem. Soc.* **2009**, *131*, 4570-4571.
- [62] Uribe-Romo, F. J.; Doonan, C. J.; Furukawa, H.; Oisaki, K.; Yaghi, O. M., *J. Am. Chem. Soc.* **2011**, *133*, 11478-11481.

- [63] Bunck, D. N.; Dichtel, W. R., *J. Am. Chem. Soc.* **2013**, *135*, 14952-14955.
- [64] Kuhn, P.; Antonietti, M.; Thomas, A., *Angew. Chem. Int. Ed.* **2008**, *47*, 3450-3453.
- [65] Bojdys, M. J.; Jeromenok, J.; Thomas, A.; Antonietti, M., *Adv. Mater.* **2010**, *22*, 2202-2205.
- [66] Zhang, W.; Liang, F.; Li, C.; Qiu, L. G.; Yuan, Y. P.; Peng, F. M.; Jiang, X.; Xie, A. J.; Shen, Y. H.; Zhu, J. F., *J. Hazard. Mater.* **2011**, *186*, 984-990.
- [67] Guo, J.; Xu, Y.; Jin, S.; Chen, L.; Kaji, T.; Honsho, Y.; Addicoat, M. A.; Kim, J.; Saeki, A.; Ihee, H.; Seki, S.; Irle, S.; Hiramoto, M.; Gao, J.; Jiang, D., *Nature Commun.* **2013**, *4*, 2736.
- [68] Dalapati, S.; Jin, S.; Gao, J.; Xu, Y.; Nagai, A.; Jiang, D., *J. Am. Chem. Soc.* **2013**, *135*, 17310-17313.
- [69] Lukose, B.; Kuc, A.; Heine, T., *Chem. Eur. J.* **2011**, *17*, 2388-2392.
- [70] Dören, T.; Millange, F.; Férey, G.; Walton, K. S.; Snurr, R. Q., *J. Phys. Chem. C* **2007**, *111*, 15350-15356.
- [71] Kandambeth, S.; Mallick, A.; Lukose, B.; Mane, M. V.; Heine, T.; Banerjee, R., *J. Am. Chem. Soc.* **2012**, *134*, 19524-19527.
- [72] Biswal, B. P.; Chandra, S.; Kandambeth, S.; Lukose, B.; Heine, T.; Banerjee, R., *J. Am. Chem. Soc.* **2013**, *135*, 5328-5331.
- [73] Chandra, S.; Kundu, T.; Kandambeth, S.; Babarao, R.; Marathe, Y.; Kunjir, S. M.; Banerjee, R., *J. Am. Chem. Soc.* **2014**, *136*, 6570-6573.
- [74] Aradi, B.; Hourahine, B.; Frauenheim, T., *J. Phys. Chem. A* **2007**, *111*, 5678-5684.
- [75] Lukose, B.; Kuc, A.; Heine, T., *J. Mol. Model.* **2013**, *19*, 2143-2148.

**Chapter 4.**  
**Chiral Covalent Organic Frameworks for**  
**High-Performance Heterogeneous**  
**Asymmetric Catalysis**

*Preparing Manuscript*

Hong Xu, Hao Wei, Jia Gao and Donglin Jiang

## **Abstract**

Periodic polygon networks and ordered open nanochannels found in covalent organic frameworks (COFs) render them able to construct catalytic scaffolds. However, the COFs' lack of unification of stability, crystallinity, and porosity has thus far impeded any practical implementation. Here we report an imine-linked COF to assure stability, crystallinity, and porosity that lead to the finding of a high-performance open catalytic framework. The stability is gained by exceptional crystal stacking energy in COFs that enable chemical anchoring chiral catalytic sites to their channel walls while retaining crystallinity and porosity. The chiral COFs serve as heterogeneous organocatalysts that are exceptionally active in water, catalyze asymmetric C–C bond formations smoothly and cleanly, and combine enantioselectivity, diastereoselectivity, recyclability, and environmental benignity. The open frameworks with these advancements are promising for practical heterogeneous catalysis.

## 4.1 Introduction

Michael addition is one of the basic C–C bond formation reactions and a powerful synthetic tool that provides access to synthons of many important natural and biologically active products.<sup>[1]</sup> Its versatile utility in organic synthesis has stimulated tremendous research interests in the development of asymmetric Michael catalysts, especially metal-free organocatalysts.<sup>[2-4]</sup> However, the field of homogenous organocatalysts remains problematic with respect to the practical application owing to the difficulty in the separation of expensive catalysts for repeated use. To overcome these problems, the development of immobilized, easily recoverable, and reusable catalysts appears as one of the most promising strategies.<sup>[5]</sup>

Most of heterogeneous organocatalysts are using linear polymers as catalyst supporters, which however, give low activity as a result of inefficient access to catalytic sites.<sup>[6-8]</sup> Polymer particles could enhance the reaction interface on surface; however, they involve complicated surface modification while the inner part of the particles is unavailable for catalysis. To overcome this issue, metal-organic framework (MOF)-based organocatalysts have been developed, utilizing coordination chemistry to introduce the catalytic sites into the open frameworks.<sup>[9-11]</sup> However, the MOF-based organocatalysts are problematic in terms of pore size, enantioselectivity and the stability issue of the coordination bonds. Recently, we have developed microporous COFs as heterogeneous organocatalysts.<sup>[5]</sup> However, these COFs are active to only small reactants, yield medium enantioselectivity, and are not stable enough for cycle use. A variety of COFs have been explored for heterogeneous catalysis, including an imine-linked COF with coordinated Pd(II) complexes on walls for Suzuki cross-coupling reactions,<sup>[12]</sup> encapsulated Au(0) nanoparticles for nitrophenol reduction,<sup>[13]</sup> imine-linkages in COFs for Knoevenagel condensation reactions,<sup>[14]</sup> and  $\pi$ -systems as photocatalysts for oxygen activation<sup>[15]</sup> and hydrogen production.<sup>[16]</sup> Cycle performance is crucial for applications, however, satisfying results are rarely achieved for COF catalysts thus far reported; the stability issue remains to be well explored.

In this study, we develop a stable, crystalline, and porous COF and show its utility in synthesizing high-performance open-framework heterogeneous catalysts. The stability originates from the  $\pi$ - $\pi$  interactions between layers in COFs that give rise to exceptional crystal stacking energy. By virtue of stability, the mesoporous imine-linked COF enables the engineering of channel walls with chiral catalytic sites in a synthetically controlled manner while retaining high crystallinity and porosity. The resulting chiral COFs consist of catalytic open frameworks that are accessible to reactants and show exceptional catalytic activity in water under ambient conditions. The COFs function as heterogeneous catalysts to activate deactivated reactants for straightforward asymmetric Michael C-C formation reactions and achieve high enantioselectivity, diastereoselectivity, recyclability, and environmental benignity that meet the requirements of catalysts for practical application. These results unambiguously reveal the significance of a stable COF in disclosing inherent functions and applications of open organic frameworks.

## 4.2 Results and Discussions

### 4.2.1 Synthesis and Structural Characterization

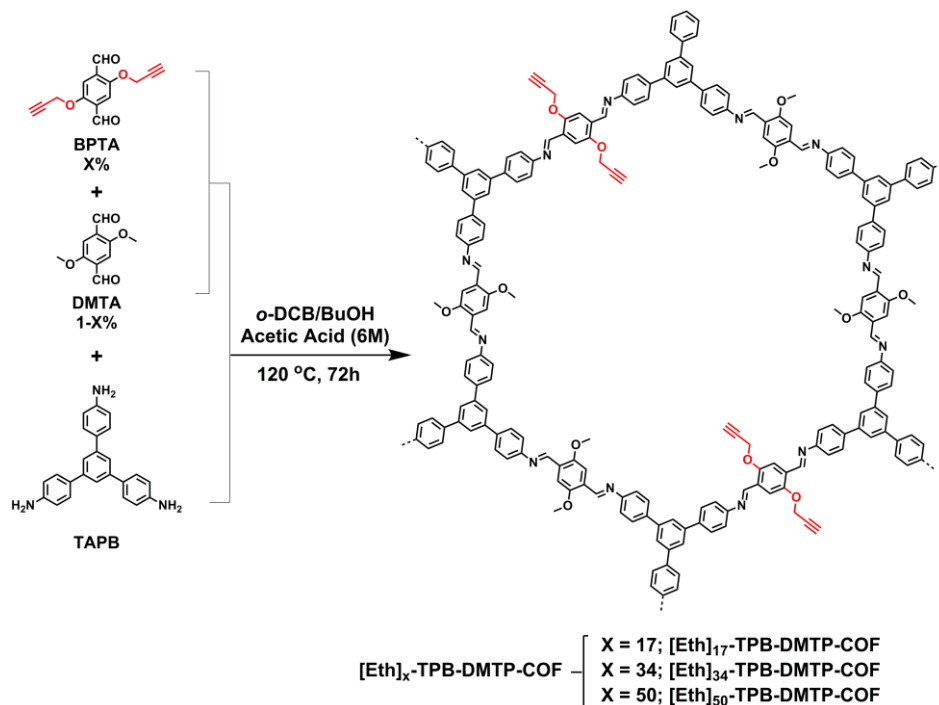


**Figure 1.** Synthesis of COF-organocatalysts ( $[\text{Py}]_x\text{-TPB-DMTP-COFs}$ ,  $X = [\text{BPTA}]/([\text{BPTA}] + [\text{DMTA}]) = 17, 34, \text{ and } 50$ ) via channel-wall engineering using a three-component condensation.

The TPB-DMTP-COF provides a stable, crystalline, and mesoporous framework, which satisfies the requirements of COF materials for functional exploration. In this study, we focused on developing heterogeneous catalytic open frameworks. We embedded the catalytic sites on the channel walls, because this structure takes the full advantage of open channels in which the active sites are easily accessible to reactants and substrates. For this purpose, we employed a three-component condensation system to synthesize the  $[\text{Eth}]_x\text{-TPB-DMTP-COFs}$  as intermediates (**Figure 1**), followed by the azide-ethynyl click reaction for appending chiral pyrrolidine species onto the pore walls of the chiral  $[\text{Py}]_x\text{-TPB-DMTP-COFs}$  (**Figure 2**), according to an established methodology.<sup>[5, 17]</sup> The content ( $X$ ) of catalytic pyrrolidine units in the  $[\text{Py}]_x\text{-TPB-DMTP-COFs}$  was adjusted by the loading content of 2,5-bis(2-

propynyloxy)terephthalaldehyde (BPTA) and 2,5-dimethoxyterephthalaldehyde (DMTA) ( $X = [\text{BPTA}] / ([\text{BPTA}] + [\text{DMTA}]) \times 100 = 0, 17, 34, \text{ and } 50$ ) for the three-component condensation reactions. Note that the X value of 17, 34, and 50 corresponds to a series of COFs in which each hexagonal macrocycle has one, two, and three catalytically active pyridine units, respectively. These reactions exhibited similar isolated yields to each other (experimental section), indicating that the reactivity of BPTA and DMTA is similar under the solvothermal condition.

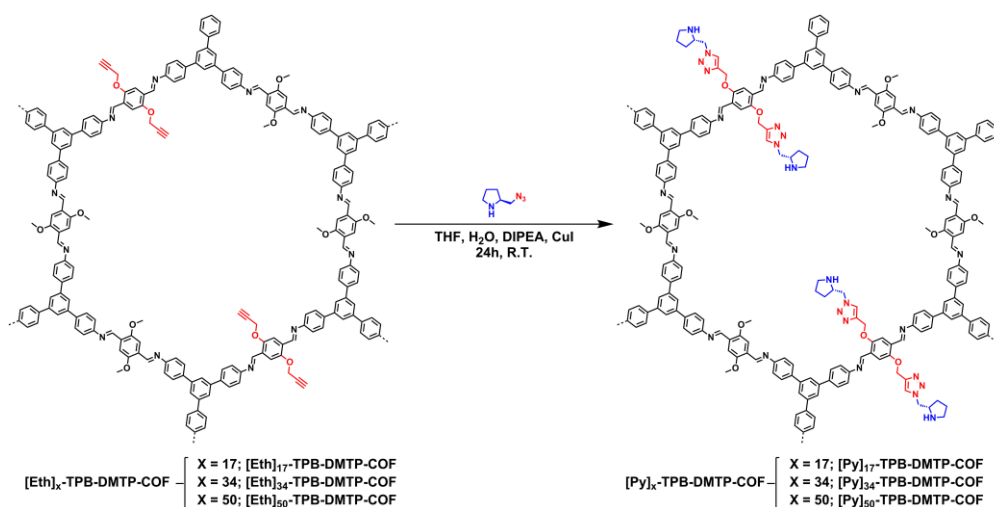


**Figure 2.** The general strategy for the pore surface engineering of the ethynyl-modified COFs via click chemistry (the case for  $x = 34$  was exemplified)

#### 4.2.2 Preparation of the COF Catalysts

The three-component reaction system allows the integration of the ethynyl units onto the pore walls with synthetically controlled density. The ethynyl units undergo a quantitative click reaction with azide compounds to construct functional interfaces via triazole linkages. The density of the pyrrolidine units on the pore walls was determined by the ethynyl content of  $[\text{Eth}]_x\text{-TPB-DMTP-COFs}$ . After the click reaction, the FT-IR spectra demonstrated the disappearance of the vibration bands at  $2120$  and  $3290\text{ cm}^{-1}$  that were attributed to the  $\text{H-C}\equiv\text{C}$  units (**Figure 4**), indicating all the  $\text{C}\equiv\text{C}$  units are clicked to bear the catalytic sites. The XRD intensity tended to decrease with increasing ethynyl content (**Figure 3**). The COF-X exhibited the highest XRD intensity of  $135 \times 10^3$  cps with  $51 \times 10^3$  cps for  $[\text{Eth}]_{50}\text{-TPB-DMTP-COFs}$ . This decrease in intensity is

caused by the large number of amorphous ethynyl chains on the pore walls. The presence of ethynyl groups does not create new XRD peaks. [Eth]<sub>x</sub>-TPB-DMTP-COFs possess the same crystalline structure as TPB-DMTP-COF, as evident by their similar XRD patterns. As more catalytic active groups were integrated into the pore walls, the XRD intensity decreased, a similar phenomenon was observed for the [Eth]<sub>x</sub>-TPB-DMTP-COF. Similarly, the XRD peak positions remained unaffected, indicating that the crystalline skeleton was well retained.

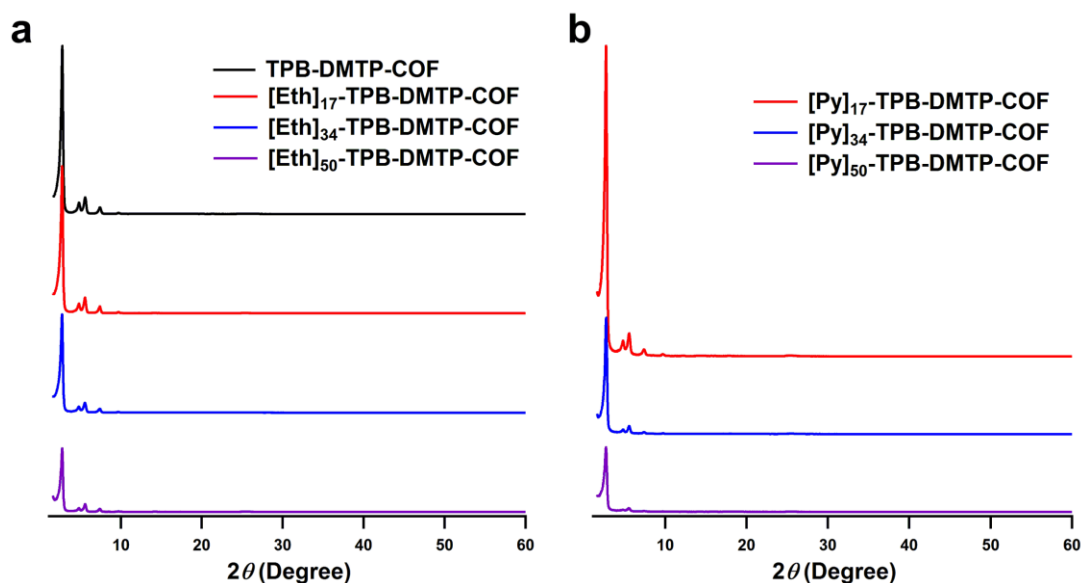


**Figure 3.** XRD patterns of **a.** TPB-DMTP-COF and [Eth]<sub>x</sub>-TPB-DMTP-COFs; **b.** [Pyr]<sub>x</sub>-TPB-DMTP-COFs

After the click reaction, a nitrogen rich unit was introduced to the COF pore walls, which cause a significant increase of the nitrogen content; meanwhile, the experimental content of carbon, hydrogen and nitrogen is quite close to the theoretical value (**Table 1**). Further, IR spectra demonstrated the disappearance of the vibration bands at 2120 and 3290  $\text{cm}^{-1}$  that were attributed to the  $\text{H-C}\equiv\text{C}$  units (**Figure 4**), indicating all the  $\text{C}\equiv\text{C}$  units are quantitatively transformed. Meanwhile the broad peaks at 2750-3000  $\text{cm}^{-1}$  which corresponding to the characteristic absorption peaks of the aliphatic chain are significantly increased;

besides, the strength of these peaks are increasing along with the increase of the catalytic sites content.

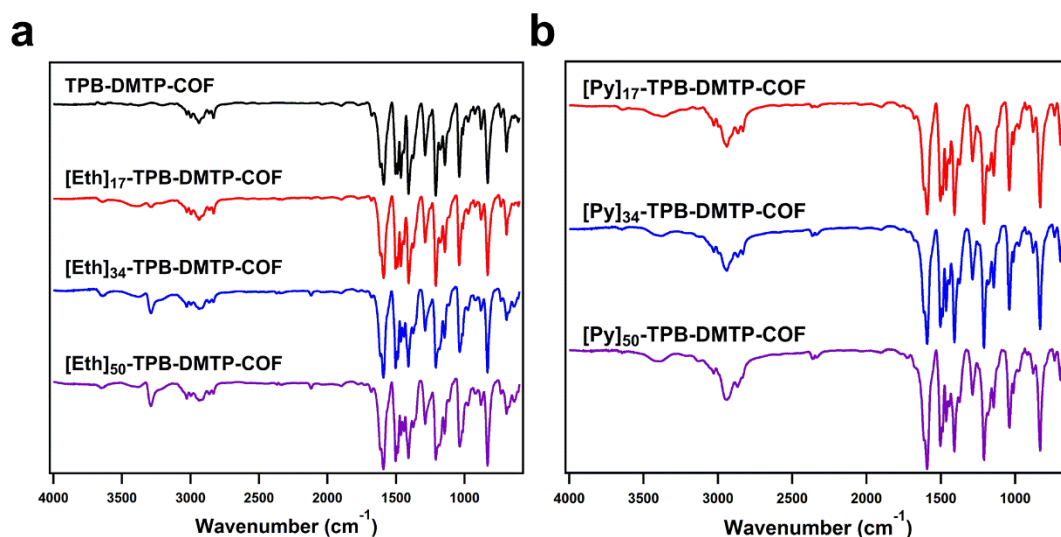


**Figure 4.** IR Spectra of **a.** TPB-DMTP-COF and [Eth]<sub>x</sub>-TPB-DMTP-COFs; **b.** [Pyr]<sub>x</sub>-TPB-DMTP-COFs.

**Table 1.** Elemental analysis of the COFs.

COFs		C (%)	H (%)	N (%)
TPB-DMTP-COF	Calcd.	79.57	5.14	7.14
	Found	78.34	5.77	6.35
[Eth] <sub>17</sub> -TPB-DMTP-COF	Calcd.	79.98	5.03	7.00
	Found	78.32	5.57	6.25
[Eth] <sub>34</sub> -TPB-DMTP-COF	Calcd.	80.37	4.93	6.86
	Found	78.31	5.64	5.94
[Eth] <sub>50</sub> -TPB-DMTP-COF	Calcd.	80.75	4.84	6.73
	Found	77.89	5.28	5.81
[Pyr] <sub>17</sub> -TPB-DMTP-COF	Calcd.	76.90	5.31	10.55
	Found	74.11	5.28	10.05
[Pyr] <sub>34</sub> -TPB-DMTP-COF	Calcd.	74.78	5.46	13.27
	Found	72.22	5.43	12.38
[Pyr] <sub>50</sub> -TPB-DMTP-COF	Calcd.	73.04	5.57	15.49
	Found	70.20	5.45	14.75

The density of the pyrrolidine units on the pore walls was determined by the ethynyl content of COF-Eth-x, since only the ethynyl groups could selectively react with the azide units to introduce the catalytic active sites; and mild reaction condition of the ‘Click reaction’ guarantee the COF network remain stable. Since the isolated yield of the click reaction is almost 100% and the elementary analysis result of the COF-catalyst is quite close to the theoretical value, further, there is no obvious absorption peak of the residue groups (aldehyde- or amino- groups). As shown in **Figure 5**, the pores become smaller and more crowded as the density of pyrrolidine units increases in [Pyr]<sub>x</sub>-H<sub>2</sub>P-COFs. This is further supported by the nitrogen sorption results (**Figure 6 and Table 2**).

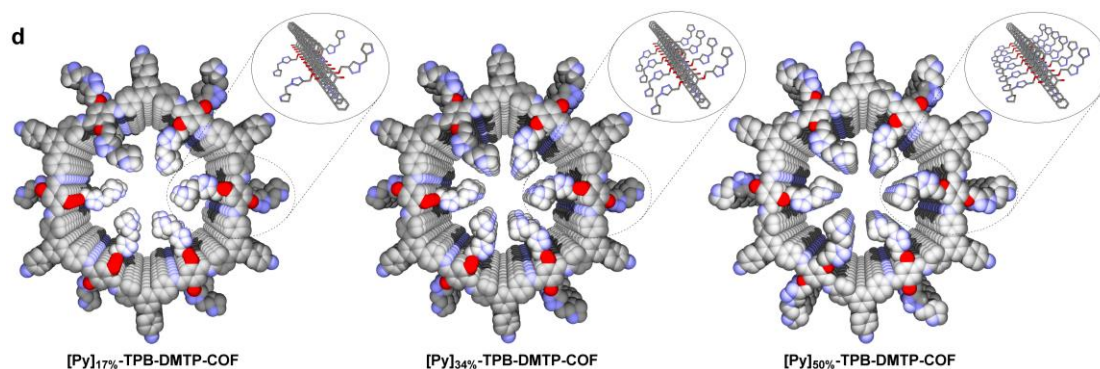


**Figure 5.** The graphical representation of [Pyr]<sub>x</sub>-TPB-DMTP-COF with different densities of catalytic sites on the pore walls.

#### 4.2.3 Gas Sorption Property

As the ethynyl content increased, COF-Eth-x exhibited a decrease in the BET surface area. For example, the TPB-DMTP-COF had a BET surface area of 2105, which decreased to 1973, 1760, and 1642 m<sup>2</sup>g<sup>-1</sup> for [Eth]<sub>17</sub>-TPB-DMTP-COF, [Eth]<sub>34</sub>-TPB-DMTP-COF, [Eth]<sub>50</sub>-TPB-DMTP-COF, respectively. Pore size distribution was estimated from the nitrogen uptake isotherm by nonlocal density functional theory (NLDFT) and revealed one pore type in their skeletons. The pore sizes decreased from 3.26 to 3.17, 3.10, and 3.03 nm, as the ethynyl content increased from 0 to 17, 34, and 50, respectively (**Table 2 and Figure 7**). After the click reactions, much bulky groups

were introduced into the pore walls of the COFs. Thus, [Pyr]<sub>x</sub>-TPB-DMTP-COFs exhibited a distinct decrease in the surface area. For example, [Pyr]<sub>17</sub>-TPB-DMTP-COF had a surface area of 1970, which decreased to 1802 and 1612 m<sup>2</sup>g<sup>-1</sup> for [Pyr]<sub>34</sub>-TPB-DMTP-COF and [Pyr]<sub>50</sub>-TPB-DMTP-COF. The pore sizes decreased from 3.07 to 2.95 and 2.86 as the pyrrolidine content increased from 17 to 34 and 50. The pore size distribution profile revealed that only one pore type existed, indicating that the pyrrolidine units are homogeneously engineered onto the walls.

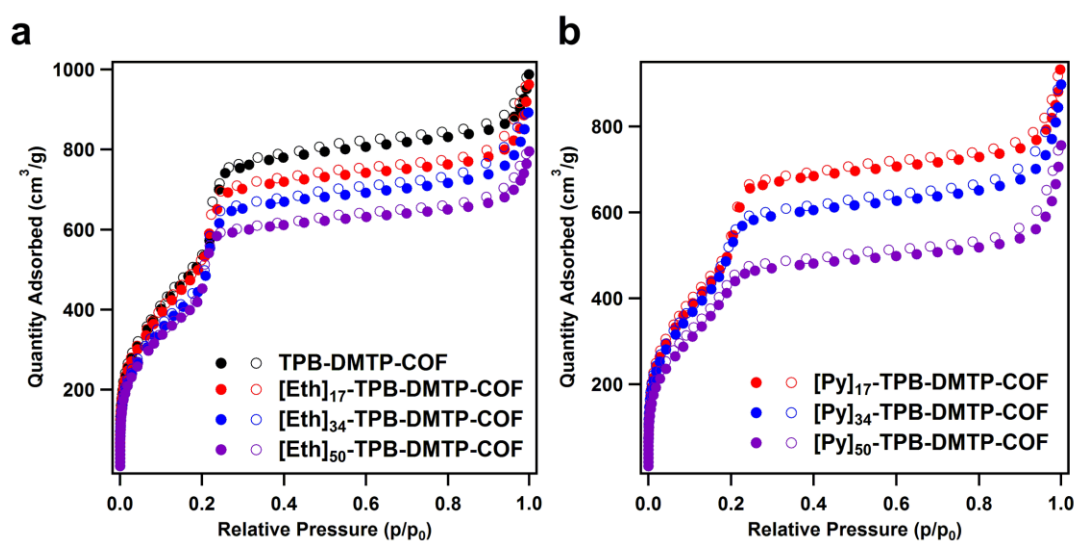


**Figure 6.** Nitrogen sorption isotherm profiles of **a.** TPB-DMTP-COF and [Eth]<sub>x</sub>-TPB-DMTP-COFs; **b.** [Pyr]<sub>x</sub>-TPB-DMTP-COFs.

**Table 2.** Pore size and pore volume of the COFs.

	BET Surface Area (m <sup>2</sup> /g)	Pore Size (nm)	Pore Volume (cm <sup>3</sup> /g)
TPB-DMTP-COF	2105	3.26	1.53
[Eth] <sub>17</sub> -TPB-DMTP-COF	1973	3.17	1.49
[Eth] <sub>34</sub> -TPB-DMTP-COF	1760	3.1	1.38
[Eth] <sub>50</sub> -TPB-DMTP-COF	1642	3.03	1.23
[Pyr] <sub>17</sub> -TPB-DMTP-COF	1970	3.07	1.44
[Pyr] <sub>34</sub> -TPB-DMTP-COF	1802	2.95	1.35

[Pyr] <sub>17</sub> -TPB-DMTP-COF	1612	2.86	1.18
Recycled [Eth] <sub>17</sub> -TPB-DMTP-COF	1916	2.98	1.46

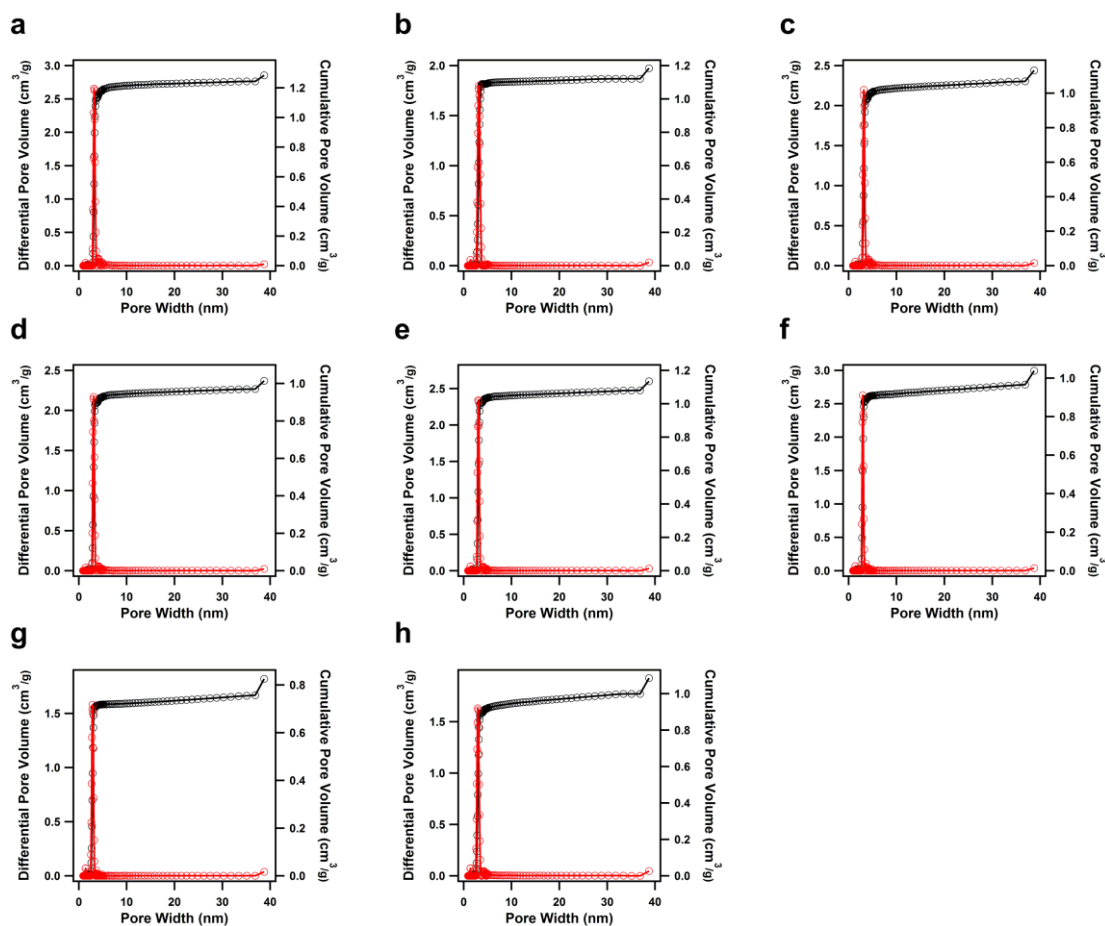
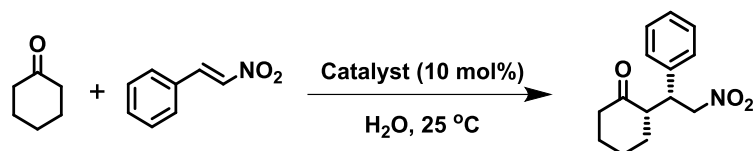


**Figure 7. a-k**, Pore size distribution (red) and cumulative pore volume (black) profiles of the COFs. (a: TPB-DMTP-COF; b: [Eth]<sub>17</sub>-TPB-DMTP-COF; c: [Eth]<sub>34</sub>-TPB-DMTP-COF; d: [Eth]<sub>50</sub>-TPB-DMTP-COF; e: [Py]<sub>17</sub>-TPB-DMTP-COF; f: [Py]<sub>34</sub>-TPB-DMTP-COF; g: [Py]<sub>50</sub>-TPB-DMTP-COF; h: Recycled COF-Pyr-17.)

#### 4.2.4 Heterogeneous Organocatalysis

Michael reactions are typically conducted in organic solvents or in mixed organic-aqueous solutions; the use of neat water as solvent is of particular environmental and economic concerns.

**Table 3.** Asymmetric Michael reaction catalyzed by the [Py]<sub>x</sub>-TPB-DMTP-COFs



Entry	Catalyst	Time (h)	Conversion (%)	Yield (%)	ee (%)	dr
1	[Py] <sub>17</sub> -TPB-DMTP-COF	12	100	95	92	90/10
2	[Py] <sub>34</sub> -TPB-DMTP-COF	17	100	93	91	90/10
3	[Py] <sub>50</sub> -TPB-DMTP-COF	34	100	95	89	88/12
4	Py <sup>b</sup>	22	100	96	92	91/9
5	[Pyr] <sub>25</sub> -H <sub>2</sub> P-COF <sup>a</sup>	36	–	–	–	–

<sup>a</sup>no reaction. <sup>b</sup> Py =

We conducted the Michael reactions in neat water at room temperature of 25 °C by dispersing the [Py]<sub>x</sub>-TPB-DMTP-COFs in the reaction mixture. **Table 3** summarized the results of the Michael reactions. We utilized the low active cyclohexanone instead of aldehydes as the reactant for the Michael reactions. The insoluble [Py]<sub>x</sub>-TPB-DMTP-COFs give rise to a heterogeneous catalytic system. Outstanding catalytic activity was observed for the [Py]<sub>17</sub>-TPB-DMTP-COF (entry 1). As a result, we are able to lower the catalyst load to 10 mol%. For example, the Michael reaction of cyclohexanone and β-nitrostyrene proceeded cleanly and highly efficiently in neat water at 25 °C (**Table 3**), achieved 100% conversion in 12 h and yielded the enantioselectivity (ee) and diastereoselectivity (dr) as high as 92% and 90/10, respectively (entry 1). As a control, we utilized the molecular catalyst with a same catalytic structure as those integrated on the pore walls of the [Py]<sub>x</sub>-TPB-DMTP-COFs (entry 4) for the same reaction. The molecular catalyst requires a much longer reaction time of 22 h to complete 100% conversion with ee and dr values of 92% and 91/9, respectively.

The enantioselectivity and diastereoselectivity observed for the heterogeneous [Py]<sub>17</sub>-TPB-DMTP-COF catalyst were similar to those of the molecular catalyst, which indicates that the catalytic sites on the channel walls are well retained in both enantio-control and diastereo-control by the chiral centers during the surface-engineering process that were conducted under mild room-temperature click reaction conditions. These results of the COF catalyst are remarkable because the heterogeneous catalytic systems typically have much lower enantioselectivity and diastereoselectivity compared to molecular catalysts.

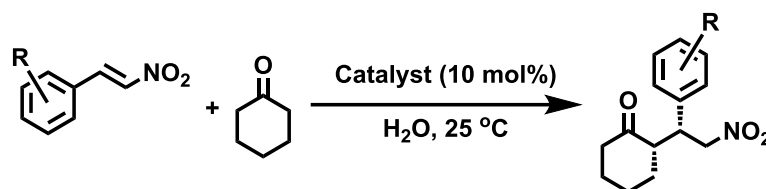
Notably, the heterogeneous [Py]<sub>17</sub>-TPB-DMTP-COF catalyst has a greatly enhanced activity; the significantly shortened reaction time compared to the molecular catalyst suggests that the nano-channels of COFs can accumulate the reactants and substrates from the water phase and promote the asymmetric reactions in the confined nanospace. **Table 6** summarizes the heterogeneous organocatalytic systems; the majority of catalysts are developed for Aldol reactions that utilize highly active and small reactants. To the best of our knowledge, the [Py]<sub>17</sub>-TPB-DMTP-COF exhibits the highest catalytic activity reported to date for the heterogeneous asymmetric Michael reactions.

We utilized [Py]<sub>34</sub>-TPB-DMTP-COF and [Py]<sub>50</sub>-TPB-DMTP-COF as a catalyst, which also give rise to heterogeneous reaction systems (**Table 3**, entries 2 and 3). Notably, the [Py]<sub>34</sub>-TPB-DMTP-COF and [Py]<sub>50</sub>-TPB-DMTP-COF achieved the ee values of 91, 89 and the dr values of 90/10, 88/12, respectively, which are similar to those of the [Py]<sub>17</sub>-TPB-DMTP-COF. These results indicate that the chiral catalytic sites on the channel walls are effective for both the enantio-control and diastereo-control in the asymmetric reactions, irrespective of their densities.

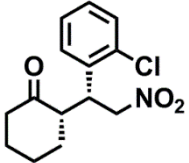
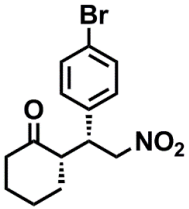
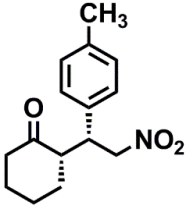
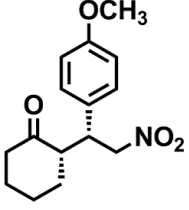
We observed that the densities of the chiral catalytic sites significantly affect the reaction rate. The [Py]<sub>34</sub>-TPB-DMTP-COF and [Py]<sub>50</sub>-TPB-DMTP-COF need a longer time of 17 and 34 h, respectively, to complete the reaction under otherwise same conditions (**Table 3**, entries 2 and 3). The elongated reaction time suggests that the mass transport becomes sluggish when the nano-channel walls are loaded with the dense side

chains; the channels become more crowded when more catalytic sites were anchored to the walls, as illustrated in **Figure 5**. This is further supported by control experiments using a microporous COF with the same catalytic active sites on the channel walls as a catalyst. Surprisingly, when the pore size was decreased to the microporous region, the Michael reactions were deeply suppressed. For example, the [Pyr]<sub>25</sub>-H<sub>2</sub>P-COF with the same chiral catalytic structures on the pore walls but a pore size of 1.9 nm cannot catalyze the Michael reaction; after 36 h, no reaction occurs (**Table 3**, entry 5). This catalytic silence is related to the fact that the Michael reactions involve large-size substrates; this catalytic feature sets a must for the heterogeneous Michael catalysts to have sufficiently large open pores. Synthesis of large mesopores and stable skeletons remains a major challenge for MOFs and COFs; no examples of MOF catalysts thus far reported can catalyze the Michael reactions. The COF-catalysts are the first example of crystalline porous catalysts including MOFs and COFs for catalyzing the Michael reactions.

**Table 4.** Investigating the substrate scope of Michael Addition catalyzed by [Py]<sub>17</sub>-TPB-DMTP-COF organocatalyst



Product	Reaction time to 100% conversion (h)	Yield (%)	d.r.	ee (%)
	12	95	90/10	92
	10	97	90/10	90

	6	95	97/3	94
	12	97	93/7	95
	16	94	92/8	93
	26	95	94/6	96

We investigated different reactants to confirm the generality of the Michael reactions (**Table 4**). The  $\beta$ -nitrostyrene compounds with different substituents on the phenyl ring, including various electron-donating and -withdrawing groups, were utilized for the Michael reaction. High activities were achieved using the [Py]<sub>17</sub>-TPB-DMTP-COF catalyst for activated  $\beta$ -nitrostyrenes, such as 4-bromo- $\beta$ -nitrostyrene, 4-chloro- $\beta$ -nitrostyrene; the reactions complete in 12 and 10 h. The enantioselectivity and diastereoselectivity were good to yield the ee values of 95% and 90% and the dr values of 93/7 and 90/10, respectively. The ortho-chloro-substituted  $\beta$ -nitrostyrene exhibited the highest activity among the series; the reaction reached 100% conversion in only 6 h, whereas the ee and dr values were as high as 94% and 97/3, respectively. Notably, the [Py]<sub>17</sub>-TPB-DMTP-COF catalyzed efficiently the Michael reactions of  $\beta$ -nitrostyrene in which the electron-donating groups at para-positions relative to the C=C double bonds are deactivated and are typically difficult to accomplish. Notably, the

[Py]<sub>17</sub>-TPB-DMTP-COF successfully facilitated the reaction of the 4-methyl- $\beta$ -nitrostyrene and cyclohexanone. The reaction was achieved in high conversion in 16 h and reached the ee and dr values of 93% and 92/8, respectively. Even for the severely deactivated substrate, such as 4-methoxy- $\beta$ -nitrostyrene, the [Py]<sub>17</sub>-TPB-DMTP-COF catalyst completed the reaction in 26 h and achieved 96% ee and 94/6 dr. These results indicate that the [Py]<sub>17</sub>-TPB-DMTP-COF catalyst is highly active to both deactivated reactants and substrates.

#### 4.2.5 Kinetic Study

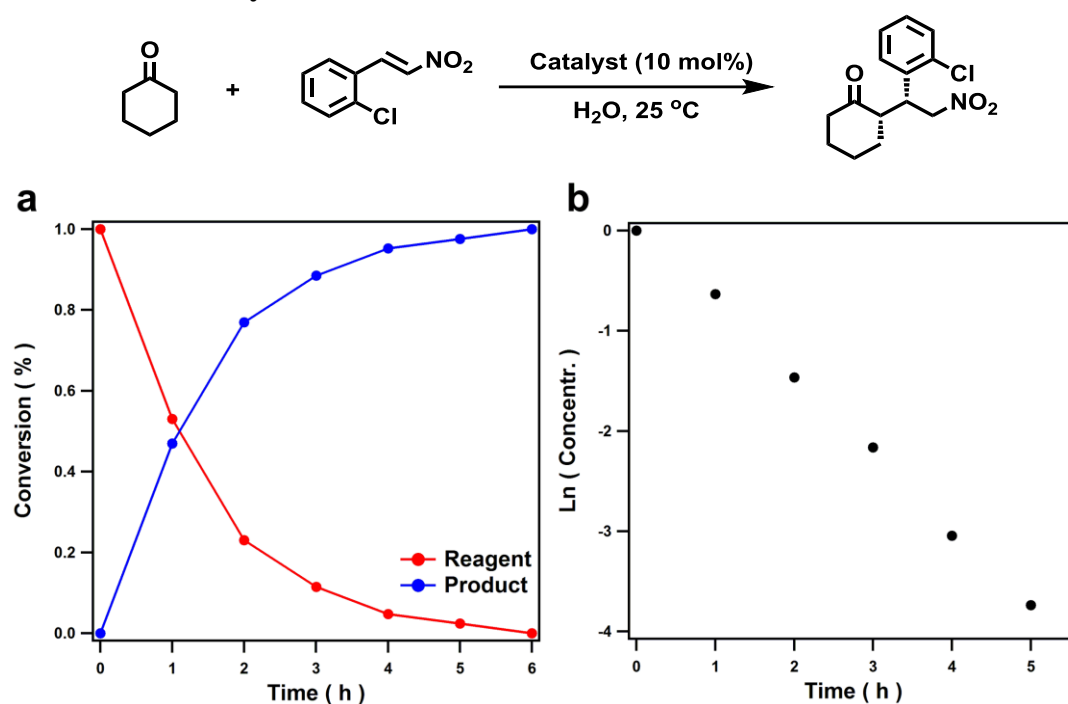


**Figure 8.** **a.** Conversion of the reagent (trans-2-chloro- $\beta$ -nitrostyrene) and concentration of the corresponding product in the reaction system. Determined by <sup>1</sup>H-NMR. **b.** Natural logarithm of the concentration (product) versus reaction time.

Kinetic studies were conducted through the entire reaction region between 0% and 100% conversion, with each experiment performed at least in duplicate, whereas the average conversions were used for kinetics evaluations. The decrease of trans-2-chloro- $\beta$ -nitrostyrene (red dots) and increase of the product (blue dot) in the Michael reactions are straightforward and the catalytic reactions proceed smoothly (**Figure 8a**). It is

noteworthy that no induction periods are observable for these heterogeneous [Py]<sub>17</sub>-TPB-DMTP-COF catalytic systems.

Under the reported conditions, the reactions exhibited apparent first-order behavior to the concentration of trans-2-chloro- $\beta$ -nitrostyrene (**Figure 8b**), which is in consistent with its role in rate-determining step (see below). The rate constant ( $k_{\text{obs}}$ ) and lifetime ( $t_{1/2}$ ) were calculated to be  $k_{\text{obs}} = 0.78 \text{ h}^{-1}$  and  $t_{1/2} = 0.9 \text{ h}$  for the Michael reaction. The reaction rate by the [Py]<sub>17</sub>-TPB-DMTP-COF is among the highest thus far reported for the Michael reactions.

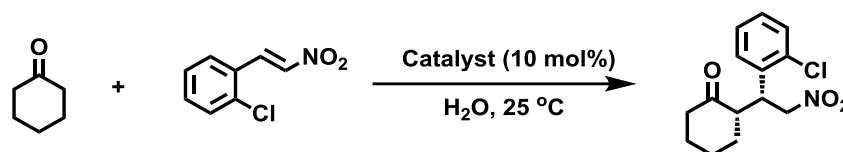
A plausible explanation for the observed first-order rate may involve the quick addition of cyclohexanone to the pyrrolidine catalyst to form an enamine intermediate, followed by the addition of styrene substrate to the enamine intermediate as the rate-determining step, with a consequent rapid hydrolysis to yield the corresponding products. The observed (2S, 1R) absolute configuration of the major syn Michael adduct as determined by the literature comparison of HPLC elution order, is consistent with the transient state of the nitrostyrene to attack the re-face of the enamine.<sup>[18]</sup>

#### 4.2.6 Cycle Performance

A long catalyst lifetime and the capability of repeated use are highly desired for practical applications. The [Py]<sub>x</sub>-TPB-DMTP-COFs are easily separated from the reaction mixture and recovered; filtration and subsequent rinsing with solvents and water refreshed the catalyst for the next round of catalyst cycle. In general, organocatalysts undergo considerable decomposition during reactions and finally lose activity, which is the reason why the catalyst loading in homogeneous systems reaches even 50 mol% of the substrates. The [Py]<sub>17</sub>-TPB-DMTP-COF catalyst was subjected to repeated use at a 10 mol% catalyst loading for the Michael reactions in water at 25 °C. Notably, the [Py]<sub>17</sub>-TPB-DMTP-COF catalyst retained high activity and achieved high yields, while retaining high enantioselectivity and diastereoselectivity even after five cycles (**Table 5**), without the use of elevated reaction temperature or the increased loading of the catalyst. The [Py]<sub>17</sub>-TPB-DMTP-COF catalyst exhibits the longest catalyst lifetime reported to date for the heterogeneous Michael reactions. Organocatalysts based on porous organic polymers<sup>[19]</sup> and MOFs<sup>[9-11]</sup> exhibit drastically

decreased activity to require much longer reaction time upon cycle (**Table 6**). Together with the high activity and broad substrate scope, the excellent extended performance renders the [Py]<sub>17</sub>-TPB-DMTP-COF a more economic and environmentally benign process.

**Table 5.** Recycling experiment of the [Py]<sub>17</sub>-TPB-DMTP-COF for the Michael addition reaction.



Catalyst	Time (h)	Yield	d.r.	ee (%)	Wt (%)
Fresh	6	95%	97/3	94	>99
Cycle 1	7	93%	97/3	94	>99
Cycle 2	9	94%	97/3	94	>99
Cycle 3	11	92%	97/3	94	>99
Cycle 4	13	92%	97/3	93	>99

To gain structural insights into the excellent performance of the [Py]<sub>17</sub>-TPB-DMTP-COF, we characterized the cycled catalyst using various analytical methods. Firstly, the XRD patterns of the [Py]<sub>17</sub>-TPB-DMTP-COF after each cycle were recorded (**Figure 9a**), which indicate that the crystallinity of the [Py]<sub>17</sub>-TPB-DMTP-COF catalyst could be perfectly maintained during cycle. Secondly, the nitrogen sorption behavior of the [Py]<sub>17</sub>-TPB-DMTP-COF catalyst upon five cycles was investigated at 77 K. The [Py]<sub>17</sub>-TPB-DMTP-COF catalyst exhibited a typical type-IV isotherm curve (**Figure 9b**), which is identical to that of the fresh catalyst. The BET surface area is 1916 m<sup>2</sup> g<sup>-1</sup>, whereas the pore size and pore volume were evaluated to be 2.98 nm and 1.08 cm<sup>3</sup> g<sup>-1</sup>, respectively (**Table 2**). Notably, these porosity parameters are very similar to the original ones of the fresh catalyst. Thirdly, the IR spectrum of the [Py]<sub>17</sub>-TPB-DMTP-COF catalyst upon five cycles was almost identical to that of the fresh catalyst (**Figure 9c**). The good stability renders the [Py]<sub>17</sub>-TPB-DMTP-COF enable to cycle use

while retaining high crystallinity, large porosity, and excellent activity. With these features, the COF-catalyst is also the best example of the heterogeneous catalysts thus far developed for the asymmetric Michael reactions in terms of cycle performance.

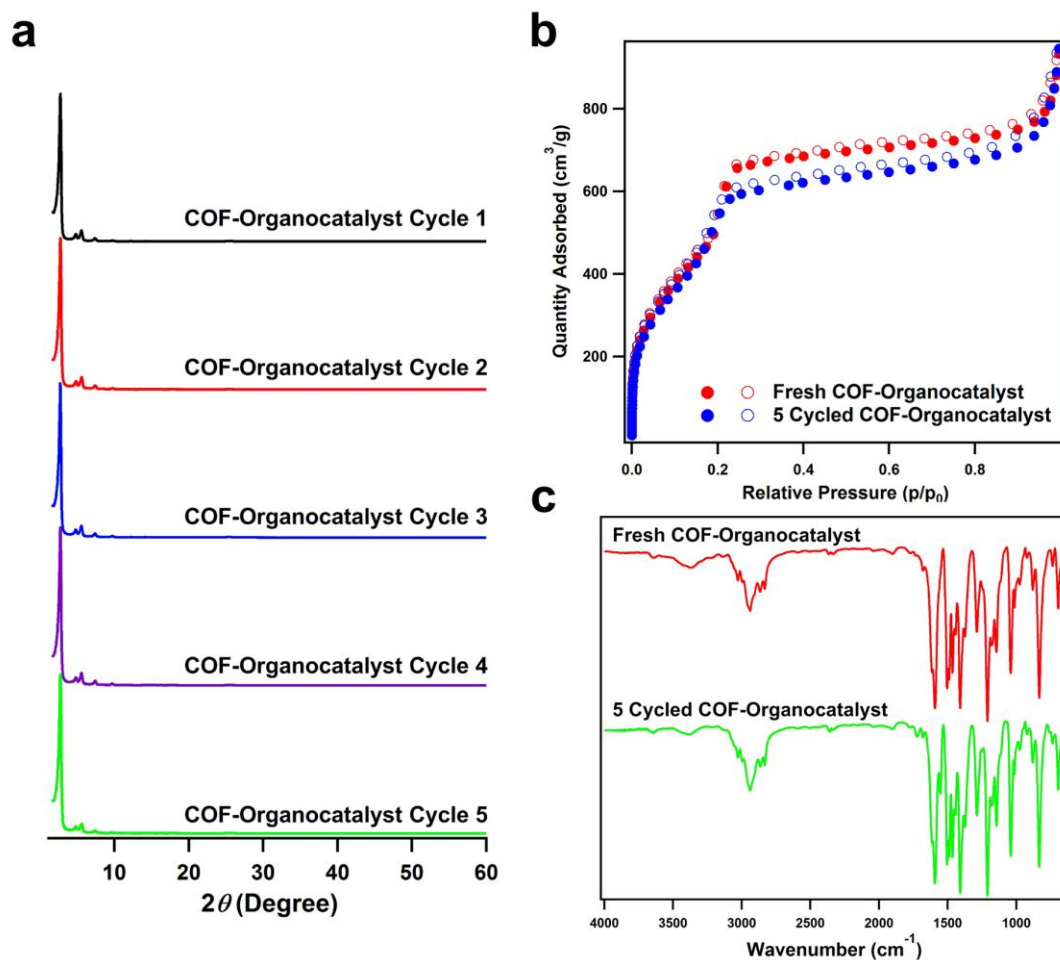


**Figure 9.** **a.** XRD patterns; **b.** Nitrogen sorption isotherm profiles; **c.** IR Spectra of the recycled COF-Organocatalyst, [Py]<sub>17</sub>-TPB-DMTP-COF.

### 4.3 Conclusion

In summary, we have developed a mesoporous COF that satisfies the requirements on stability, crystallinity, and porosity for functional exploration. The stability renders the COFs able to be chemically functionalized while retaining crystallinity and porosity; the chiral COF catalysts engineered with active sites on the channel walls were synthesized in a facile yet controlled manner. This novel class of open framework catalysts, unlike previous catalysts thus far reported, merges a number of striking features, including activity, enantioselectivity, diastereoselectivity, stability, recyclability, and environmental benignity; these advantages offer a plausible solution to long-standing challenges for real application of organocatalysts. Therefore, these advancements open new perspectives in the design of heterogeneous catalysts for the sustainable production of chemicals and fuels; the utilization of stable open framework architectures may facilitate the design of other functions and applications.

## 4.4 Experimental Sections

### 4.4.1 Materials and Methods

Flash column chromatography was carried out with silica gel (200-300 mesh).  $^1\text{H}$  nuclear magnetic resonance (NMR) spectra were recorded on JEOL models JNM-LA400 NMR spectrometers, where chemical shifts ( $\delta$  in ppm) were determined with a residual proton of the solvent as standard. Fourier transform infrared (IR) spectra were recorded on a JASCO model FT-IR-6100 infrared spectrometer. X-ray diffraction (XRD) data were recorded on a Rigaku model RINT Ultima III diffractometer by depositing powder on glass substrate, from  $2\theta = 1.5^\circ$  up to  $60^\circ$  with  $0.02^\circ$  increment. Nitrogen sorption isotherms were measured at 77 K with a Micromeritics Instrument Corporation model 3Flex surface characterization analyzer. The Brunauer-Emmett-Teller (BET) method was utilized to calculate the specific surface areas. By using the non-local density functional theory (NLDFT) model, the pore volume was derived from the sorption curve. Elemental analysis was performed on a Yanako model CHN CORDER MT-6 elemental analyzer. High performance liquid chromatography were performed on a JASCO model HPLC model with Daicel chiral AD-H columns with *i*-PrOH/*n*-hexane as the eluent.

The crystalline structure of COF were determined using the density-functional tight-binding (DFTB) method including Lennard-Jones (LJ) dispersion. The calculations were carried out with the DFTB+ program package version 1.2.<sup>[20]</sup> DFTB is an approximate density functional theory method based on the tight binding approach and utilizes an optimized minimal LCAO Slater-type all-valence basis set in combination with a two-center approximation for Hamiltonian matrix elements. The Coulombic interaction between partial atomic charges was determined using the self-consistent charge (SCC) formalism. Lennard-Jones type dispersion was employed in all calculations to describe van der Waals (vdW) and  $\pi$ -stacking interactions. The lattice dimensions were optimized simultaneously with the geometry. Standard DFTB parameters for X–Y element pair (X, Y = C, O, H and N) interactions were employed from the mio-0-1 set. The monolayer formation energy (condensation energy,  $E_c$ ) is

calculated from the total energies of the monolayer and of the individual building blocks.<sup>[21]</sup> The accessible surface areas were calculated from the Monte Carlo integration technique using a nitrogen-size probe molecule (diameter = 3.68 Å) roll over the framework surface with a grid interval of 0.25 Å.<sup>[22]</sup>

Dehydrated N,N-dimethylformide (DMF), N,N-dimethylacetamide (DMAc), dehydrated tetrahydrofuran (THF), and o-dichlorobenzene (o-DCB) were purchased from Kanto Chemicals. Hydrobromic acid, p-toluenesulonyl chloride, trifluoroacetic acid, toluene, dioxane, mesitylene, 1-butanol, ethanol, and acetic acid were purchased from Wako Chemicals. Propargyl bromide, 1,4-dimethoxybenzene, N-(tert-butoxycarbonyl)-L-prolinol, tert-butyl alcohol, 1,3,5-tri(4-aminophenyl) benzene and benzoic acid were purchased from TCI. trans-beta-Nitrostyrene, N,N-diisopropylethylamine, trans-4-chloro-beta-nitrostyrene, trans-2-chloro-beta-nitrostyrene, trans-4-bromo-beta-nitrostyrene, trans-4-methyl-beta-nitrostyrene, and trans-4-methoxy-beta-nitrostyrene were purchased from Sigma-Aldrich Co.

2,5-Dimethoxyterephthalaldehyde (DMTA), 2,5-dihydroxyterephthalaldehyde (DHTA) and 2,5-bis(2-propynyloxy) terephthalaldehyde (BPTA) and (S)-2-(Azidomethyl)pyrrolidine were synthesized according to the procedures described in Chapter 2, Section 2.4.3.

**TPB-DMTP-COF.** An o-DCB/BuOH (0.5 mL / 0.5 mL) mixture of TAPB (0.080 mmol, 28.1 mg) and DMTA (0.120 mmol, 23.3 mg) in the presence of acetic acid catalyst (6 M, 0.1 mL) in a Pyrex tube (10 mL) was degassed by three freeze–pump–thaw cycles. The tube was sealed off by flame and heated at 120 °C for 3 days. The precipitate was collected via centrifuge, washed with THF for 6 times and then soaked in THF for 1 day to remove trapped guest molecules. The powder was collected and dried at 120 °C under vacuum overnight to give the COF-X in isolated yield of 81%.

**[Eth]<sub>x</sub>-TPB-DMTP-COF.** An o-DCB/BuOH (0.5 mL / 0.5 mL) mixture of TAPB (0.080 mmol, 28.1 mg) and DMTA/BPTA (total 0.120 mmol) at different molar ratios of 5/1, 4/2, and 3/3 in the presence of acetic acid catalyst (6 M, 0.1 mL) in a Pyrex tube

(10 mL) was degassed by three freeze–pump–thaw cycles. The tube was sealed off by flame and heated at 120 °C for 3 days. The precipitate was collected via centrifuge, washed with THF for 6 times and then soaked in THF for 1 day to remove trapped guest molecules. The powder was collected and dried at 120 °C under vacuum overnight to give the corresponding COFs in isolated yields of 80%, 79%, and 81% for the COF-Eth-17, COF-Eth-34, and COF-Eth-50, respectively.

**[Py]<sub>x</sub>-TPB-DMTP-COF.** A THF/H<sub>2</sub>O (2.1 mL / 0.7 mL) mixture of COF-Eth-17 (65 mg) in the presence of CuI (6 mg) and DIPEA (THF solution; 1M; 108 μL) in a flask (25 mL) was added with (S)-2-(azidomethyl)pyrrolidine (toluene solution; 1 M; 60 μL). The flask was degassed via three freeze–pump–thaw cycles and the mixture was stirred at room temperature for 4 h. The precipitate was collected via centrifuge, washed with THF 5 times, and dried at room temperature under vacuum, to produce COF-Pyr-17 as a dark green solid in quantitative yield. The ethynyl groups were quantitatively reacted with the azide units as evident by the IR spectra. The click reaction of COF-Eth-x (x = 34 and 50) with (S)-2-(azidomethyl)pyrrolidine were performed according to this method under otherwise same conditions.



**Control: (S)-4-(Phenoxymethyl)-1-(pyrrolidin-2-ylmethyl)-1H-1,2,3-triazole**

**(S)-4-(Phenoxymethyl)-1-(pyrrolidin-2-ylmethyl)-1H-1,2,3-triazole.** The click reaction to synthesize this monomeric catalyst control was prepared according to the above procedure for COF-Pyr-17, using phenyl propargyl ether (toluene solution; 1M, 80 μL) in place of COF-Eth-17 as a reactant.

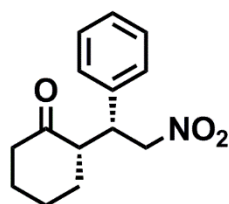
**Michael addition reaction.** To an H<sub>2</sub>O (1/1 v/v 0.4 mL) suspension of COF-Eth-17 (0.01 mmol) was added with cyclohexanone (2 mmol), nitrostyrene (0.1 mmol),

benzoic acid (0.025 mmol) and DIPEA (water suspension; 0.5M; 32 $\mu$ L). The mixture was stirred at room temperature for a period to reach 100% conversion. After addition of EtOH, the organic layer was removed via centrifuge. The catalyst was washed with EtOH twice and with ethyl acetate 3 times, the organic layer was then combined and concentrated under reduced pressure.  $^1\text{H-NMR}$  spectra were utilized to calculate diastereomeric ratio (dr). The enantiomeric excess (ee) was determined by HPLC on a chiral phase chiralpak AD-H column.

**Recycle procedure of [Py]<sub>17</sub>-TPB-DMTP-COF.** The COF catalyst was recovered via centrifuge, washed with ethyl acetate and a mixture of triethylamine/ethanol solution (5% v) to remove the product and reactants and simply dried before reuse.

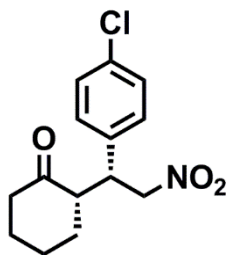
#### 4.4.2 Characterization of Products

(S)-2-((R)-2-nitro-1-phenylethyl)cyclohexanone<sup>[23-25]</sup>



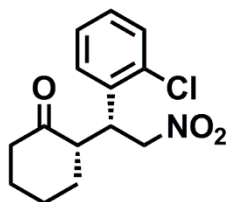
Major diastereomer:  $^1\text{H NMR}$  (400 MHz,  $\text{CDCl}_3$ ):  $\delta$  = 7.34-7.25 (m, 3H), 7.15 (d,  $J$  = 7.2 Hz, 2H), 4.93 (dd,  $J$  = 12.4, 4.4 Hz, 1H), 4.62 (dd,  $J$  = 12.4, 10 Hz, 1H), 3.75 (dt,  $J$  = 10, 4.4 Hz, 1H), 2.72-2.64 (m, 1H), 2.51-2.44 (m, 1H), 2.42-2.33 (m, 1H), 2.11-2.03 (m, 1H), 1.81-1.66 (m, 4H), 1.28-1.16 (m, 1H). HPLC conditions: The enantiomeric excess was determined by HPLC (Chiralcel AD-H), hexane : *i*-PrOH = 90 : 10, UV = 206 nm, 25  $^\circ\text{C}$ , 0.5 mL  $\text{min}^{-1}$ , syn:  $t_{\text{R}}$  = 24.2 min (minor) and  $t_{\text{R}}$  = 29.8 min (major).

(S)-2-((R)-1-(4-chlorophenyl)-2-nitroethyl)cyclohexanone<sup>[26]</sup>



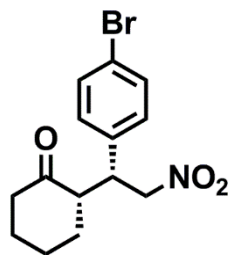
Major diastereomer:  $^1\text{H NMR}$  (400 MHz,  $\text{CDCl}_3$ ):  $\delta$  = 7.29 (d,  $J$  = 8.4 Hz, 2H), 7.10 (d,  $J$  = 8.4 Hz, 2H), 4.92 (dd,  $J$  = 12.4, 4.8 Hz, 1H), 4.59 (dd,  $J$  = 12.4, 9.6 Hz, 1H), 3.74 (dt,  $J$  = 9.8, 4.8 Hz, 1H), 2.68-2.59 (m, 1H), 2.50-2.43 (m, 1H), 2.41-2.31 (m, 1H), 2.12-2.04 (m, 1H), 1.83-1.76 (m, 1H), 1.75-1.53 (m, 3H), 1.28-1.16 (m, 1H). HPLC conditions: The enantiomeric excess was determined by HPLC (Chiralcel AD-H), hexane : *i*-PrOH = 90 : 10, UV = 206 nm, 20 °C, 0.5 mL min<sup>-1</sup>, syn:  $t_{\text{R}}$  = 34.6 min (minor) and  $t_{\text{R}}$  = 50.5 min (major).

(S)-2-((R)-1-(2-chlorophenyl)-2-nitroethyl)cyclohexanone<sup>[26]</sup>



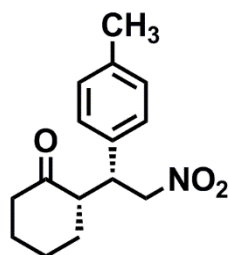
Major diastereomer:  $^1\text{H NMR}$  (400 MHz,  $\text{CDCl}_3$ ):  $\delta$  = 7.37 (dd,  $J$  = 8.4, 1.6 Hz, 1H), 7.26-7.17 (m, 3H), 4.92-4.86 (m, 2H), 4.31-4.23 (m, 1H), 2.96-2.85 (m, 1H), 2.50-2.43 (m, 1H), 2.42-2.33 (m, 1H), 2.13-2.05 (m, 1H), 1.85-1.56 (m, 4H), 1.38-1.28 (m, 1H). HPLC conditions: The enantiomeric excess was determined by HPLC (Chiralcel AD-H), hexane : *i*-PrOH = 90 : 10, UV = 206 nm, 20 °C, 0.5 mL min<sup>-1</sup>, syn:  $t_{\text{R}}$  = 24.0 min (minor) and  $t_{\text{R}}$  = 39.2 min (major).

(S)-2-((R)-1-(4-bromophenyl)-2-nitroethyl)cyclohexanone<sup>[27]</sup>



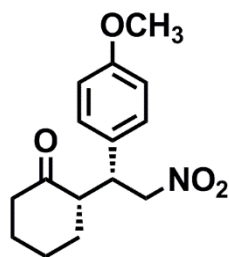
Major diastereomer:  $^1\text{H}$  NMR (400 MHz,  $\text{CDCl}_3$ ):  $\delta$  = 7.44 (d,  $J$  = 8.4 Hz, 2H), 7.05 (d,  $J$  = 8 Hz, 2H), 4.92 (dd,  $J$  = 12.8, 4.8 Hz, 1H), 4.59 (dd,  $J$  = 12.8, 10 Hz, 1H), 3.73 (dt,  $J$  = 10, 4.4 Hz, 1H), 2.67-2.59 (m, 1H), 2.50-2.43 (m, 1H), 2.41-2.32 (m, 1H), 2.12-2.05 (m, 1H), 1.83-1.56 (m, 4H), 1.28-1.17 (m, 1H). HPLC conditions: The enantiomeric excess was determined by HPLC (Chiralcel AD-H), hexane : *i*-PrOH = 90 : 10, UV = 208 nm, 25  $^\circ\text{C}$ , 1.0 mL  $\text{min}^{-1}$ , syn:  $t_{\text{R}}$  = 16.4 min (minor) and  $t_{\text{R}}$  = 24.7 min (major).

(S)-2-((R)-1-(4-methylphenyl)-2-nitroethyl)cyclohexanone<sup>[26]</sup>



Major diastereomer:  $^1\text{H}$  NMR (400 MHz,  $\text{CDCl}_3$ ):  $\delta$  = 7.11 (d,  $J$  = 8 Hz, 2H), 7.03 (d,  $J$  = 8.4 Hz, 2H), 4.90 (dd,  $J$  = 12.4, 4.8 Hz, 1H), 4.59 (dd,  $J$  = 12, 9.6 Hz, 1H), 3.70 (dt,  $J$  = 10, 4.8 Hz, 1H), 2.69-2.61 (m, 1H), 2.50-2.43 (m, 1H), 2.41-2.32 (m, 1H), 2.30 (s, 3H), 2.10-2.02 (m, 1H), 1.81-1.56 (m, 4H), 1.28-1.18 (m, 1H). HPLC conditions: The enantiomeric excess was determined by HPLC (Chiralcel AD-H), hexane : *i*-PrOH = 90 : 10, UV = 206 nm, 20  $^\circ\text{C}$ , 0.5 mL  $\text{min}^{-1}$ , syn:  $t_{\text{R}}$  = 22.0 min (minor) and  $t_{\text{R}}$  = 28.2 min (major).

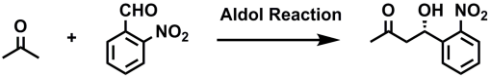
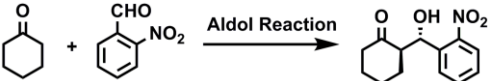
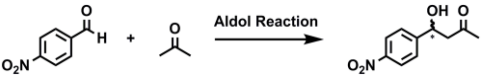
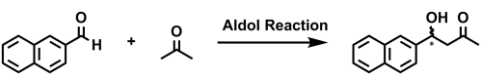
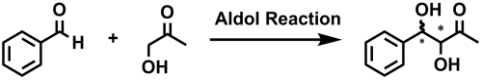
(S)-2-((R)-1-(4-methoxyphenyl)-2-nitroethyl)cyclohexanone<sup>[26, 28]</sup>

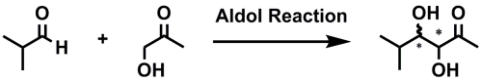
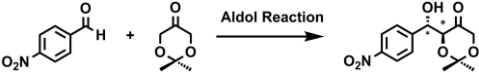
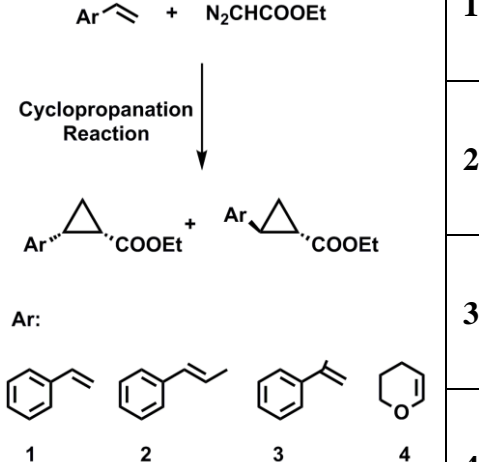


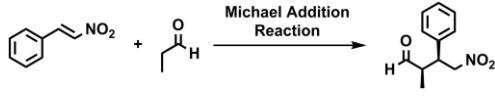
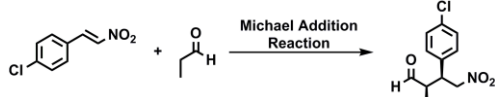
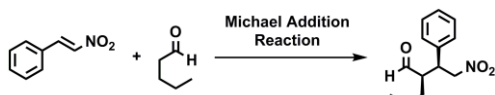
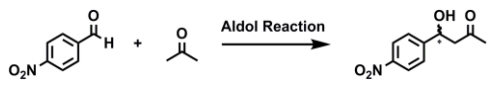
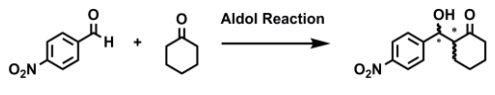
Major diastereomer:  $^1\text{H}$  NMR (400 MHz,  $\text{CDCl}_3$ ):  $\delta$  = 7.06 (d,  $J$  = 8.8 Hz, 2H), 6.83 (d,  $J$  = 9.2 Hz, 2H), 4.89 (dd,  $J$  = 12.4, 4.8 Hz, 1H), 4.57 (dd,  $J$  = 12.8, 10 Hz, 1H), 3.77 (s, 3H), 3.70 (dt,  $J$  = 10, 4.4 Hz, 1H), 2.67-2.59 (m, 1H), 2.49-2.43 (m, 1H), 2.41-2.32 (m, 1H), 2.10-2.02 (m, 1H), 1.81-1.52 (m, 4H), 1.28-1.18 (m, 1H). HPLC conditions: The enantiomeric excess was determined by HPLC (Chiralcel AD-H), hexane : *i*-PrOH = 80 : 20, UV = 206 nm, 20  $^\circ\text{C}$ , 0.5 mL  $\text{min}^{-1}$ , syn:  $t_{\text{R}}$  = 21.7 min (minor) and  $t_{\text{R}}$  = 26.0 min (major).

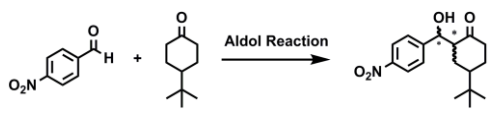
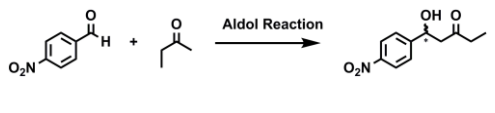
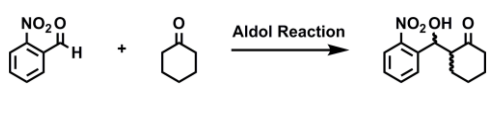
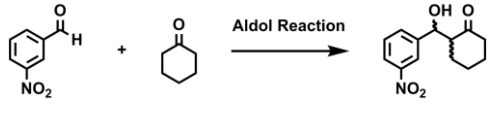
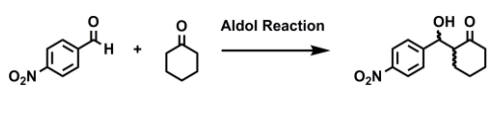
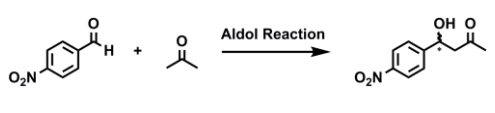
## 4.4.3 Comparison of Different Heterogeneous Organocatalysts

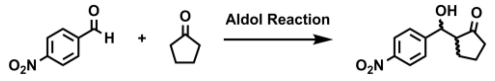
Table 6. Heterogeneous organocatalyst in porous materials.

	Preparation Strategy	Reaction	Solvents	Cata. Load	Temp.	Time	Yield	ee & dr	Cycle Performance	Surface Area & Pore Size
Graphenes	Immobilized to Graphene oxide via hydrogen binding <sup>[29]</sup>		Acetone	30%	30	6h	96%	79%	The cycled catalyst could maintain the yield and ee; however the activity issue is not mentioned.	Not mentioned
			DMF	30%	30	24h	96%	92% (93/7)		
Zeolites	The proline was immobilized on zeolite by adsorption to create heterogeneous catalyst. <sup>[30]</sup>		Acetone	30%	25	5.5h	78%	-21%	The cycle performance is not mentioned.	209 m <sup>2</sup> g <sup>-1</sup>
			Acetone	30%	25	40h	18%	-8%		
	The triethoxysilyl-modified proline was introduced to MCM-41 <sup>[31]</sup> via a post-functionalization strategy. <sup>[32]</sup>		DMSO	20%	90	24h	55%	70% (58/42)	After 3 cycles, the yield (from 55% to 50%) and dr (from 58/42 to 56/44) could be well maintained.	MCM-41 (1030 m <sup>2</sup> g <sup>-1</sup> ) Surface area of the catalyst is not
			Toluene	20%	90	24h	60%	70% (61/39)		
			DMSO	20%	90	24h	60%	70% (95/5)		
	Toluene	20%	90	24h	55%	70% (95/5)				
	DMSO	20%	90	24h	55%	99%				

								(95/5)	(ee not mentioned)	mentioned.
The triethoxysilyl-modified proline was grafted into MCM-41 <sup>[31]</sup> to create the heterogeneous catalyst. <sup>[33]</sup>		Toluene	20%	90	24h	55%	99% (95/5)	After 1 recycle, the conversion is changed from 96% to 93% at same period of time, ee decreased from 67% to 65%.	MCM-41 (1030 m <sup>2</sup> g <sup>-1</sup> ) Surface area of the catalyst is not mentioned.	
		MeCN	30%	25	96h	20%	63% (66/34)			
		DMF	30%	25	61h	80%	82% (83/17)			
		Formamide	30%	25	13h	96%	67% (66/34)			
Porous Organic Polymers	<p>Introducing proline to the polymer network via amidation reaction and deprotection of the t-Boc; further coordinate with Cu (II) yielded the heterogeneous metal-proline catalyst.<sup>[34]</sup></p> 	1	ClCH <sub>2</sub> CH <sub>2</sub> Cl	10% (5%)*	60	18h (18h)	90% (60%)	40% (60%)	This catalyst could be reused 10 times. (No detailed data)	190 m <sup>2</sup> g <sup>-1</sup> 10.9 nm <sup>3</sup> g <sup>-1</sup>
		2	ClCH <sub>2</sub> CH <sub>2</sub> Cl	10% (5%)	60	18h (18h)	92% (60%)	40% (30%)		
		3	ClCH <sub>2</sub> CH <sub>2</sub> Cl	10% (5%)	60	18h (2h)	96% (72%)	5% (3%)		
		4	ClCH <sub>2</sub> CH <sub>2</sub> Cl	10% (5%)	60	18h (2h)	96% (97%)	85% (47%)		

	The ethynyl-modified Jørgensen–Hayashi catalyst <sup>[35-37]</sup> was introduced into pores via the trimerization of the ethynes; further deprotection of the t-Boc group yielded the heterogeneous organocatalyst. <sup>[19]</sup>		EtOH/H <sub>2</sub> O	10%	25	1.5h	99%	98% (92/8)	After 4 cycles, the ee and dr could be well maintained, however, the yield is decreased from 96% to 39%, and the reaction time (to achieve 100% conversion) is extended from 2h to 30h.	881 m <sup>2</sup> g <sup>-1</sup> 0.50 cm <sup>3</sup> g <sup>-1</sup> Micropore (49.7%) Mesopore (50.3%)
			EtOH/H <sub>2</sub> O	10%	25	2h	96%	99% (92/8)		
			EtOH/H <sub>2</sub> O	10%	25	6h	86%	97% (95/5)		
MOFs	A pyridin-modified proline was introduced to the MIL-101 <sup>[38]</sup> via the coordination chemistry, led to the heterogeneous		Neat condition	10%	25	24h	66%	69%	After 3 cycles, the reaction time was extended from 24h to 48h (14% starting material residue); yield was	1420 m <sup>2</sup> g <sup>-1</sup> 0.73 cm <sup>3</sup> g <sup>-1</sup> (before introducing catalyst: 3850 m <sup>2</sup> g <sup>-1</sup> )
			Neat condition	10%	25	24h	81%	66% (80/20)		

organocatalytic MOF. <sup>[9]</sup>		DMF	10%	25	36h	86%	68% (83/17)	decreased from 66% to 48% and ee was decreased from 69% to 58%. In this last cycle, 11% of ligand was observed in the solution.	2.06 cm <sup>3</sup> g <sup>-1</sup> )
		Neat condition	10%	25	36h	49%	81%		
A imidazole-modified proline was introduced to MOF via copolymerization with other building blocks at 100 °C or 120 °C. <sup>[10]</sup>		MeOH/H <sub>2</sub> O	5%	25	10d	42%	60%	After 3 cycles, the ee could be well maintained, and the yield is slightly decreased from 97% to 89%. (10 days)	The surface area information is not mentioned.
		MeOH/H <sub>2</sub> O	5%	25	10d	77%	61%		
		MeOH/H <sub>2</sub> O	5%	25	10d	97%	58%		
The proline was introduced to the ligand and protected by t-		Acetone	100%	25	40h	-	29%	After 3 cycles, the reaction time was extended	138 m <sup>2</sup> g <sup>-1</sup>

	Boc group during MOF synthesis and then unveiled by thermal treatment (165°C, 4h). <sup>[11]</sup>		Cyclopentanone	100%	25	30h	-	14% (75/25)	from 30h to 72h.	
--	--	--	----------------	------	----	-----	---	----------------	------------------	--

\* Data in the parenthesis refer to the result of the small molecule catalyst.

## 4.5 References

- [1] Berner, O. M.; Tedeschi, L.; Enders, D., *Eur. J. Org. Chem.* **2002**, 2002, 1877-1894.
- [2] List, B., *Tetrahedron* **2002**, 58, 5573-5590.
- [3] Notz, W.; Tanaka, F.; Barbas, C. F., 3rd, *Acc. Chem. Res.* **2004**, 37, 580-591.
- [4] MacMillan, D. W., *Nature* **2008**, 455, 304-308.
- [5] Xu, H.; Chen, X.; Gao, J.; Lin, J.; Addicoat, M.; Irle, S.; Jiang, D., *Chem. Commun.* **2014**, 50, 1292-1294.
- [6] Benaglia, M.; Puglisi, A.; Cozzi, F., *Chem. Rev.* **2003**, 103, 3401-3429.
- [7] Lee, J.; Farha, O. K.; Roberts, J.; Scheidt, K. A.; Nguyen, S. T.; Hupp, J. T., *Chem. Soc. Rev.* **2009**, 38, 1450-1459.
- [8] Yoon, M.; Srirambalaji, R.; Kim, K., *Chem. Rev.* **2012**, 112, 1196-1231.
- [9] Banerjee, M.; Das, S.; Yoon, M.; Choi, H. J.; Hyun, M. H.; Park, S. M.; Seo, G.; Kim, K., *J. Am. Chem. Soc.* **2009**, 131, 7524-7525.
- [10] Dang, D.; Wu, P.; He, C.; Xie, Z.; Duan, C., *J. Am. Chem. Soc.* **2010**, 132, 14321-14323.
- [11] Lun, D. J.; Waterhouse, G. I.; Telfer, S. G., *J. Am. Chem. Soc.* **2011**, 133, 5806-5809.
- [12] Ding, S. Y.; Gao, J.; Wang, Q.; Zhang, Y.; Song, W. G.; Su, C. Y.; Wang, W., *J. Am. Chem. Soc.* **2011**, 133, 19816-19822.
- [13] Pachfule, P.; Kandambeth, S.; Diaz Diaz, D.; Banerjee, R., *Chem. Commun.* **2014**, 50, 3169-3172.
- [14] Fang, Q.; Gu, S.; Zheng, J.; Zhuang, Z.; Qiu, S.; Yan, Y., *Angew. Chem. Int. Ed.* **2014**, 53, 2878-2882.
- [15] Stegbauer, L.; Schwinghammer, K.; Lotsch, B. V., *Chem. Sci.* **2014**, 5, 2789.
- [16] Thote, J.; Aiyappa, H. B.; Deshpande, A.; Diaz Diaz, D.; Kurungot, S.; Banerjee, R., *Chem. Eur. J.* **2014**, 20, 15961-15965.
- [17] Nagai, A.; Guo, Z.; Feng, X.; Jin, S.; Chen, X.; Ding, X.; Jiang, D., *Nature Commun.* **2011**, 2, 536.
- [18] Bock, D. A.; Lehmann, C. W.; List, B., *Proc. Natl. Acad. Sci. USA* **2010**, 107, 20636-20641.
- [19] Wang, C. A.; Zhang, Z. K.; Yue, T.; Sun, Y. L.; Wang, L.; Wang, W. D.; Zhang, Y.; Liu, C.; Wang, W., *Chem. Eur. J.* **2012**, 18, 6718-6723.
- [20] Aradi, B.; Hourahine, B.; Frauenheim, T., *J. Phys. Chem. A* **2007**, 111, 5678-5684.
- [21] Lukose, B.; Kuc, A.; Heine, T., *J. Mol. Model.* **2013**, 19, 2143-2148.

- [22] Dören, T.; Millange, F.; Férey, G.; Walton, K. S.; Snurr, R. Q., *J. Phys. Chem. C* **2007**, 111, 15350-15356.
- [23] Pansare, S. V.; Pandya, K., *J. Am. Chem. Soc.* **2006**, 128, 9624-9625.
- [24] Cobb, A. J.; Shaw, D. M.; Longbottom, D. A.; Gold, J. B.; Ley, S. V., *Org. Biomol. Chem.* **2005**, 3, 84-96.
- [25] Luo, S.; Xu, H.; Mi, X.; Li, J.; Zheng, X.; Cheng, J. P., *J. Org. Chem.* **2006**, 71, 9244-9247.
- [26] Luo, S.; Mi, X.; Zhang, L.; Liu, S.; Xu, H.; Cheng, J. P., *Angew. Chem. Int. Ed.* **2006**, 45, 3093-3097.
- [27] Cao, C. L.; Ye, M. C.; Sun, X. L.; Tang, Y., *Org. Lett.* **2006**, 8, 2901-2904.
- [28] Ishii, T.; Fujioka, S.; Sekiguchi, Y.; Kotsuki, H., *J. Am. Chem. Soc.* **2004**, 126, 9558-9559.
- [29] Tan, R.; Li, C.; Luo, J.; Kong, Y.; Zheng, W.; Yin, D., *J. Catal.* **2013**, 298, 138-147.
- [30] Zhong, L.; Xiao, J.; Li, C., *J. Catal.* **2006**, 243, 442-445.
- [31] Kresge, C. T.; Leonowicz, M. E.; Roth, W. J.; Vartuli, J. C.; Beck, J. S., *Nature* **1992**, 359, 710-712.
- [32] Calderón, F.; Fernández, R.; Sánchez, F.; Fernández-Mayoralas, A., *Adv. Synth. Catal.* **2005**, 347, 1395-1403.
- [33] Doyaguez, E. G.; Calderon, F.; Sanchez, F.; Fernandez-Mayoralas, A., *J. Org. Chem.* **2007**, 72, 9353-9356.
- [34] Verde-Sesto, E.; Pintado-Sierra, M.; Corma, A.; Maya, E. M.; de la Campa, J. G.; Iglesias, M.; Sanchez, F., *Chem. Eur. J.* **2014**, 20, 5111-5120.
- [35] Marigo, M.; Franzen, J.; Poulsen, T. B.; Zhuang, W.; Jorgensen, K. A., *J. Am. Chem. Soc.* **2005**, 127, 6964-6965.
- [36] Hayashi, Y.; Gotoh, H.; Hayashi, T.; Shoji, M., *Angew. Chem. Int. Ed.* **2005**, 44, 4212-4215.
- [37] Jensen, K. L.; Dickmeiss, G.; Jiang, H.; Albrecht, L.; Jorgensen, K. A., *Acc. Chem. Res.* **2012**, 45, 248-264.
- [38] Férey, G.; Mellot-Draznieks, C.; Serre, C.; Millange, F.; Dutour, J.; Surble, S.; Margiolaki, I., *Science* **2005**, 309, 2040-2042.

**Chapter 5.**  
**Summary and Perspectives**

Covalent organic frameworks (COFs) are a class of crystalline porous polymers that enable the atomically precise integration of building blocks into two- or three-dimensional (2D or 3D, respectively) periodicities. This covalently linked and topologically crystallized 2D architecture merges two structural characters, i.e., periodic  $\pi$  arrays and ordered one-dimensional (1D) channels. Such highly ordered skeletal alignment, high surface area together with open-channel structure of the 2D COFs provides an intriguing motif for exploring well-defined nanoreactors. However, difficulty in getting a crystalline catalytic framework and losing of catalytic activity during polymerization makes the preparation of catalytic COF a big challenge in this field; meanwhile the stability issue of the currently developed COF materials further limited their application in catalysis.

In chapter 2, I developed a pore surface engineering strategy for the controlled functionalization of imine-linked COFs using a three-component condensation system in conjunction with click chemistry. I introduced the ethynyl- group into the building blocks and optimized the solvothermal conditions to create a serious ethynyl- modified COFs. This post-synthesis strategy preserved the crystallinity of the COF skeletons which ensure the open channels accessible for the reactants; meanwhile, the ambient condition of the click reaction largely maintained the activity and selectivity of the organocatalytic active sites. Engineering pyrrolidine units onto the pore walls creates COF based heterogeneous organocatalysts, which showed significantly improved activity because of the ordered nano-channel arrays and the high surface area.

To develop catalytic systems, chemical stability of the 2D COFs thus far reported are not robust enough to maintain crystallinity and porosity in different solvents or acidic/basic conditions. In chapter 3, I discovered a novel mesoporous imine COF which combines high crystallinity, porosity and excellent stabilities. COFs are designed and synthesized utilizing the reversible formation of covalent bonds that can be formed, broken, and reformed under the principle of dynamic covalent chemistry. Consequently, the reversible reaction nature makes the high crystallinity and large porosity seem to be incompatible with a robust stability in COF materials. However, in this part I challenge

this contradiction by a synthetic discovery of highly crystallized imine-COF, which owns a chemical robust nature but shows high crystallinity. This discovery makes a breakthrough in the field of crystalline frameworks, providing an efficient solution to the contradiction of high performance with high stability.

In chapter 4, I combined the pore surface engineering strategy with the highly crystallized mesoporous imine COF to create a high-performance heterogeneous asymmetric organocatalyst. The stability renders the COFs able to be chemically functionalized while retaining crystallinity and porosity; the chiral COF catalysts engineered with active sites on the channel walls were synthesized in a facile yet controlled manner. The mesoporous nature together with highly ordered 1D nano-channels and extremely high surface area endow this crystalline catalyst a number of striking features, including enhanced activity, high enantioselectivity, excellent stability and cycle performance and environmental benignity.

In summary, through the three-year work, I developed a general strategy for the design and synthesis of chiral covalent organic frameworks and demonstrated their functions as unique platform for designing high-performance heterogeneous asymmetric organocatalysts. I introduced click chemistry for functionalize COF as porous crystalline heterogeneous catalyst, provides an efficient and powerful method for construction of COF based heterogeneous catalyst; meanwhile, the discovery of the highly crystallized imine-COF combines the crystallinity, porosity with stability, demonstrates an efficient solution to the contradiction of high performance with high stability in the crystalline materials. Combine these significant achievements, I constructed an excellent COF-based heterogeneous organocatalyst, which demonstrated high overall-performance and strong potential of the COF material in heterogeneous catalysis.

## List of Publications

### 原著論文

1. Hong Xu, Xiong Chen, Jia Gao, Jianbin Lin, Matthew Addicoat, Stephan Irle, and Donglin Jiang, “Catalytic covalent organic frameworks via pore surface engineering”. *Chem. Commun.*, **2014**, 50 (11), 1292-1294. **(Selected as Back Cover.)**
2. Hong Xu and Donglin Jiang, “Covalent organic frameworks: Crossing the channel”. *Nature Chem.*, **2014**, 6 (7), 564-566.
3. Yanhong Xu, Shangbin Jin, Hong Xu, Atsushi Nagai and Donglin Jiang, “Conjugated microporous polymers: design, synthesis and application”, *Chem. Soc. Rev.*, **2013**, 42 (20), 8012-8031. **(Selected as Cover Page)**
4. Xiong Chen, Ning Huang, Jia Gao, Hong Xu, Fei Xu and Donglin Jiang, “Towards covalent organic frameworks with predesignable and aligned open docking sites”. *Chem. Commun.*, **2014**, 50 (46), 6161-6163.
5. Hong Xu, Hao Wei, Jia Gao and Donglin Jiang, “Chiral covalent organic framework catalysts for high-performance heterogeneous asymmetric transformations”. Preparing manuscript.

学会発表リスト

1. Hong Xu and Donglin Jiang, Designing Covalent Organic Frameworks as Highly Active Asymmetric Catalysts. 日本高分子学会第63回高分子討論会 (長崎) 2014.09. (Oral)
2. Hong Xu and Donglin Jiang, Designing Covalent Organic Frameworks as Highly Active Asymmetric Catalysts. American Chemical Society 248th National Meeting and Exposition, San Francisco, California, USA, 2014.08. (Poster)
3. Hong Xu and Donglin Jiang, Catalytic Covalent Organic Frameworks via Pore Surface Engineering. 日本化学会第94春季年会 (名古屋) 2014.03. (Oral)
4. Hong Xu and Donglin Jiang, Catalytic Covalent Organic Frameworks via Pore Surface Engineering. アジア冬の学校2014 (台湾台北) 2014.02. (Poster)
5. Hong Xu, Atsushi Nagai and Donglin Jiang, Construction of New Heterogeneous Organocatalysts using Covalent Organic Frameworks. 日本高分子学会第62回高分子年次大会 (京都) 2012.05. (Oral)
6. Hong Xu, Atsushi Nagai and Donglin Jiang, Construction of New Heterogeneous Organocatalysts using Covalent Organic Frameworks. 日本化学会第93春季年会 (京都) 2012.03. (Oral)
7. Hong Xu, Xiong Chen, Atsushi Nagai, and Donglin Jiang, Heterogeneous Organocatalysts Based on Two-Dimensional Polymers and Covalent Organic Frameworks. アジア冬の学校2014 (韓国釜山) 2014.02. (Poster)

## **Acknowledgements**

I wrote my thesis with a big thankful heart. During the past 3 years at IMS, I received countless amounts of help and support from many people. I wish I could find a better way to express my thankfulness.

The first one I would like to thank is my advisor, Prof. Donglin Jiang, for all his advice, encouragement and help all these years. From him, I saw the attributes of a great scientist, and learned a lot that can never be obtained in classrooms. I was extremely fortunate to get trained under his supervision. His insight, attitude and enthusiasm have been a never-ending source of inspiration and support. His encouragement and patience have made my time working here so enjoyable, even in difficulties and failures. I know I can never repay him for what I have received, and I hope I can pass these qualities on when I have opportunities to help others.

The interdisciplinary work presented in this thesis would have not been possible without close collaborations and interactions with experts from various fields, and from different departments and universities. In particular, we collaborate very closely with Prof. Stephan Irlle and Dr. Matthew Addicoat of Nagoya University, who carried out structural calculations. Their results helps me a lot to understand the structure of the COFs.

The work in this thesis could not be done without the help from the peoples at the Instrument Center in IMS. I'm especially thankful to Dr. Motoyasu Fujiwara, Dr. Satoru Nakao, Ms. Midori Saito, Mr. Seiji Makita and Ms. Michiko Nakano, for their kind supports in PXRD, FE-SEM, HR-TEM, EA and NMR measurements.

I also owe my sincere gratitude to my friends and my labmates Prof. Atsushi Nagai, Prof. Hao Wei, Dr. Jianbin Lin, Dr. Yanhong Xu, Dr. Xuesong Ding, Dr. Xiao Feng, Dr.

Xiong Chen, Dr. Cheng Gu, Dr. Sasanka Dalapati, Dr. Shangbin Jin, Mr. Yang Wu, Mr. Ning Huang, Mr. Jia Gao, Mr. Long Chen, Mr. Fei Xu, and secretaries Ms. Hiroko Suzuki, Mrs. Masako Hamada and Mrs. Sayuri Suzuki who gave me their help and encouragements in not only research but also everyday life.

Last but not least, I would like to thank my wife Dr. Li Sheng, my mother, father, and brother for all their love, supports and encouragements almost all my life.

Hong XU

2014